About this issue

One of the roles of the IUGS Advisory Board on Remote Sensing (ABRS) is to disseminate the latest information on remote sensing to the IUGS Executive Committee, Commissions, and Affiliated Organizations. This special issue of *Episodes* commemorates the success of the workshop on "Remote Sensing in Global Geoscience Processes" that was held at the University of Colorado at Boulder (USA) in May 1991. The workshop set high standards in terms of the level of international participation and the quality of the papers presented.

Remote sensing techniques have made significant strides in the earth sciences over the past two decades and now are used routinely in geological investigations in many areas. Geoscientists are among the largest users of aircraft and satellite images, and because the current and planned satellite programs are geared toward our understanding the earth-system sciences, this trend will continue. The papers and abstracts presented in this issue represent only some of the many applications of remote sensing in our efforts to understand global geoscience processes. We hope that this issue will encourage more use of remote sensing and further discussions among discipline specialists; the planning of workshops focused more on radar geology in vegetated terrains, particularly in tropical areas; and discussions on the role of remote sensing in helping to unravel the geology of arid lands, as well as, in particular, its contributions to geological hazards studies.

Episodes will return to its regular format and features in the next issue (June 1992).□

Correction

In the last issue (December 1991), a conference report by Richard M. Corfield entitled "Global Bioevents—Innovations and revolutions in the biosphere" referred to work by Richard Corfield and Julie Cartlidge on oxygen and carbon isotopic changes that took place in the Paleozoic. The reference to the Paleozoic was incorrect; the changes actually occurred in the Paleocene, not the Paleozoic. This was entirely *Episodes'* error, not Dr. Corfield's.□

Information for Contributors to Episodes

Episodes is distributed to a wide range of earth scientists in 150 countries. It keeps readers informed of new and current developments and is a vital communications link for the IUGS and the global earth-science community.

Policy

Episodes welcomes contributed articles. Articles should be innovative and of interest to a broad audience of professional scientists having diverse cultural and linguistic backgrounds. Articles include state-of-the-art reviews, new results from a research project of more than local significance, or discussions of the infrastructure of science—techniques, research programs, organizations, science policy, or technical assistance. All contributions will be reviewed for scientific interest and soundness.

Manuscripts

Articles are normally 4,000–5,000 words in length, equivalent to 16–18 double spaced typewritten pages on 22 × 28 cm (8.5 × 11 in.) paper. Shorter articles are also acceptable. Together with illustrations, most articles generally run five to seven printed pages.

All manuscripts should be written in English, double-spaced and typed on one side of the page only. Measurements should be given in metric units, and all nonstandard abbreviations, symbols, and acronyms should be properly defined. Acknowledgments may be included in a brief statement at the end of the article.

All accepted manuscripts will be edited to conform to *Episodes'* style and to ensure clarity and effectiveness of communication. *Episodes* will endeavor to clear major changes with the author. Submissions should include telephone, telex, and telefax numbers, if possible. The author will not see galleys or page proofs.

References cited in articles should follow the style shown below. These examples include references to a serial publication, a map, an abstract, a meeting report, and a book.

Handin, J.W., and Griggs, David, 1951, Predicted fabric changes, pt. 2 *of* Deformation of Yule Marble: Geological Society of America Bulletin, v. 62, no. 8, p. 863–866.

Harrison, J.E., Griggs, A.B., and Wells, J.D., 1986, Geologic and structure maps of the Wallace 1° × 2° quadrangle, Montana and Idaho: U.S. Geological Survey Miscellaneous Investigations Series Map I–1509–A, scale 1:250,000.

Street, R.L., and Herrmann, R.B., 1974, Earthquake mechanics in southeast Missouri and adjacent areas [abs.]: Geological Society of America Abstracts with Programs, v. 6, no. 3, p. 312–313.

Thayer, T.P., 1960, Some critical differences between alpine-type and stratiform peridotite-gabbro complexes: International Geological Congress, 21st, Copenhagen, 1960, Report, pt. 13, p. 247–259.

Thompson, J.B., Jr., and Norton, S.A., 1968, Paleozoic regional metamorphism in New England and adjacent areas, *in* Zen, E-an, White, W.S., Hadley, J.B., and Thompson, J.B., Jr., eds., Studies of Appalachian geology, northern and maritime: New York, Interscience Publishers, p. 319–327.

Illustrations

Illustrations should be in the form of high-quality black and white glossy photographic prints or originals. Please ensure that lettering, patterns, and other details will stand reduction to a single column width of 9.1 cm or a double column width of 18.6 cm. All illustrations previously published and unchanged from the original must include permission from the original publisher to republish. Manuscripts must also include a photograph and a brief (100 words maximum) biographical sketch of author.□

by Vernon H. Singhroy

Remote sensing in global geoscience processes: Introductory remarks

Important global scale applications in geology can be addressed by the use of the most advanced sensors that are available now on satellites. The articles in this special issue of Episodes *have been assembled by the Advisory Board on Remote Sensing for the purpose of discussing such applications.*

Introduction

One of the primary roles of the Advisory Board on Remote Sensing (ABRS) of the International Union of Geological Sciences (IUGS) is to facilitate the use of remote sensing data by the international geological community. A 2-day workshop hosted by the ABRS and the University of Colorado in the USA in May 1991 addressed the use of existing and planned remote sensing satellites. This introductory article evolved from the 1991 workshop and presents a starting point for future discussions and for future directions of remote sensing within the IUGS. Included in this special issue of *Episodes* are more detailed reviews and applications of remote sensing data to global geoscience processes, including geologic hazards.

The degree to which rock units have been mapped on the Earth varies considerably from country to country. Vast areas in developing countries, deserts, and jungles have been mapped only at reconnaissance scales. A better understanding of the characteristics of these rock units would increase our understanding of the deformational history of the Earth, as well as the location and mode of emplacement of nonrenewable resources. A remote sensing approach would provide the synoptic view that is necessary in order to map poorly known areas, and in some cases, remote sensing would provide a detailed view as well.

Although remote sensing is a relatively young scientific discipline, its use in the geosciences over the last two decades has been quite remarkable. Currently operational satellite systems, such as the USA's Landsat and France's SPOT, and radar images from satellites and aircraft are employed widely in geological mapping and exploration programs, as well as in investigations of geologic hazards. Figure 1 shows an example of the extensive use of remote sensing techniques within the international geological community.

In general, three methods are used to extract geological information from remote sensing data. These are the spectral, photogeological, and integration methods. Examples of all these methods are evident in this issue of *Episodes*. The spectral approach involves the separation of surface materials or vegetation based on spectral reflectance, emittance, or backscatter. This approach is used for analyzing multispectral image data in both vegetated and nonvegetated areas. Laboratory and field spectral data often are employed in order to establish the physical basis for the remote determination of rocks, soils, minerals, or vegetation. The photogeological technique uses topographic expression and image textures for delineating geologic structures and geomorphic and lithologic units. This is a very common and effective approach and relies, to a large extent, on the skills of the interpreter. The integration method involves the merging of remote sensing data and geological, geophysical, or topographic information for the purpose of assisting in the interpretation of the spectral or photogeological units and for determining their relationships with the other data sets. This integration approach is being incorporated increasingly in geological remote sensing as more geological and topographic data are available in digital form.

Global land processes

Several significant developments have taken place in remote sensing in terms of the uses of existing satellites and the capabilities of planned satellites that are directly applicable to the study of geoscience processes. These developments include the higher spatial, spectral, and stereo capabilities that can provide more quantitative measurements of surface and near-surface features for the purpose of predictive modeling. For instance, the techniques developed and sensors used for geological mapping and exploration can be applied to the investigation of crustal and tectonic movements, arid lands, geology, and erosion processes, among others.

For decades, geologists have used remotely sensed images successfully in order to identify primary earth materials (rocks and minerals) and their regolith. The application of high-resolution spectrometers to mineral mapping is rapidly becoming a reality. The use of Landsat Thematic Mapper (TM) and SPOT data, when available, can provide a way to map mineral assemblages in arid and semiarid areas. However, higher spectral resolution clearly would be needed for us to be able to separate most rock types and soils. Nonetheless, the identification of minerals, rocks, soils, and vegetation from laboratory, field, and airborne spectra is a significant development in the study of global geoscience processes. Although valuable geological information has been derived from the spectral data provided by Landsat and SPOT, high-resolution imaging spectrometers have extensive capabilities in spectral geology and for global spectral measurements. Such capabilities are described by Goetz in his article in this issue.

In vegetated areas, however, other methods are needed to detect the variations in vegetation for the purpose of mapping the underlying materials. Developments in geobotanical remote sensing over the past decade have increased our knowledge of the influence of lithology, topography, and geochemistry on the distribution and density of vegetation. Bell and others (abstract in this issue) have shown that an understanding of the relationships between vegetation and lithology can provide additional insights into the distribution of global biomes. Rock (abstract in this issue), Singhroy (1988), and others have used airborne multispectral imagers to locate, monitor, and study forest damage that has resulted from natural mineral concentrations, mine wastes, and other environmental factors. The capability of remote sensing techniques to map and monitor vegetation stress that is caused by both natural and anthropogenic factors is significant in our understanding of the biogeochemical cycle.

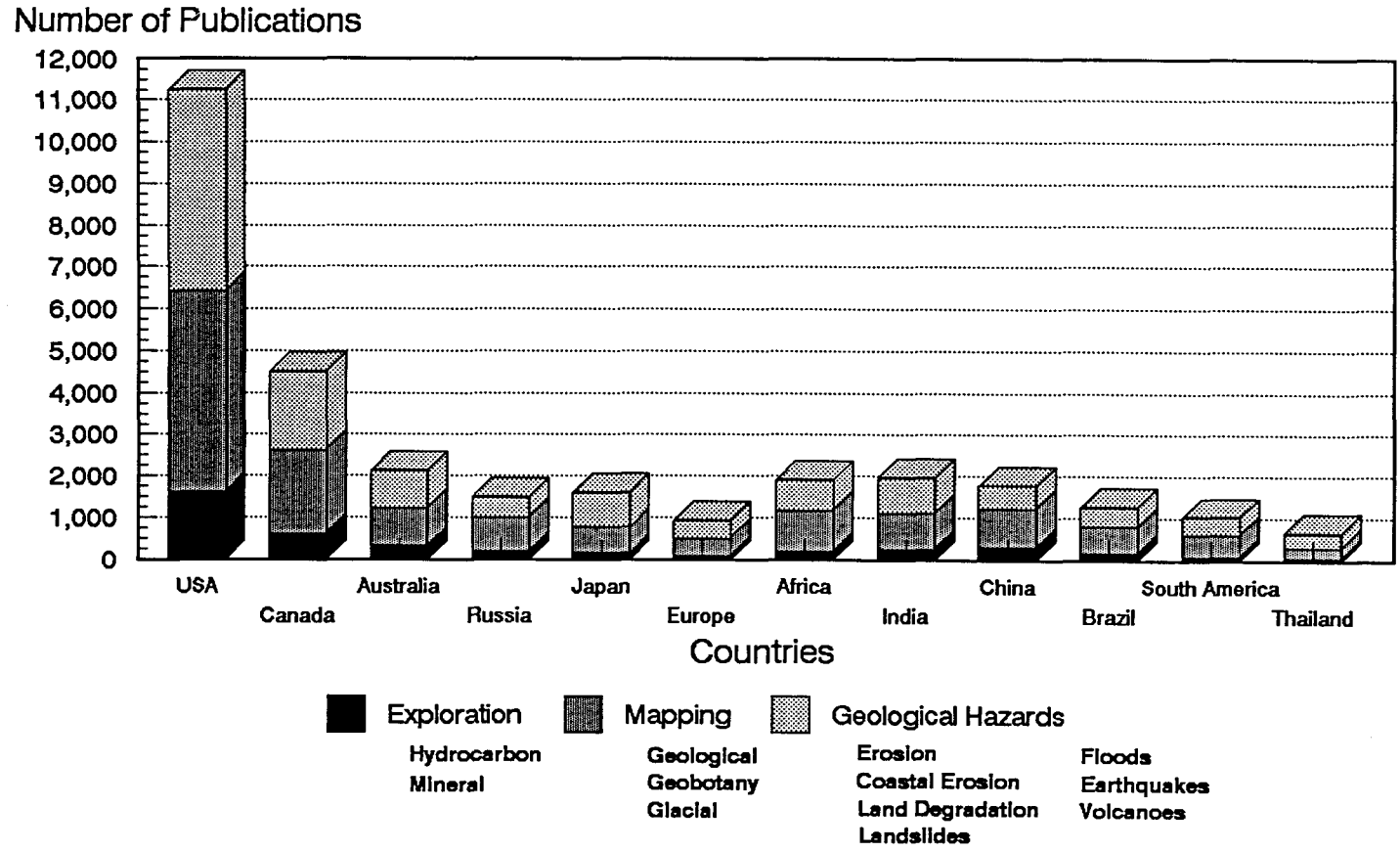

Figure 1.—International applications of geological remote sensing techniques from 1980 to 1991. Compiled by Canada Centre for Remote Sensing.

The capabilities of Synthetic Aperture Radar (SAR) for landform and geological mapping and for tectonic activity and erosion studies, as well as its potential in providing information on soil moisture, surface roughness, and topography, are described in this issue by Evans and by Singhroy. Because SAR penetrates clouds and sometimes vegetation and thin sand, it can be applied to the study of geologic processes in cloudy, vegetated, and arid areas where other sensors are limited. The use of SAR in characterizing and mapping evidence of alternating humid and arid climates, such as fossil dune fields, paleorivers, and paleolakes, is particularly significant for reconstructing the climatic history of deserts that existed during the Cenozoic (Petit-Maire and others, abstract in this issue).

The development of remote sensing methods for mapping rock units, detecting crustal movements, and monitoring selected surface processes is crucial to predictive modeling. These techniques include the mapping of fracture systems from multispectral satellite and SAR images (Halbouty, 1976, 1980; Misra and others, 1991; Abrams and others, 1985), the statistical analysis of lineament data, and the creation of lineament density maps (Misra and others, 1991). Image enhancement techniques such as principal component analysis (Loughlin, 1991; Chavez and Bowell, 1988), decorrelation stretching of bands (Dury and Hunt, 1988), and band ratios (Podwysocki and others, 1983) are some of the common image processing methods that are used by geoscientists. The integration of geophysical and remote sensing data is being carried out increasingly for geological investigations in different environments (Harris, 1991; Fernandez-Alonso and Tahon, 1991). Landsat and SPOT, when merged with geographic, geologic, and digital elevation information, have produced revised maps and realistic perspectives of the Earth's surface. Such three-dimensional spatial and dynamic modeling that results from the combination of geographic information systems (GIS) and remote sensing is crucial for geoscience applications.

Geologic hazards

In the context of the International Decade for Natural Disaster Reduction (IDNDR), remote sensing techniques are playing an increasing role in the identification and monitoring of areas of geologic hazards. In this issue, studies show that satellite and airborne remote sensing and GIS techniques have been used to study volcanic eruption processes, to produce hazard maps in mountainous areas, to monitor landslide activities, and to identify fracture zones associated with seismic activity. These remote sensing techniques can lead to disaster reduction by preventing disasters through measures such as improved construction or land-use practices; by providing warnings and forecasts; and by rendering fast, effective relief after disaster strikes (Walter, abstract in this issue).

Mouginis-Mark and Francis (this issue) review the current applications of the many remote sensing techniques as they apply to the analysis of volcanoes and volcanic terranes. Landsat TM images have been used to map the distribution of volcanic lithologies, to identify potentially active volcanoes and volcanic debris deposits,

and to monitor lava flows. Images from the Geostationary Operational Environmental Satellite (GOES) and the U.S. National Oceanic and Atmospheric Administration's NOAA 7 satellite have been employed in monitoring the downwind disposal of an eruption plume and in measuring plume temperature. The evolution of a lava flow field and its thermal characteristics can be studied over a period of time by using daily Advanced Very High Resolution Radiometer (AVHRR) satellite images. Under cloudy conditions, the potential is great that SAR data will be able to map the distribution of lava flows, cinder cones, and fault zones. In Japan, regional volcanic framework mapping has been conducted by the use of thermal infrared imagery (Yamaguchi and others, this issue).

The production of hazard maps at various scales from 1:250,000 to 1:5,000 has been accomplished by combining remote sensing and GIS techniques in mountainous areas and is described by Rengers and others (this issue). Aerial photographs, SPOT, and Landsat data were processed by the use of GIS, particularly for landslide hazard assessment. In cloudy, tropical, mountainous areas, radar images also will provide information on geologic structures, slopes, and terrain roughness. However, input into GIS could require geometrically corrected radar images.

Leroi and others (this issue) created a digital elevation model from a hybrid SPOT and Landsat stereopair and analyzed slope morphology and debris in relation to landslides in Colombia. The landslide hazard map that resulted from SPOT, Landsat, and GIS techniques is part of the Geological Application of Remote Sensing (GARS) project of the United Nations Educational, Scientific, and Cultural Organization (UNESCO). Similar techniques, described by McKean and others (1991), have employed Landsat TM data in a GIS context for the purpose of exploring the effect of vegetation type on debris flow for use in hazard modeling.

The mapping of fracture systems from several types of remotely sensed data is well documented in seismically active areas (Shibakova and others, this issue; Moon, 1991; and others). Measurements of horizontal terrain displacements associated with earthquakes have been conducted by the use of SPOT imagery (Crippen, this issue). Eliason (this issue) provides a structural analysis of fracture systems that uses topographic and seismic data. This information can be integrated with other satellite lineament maps for the structural interpretation of seismically active areas.

Future directions

Understanding global geologic and geophysical processes requires a diversity of accurate observations. The need to monitor the mechanisms of geologic hazards, crustal movements, desertification, erosion processes, and sea level changes is fundamental to our understanding the total Earth system, from which we hope to develop a capability to predict future change. The existing and planned satellite systems (fig. 2) and the techniques described in this issue are a means to study global geoscience processes. Of particular interest will be the series of radar satellites to be launched in the 1990s, such as ERS–1 (Europe), JERS–1 (Japan), and Radarsat (Canada), which will provide geologic information from the Tropics and other parts of the Earth. Clearly, important global scale research in geology is being addressed by using the most advanced sensors now available on satellites, and this research will continue as planned satellites are launched. The IUGS through the ABRS will continue to report on these developments and will encourage cooperative research in geological remote sensing. I hope that discussions resulting from this issue of *Episodes* will chart the future directions of programs on remote sensing activities within the IUGS.

References

Abrams, M.J., Conel, J.E., Lang, H.R., and Paley, H.N., 1985, The joint NASA/Geosat test case project, final report: Tulsa, Oklahoma, USA, American Association of Petroleum Geologists, v. 1 and 2, 622 p.

Chavez, P.S., and Bowell, J.A., 1988, Comparison of the spectral information content of Landsat Thematic Mapper and SPOT for three different sites in Phoenix, Arizona, region: Photogrammetric Engineering and Remote Sensing, v. 54, no. 12, p. 1699–1708.

Dury, S.A., and Hunt, G.A., 1988, Remote sensing of laterized Archean greenstone terrain: Marshall Pool area, northeastern Yilgarn Block, Western Australia: Photogrammetric Engineering and Remote Sensing, v. 54, no. 12, p. 1717–1725.

Fernandez-Alonso, M., and Tahon, A., 1991, Lithologic discrimination and structural trends in W. Rwanda (Africa) on images of airborne radiometric and aeromagnetic surveys registered to a Landsat TM scene: Photogrammetric Engineering and Remote Sensing, v. 57, no. 9, p. 1155–1162.

Halbouty, M.T., 1976, Application of Landsat imagery to petroleum and mineral exploration: American Association of Petroleum Geologists Bulletin 60, p. 745–793.

———1980, Geologic significance of Landsat data for 15 giant oil and gas fields: American Association of Petroleum Geologists Bulletin 64, p. 8–36.

Harris, J., 1991, Mapping of regional structure of eastern Nova Scotia using remotely sensed imagery: Implications for regional tectonics and gold exploration: Canadian Journal of Remote Sensing, v. 17, no. 2, p. 122–136.

Loughlin, W.P., 1991, Principal component analysis for alteration mapping: Photogrammetric Engineering and Remote Sensing, v. 57, no. 9, p. 1163–1169.

McKean, J., Buechel, S., and Gaydos, L., 1991, Remote sensing and landslide hazard assessment: Photogrammetric Engineering and Remote Sensing, v. 57, no. 9, p. 1185–1193.

Misra, K.S., Slaney, V.R., Graham, D., and Harris, J., 1991, Mapping of basement and other tectonic features using Seasat and Thematic Mapper in hydrocarbon-producing areas of the western sedimentary basin of Canada: Canadian Journal of Remote Sensing, v. 17, no. 2, p. 137–151.

Moon, W.M., Won, J.S., Li, B., Slaney, V.R., and Lamontagne, M., 1991, Application of airborne C–SAR and SPOT image data to the geological setting of the Nahanni earthquake area: Canadian Journal of Remote Sensing, v. 17, no. 3, p. 272–278.

NASA (National Aeronautics and Space Administration), 1990, EOS: A mission to planet Earth: Washington, D.C., USA, p. 6.

Podwysocki, M.H., Segal, D.B., and Abrams, M.J., 1983, Use of multispectral scanner images for assessment of hydrothermal alteration in the Marysvale, Utah, mining area: Economic Geology, v. 78, no. 4, p. 675–687.

Singhroy, V.H., 1988, An overview of geobotanical remote sensing in Canada, *in* Howarth, P.J., ed., Canadian Symposium on Remote Sensing, 11th, Waterloo, Ontario, Canada, 1987, Proceedings, p. 259–275.□

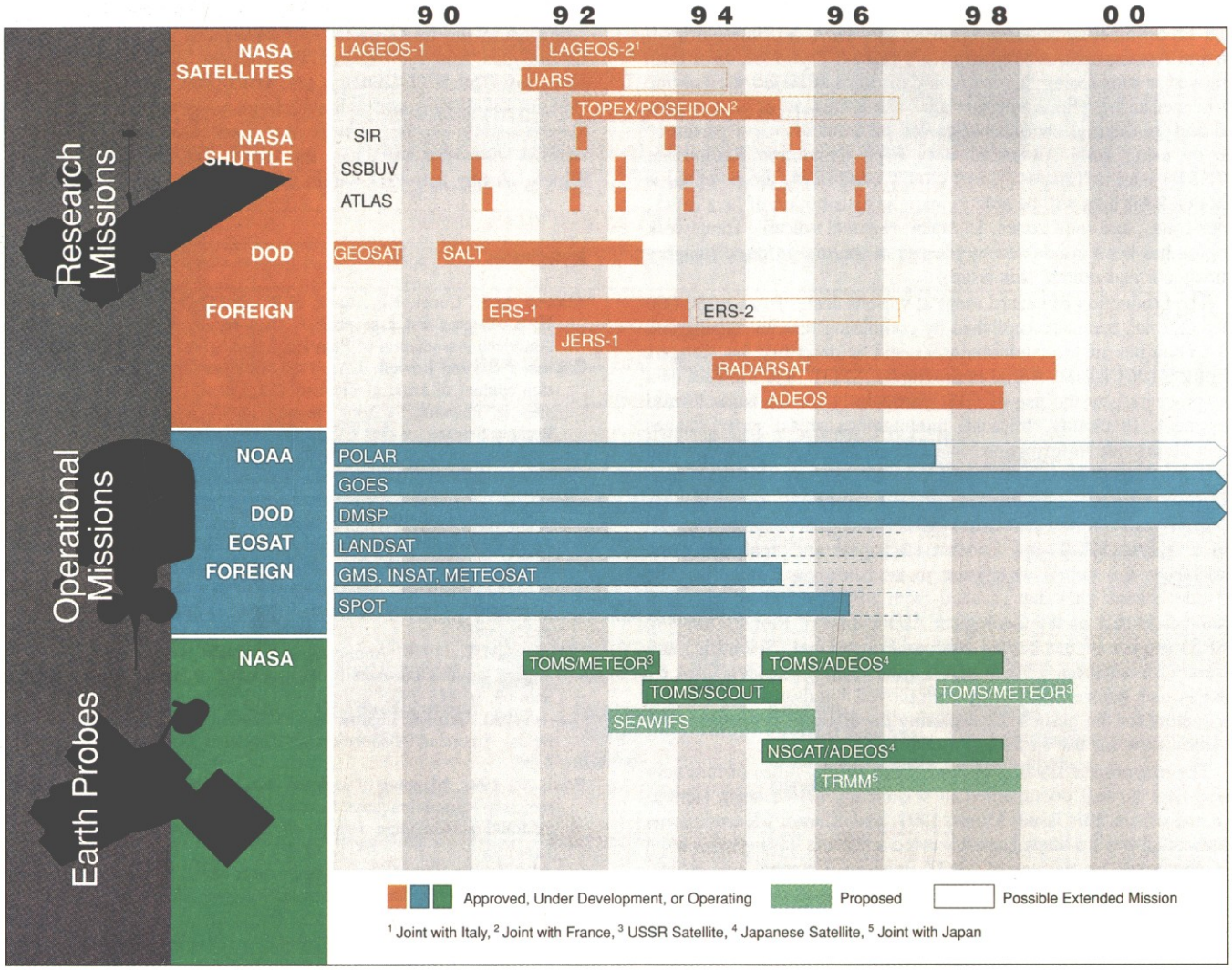

Figure 2.—Existing and planned satellite systems for the years 1988 through 2002. Taken from NASA (1990). Abbreviations: NASA, U.S. National Aeronautics and Space Administration; DOD, U.S. Department of Defense; NOAA, U.S. National Oceanic and Space Administration; EOSAT, Earth Observation Satellite Company, USA.

Dr. V.H. Singhroy *is Chairman of the Advisory Board on Remote Sensing of the International Union of Geological Sciences, Research Scientist in geological remote sensing, and Scientific Advisor at the Canada Centre for Remote Sensing in Ottawa, Ontario, Canada.*

by Alexander F.H. Goetz

Imaging spectrometry for Earth observations

Imaging spectrometry is defined as the simultaneous acquisition of images in a large number of contiguous spectral bands. Today, several airborne imaging spectrometers are operational, and in the beginning of the next decade, the High Resolution Imaging Spectrometer will provide data from orbit. This is a facility instrument that is slated for flight on the second series of the National Aeronautics and Space Administration's Earth Observing System platforms. The instrument is designed to acquire 24-kilometer wide, 30-meter pixel images in 192 spectral bands simultaneously in the 0.4–2.45-micrometer wavelength region. By the use of pointing mirrors, it will be able to sample any place on Earth, except the poles, every 2 days. It will operate at the intermediate scale between the human and the global and, therefore, will link studies of the Earth's surface processes to the global monitoring that is carried out by lower resolution instruments. So far, over 50 science data products from images of this instrument have been identified in the fields of atmospheric gases, clouds, snow and ice, water, vegetation, and rocks and soils. The key attribute of imaging spectrometry that makes it possible to derive quantitative information from the data is the large number of contiguous spectral bands. Therefore, spectrum matching techniques can be applied. Such techniques are not possible by using today's multispectral scanner data.

Introduction

Imaging spectrometry for Earth observations has been developed over the last decade in order to provide more definitive and quantitative information from remote sensing about the surface of the Earth. The space-based multispectral scanners, USA's Landsat and France's SPOT, showed many of the advantages of the perspective from space. The short-wavelength infrared bands of the Landsat Thematic Mapper (TM) have yielded information about the Earth's surface, but in many instances, the information is ambiguous as a result of the small number of spectral bands available. Because the emphasis now is being placed on global measurements in an effort to understand global change, more sophisticated sensors are necessary in order to provide the quantitative information that is important to the development of predictive models. Imaging spectrometry has the potential to acquire all the information that is available in the radiance reflected from the Earth's surface.

Imaging spectrometry is defined as the simultaneous acquisition of image data in hundreds of contiguous spectral bands, which makes it possible to produce laboratory-like reflectance spectra for each pixel in the image, as shown in figure 1 (Goetz and others, 1985). The High Resolution Imaging Spectrometer, slated for flight on the second of the National Aeronautics and Space Administration's (NASA) Earth Observing System's (EOS–A) series of platforms, will have 192 spectral bands covering the wavelength region of 0.4–2.45 μm.

Background

Landsat 1, launched in 1972, provided the first multispectral images that could be calibrated radiometrically and that were provided in digital form. The spectral bands were designed primarily for use in agricultural studies. However, the geological community rapidly took advantage of the synoptic view, as well as the spectral coverage that extended beyond the visible part of the spectrum. The need to understand the spectral reflectance characteristics of natural surfaces hastened the development of portable spectrometers that would aid in interpreting Landsat Multispectral Scanner (MSS) images and would provide a fundamental data set for developing the requirements of more sophisticated spectral imaging systems. One of the early instruments was the Portable Field Reflectance Spectrometer (PFRS) (Goetz and others, 1975). Its spectra and laboratories' spectra were reproduced in a series of papers during the 1970s that were summarized by Hunt (1980), and these papers made it clear that direct mineral identification would be possible if imaging was possible in narrow, contiguous spectral bands. Field spectrometry and multiband airborne imaging produced the rational for the seventh band (2.08–2.36 μm) on the TM (Abrams and others, 1977).

Although imaging spectrometry was not feasible at that time, the next step beyond field spectrometry was airborne and spaceborne profiling in many spectral bands simultaneously. Two instruments were developed during that period. In 1976 work was begun on the Shuttle Multispectral Infrared Radiometer (SMIRR), a 10-band spinning filter wheel radiometer that flew with the second flight of the space shuttle in 1981. Data from this instrument provided the first direct identification of limestone and the clay kaolinite from orbit (Goetz and others, 1982).

In the late 1970s, an airborne 500-band profiler was developed by Geophysical Environmental Research in Millbrook, New York, USA, and was used to produce mineralogical maps, as well as to identify trees that were stressed by excess copper in the soil. This profiler led to the discovery of the "blue shift" in the red edge of the chlorophyll absorption feature at 0.68 μm (Collins and others, 1983).

In 1981 an imaging spectrometer program was begun at NASA's Jet Propulsion Laboratory in Pasadena, California, USA. This program had as its goal two different airborne imaging spectrometer systems, a shuttle experiment and finally a free-flying version known as the High Resolution Imaging Spectrometer (HIRIS). The first airborne system was the Airborne Imaging Spectrometer (AIS) (Vane and Goetz, 1988), which was, in fact, a detector test

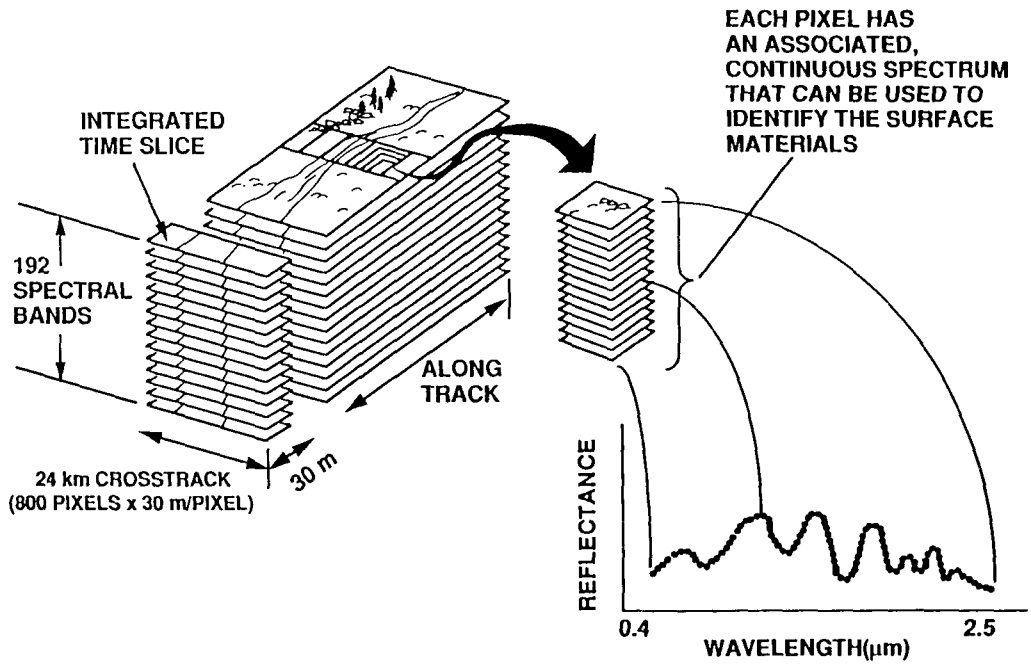

Figure 1.—Concept of imaging spectrometry.

bed. It covered 128, 9.3-nm bands in the 1.2–2.4 μm region. The spatial swath coverage was only 32 and later 64 picture elements. A coincident development was a new portable spectrometer known as the Portable Instant Display and Analysis Spectrometer (PIDAS) (Goetz, 1987) that recorded a complete spectrum from 0.4 to 2.5 μm in 2 seconds. The second airborne system was the 224-band Airborne Visible and Infrared Imaging Spectrometer (AVIRIS) that flies at 20-km altitude on the NASA ER–2 aircraft (Porter and Enmark, 1988). AVIRIS is an optomechanical whiskbroom scanner that has a 1-milliradian (mrad) instantaneous field of vision (20-m pixels). AVIRIS is operational now and provides unique imaging spectrometry data for atmosphere, land, and water studies.

In 1988 NASA announced that HIRIS would be a facility instrument as part of the EOS package aboard the Polar-Orbiting Platform. The 14-member HIRIS team (table 1) was chosen in 1989. In early 1991, NASA confirmed that HIRIS would be part of the second EOS–A platform scheduled to be flown in 2003.

Table 1.—HIRIS science team members and their affiliations

John Aber University of New Hampshire	Hugh Kieffer U.S. Geologial Survey Flagstaff, Arizona
Kendall L. Carder University of South Florida	David A. Landgrebe Purdue University
Roger N. Clark U.S. Geological Survey Denver, Colorado	John M. Melack University of California, Santa Barbara
Curtiss O. Davis Jet Propulsion Laboratory, California Institute of Technology	Lawrence C. Rowan U.S. Geological Survey Reston, Virginia
Jeffrey Dozier University of California, Santa Barbara, and Goddard Space Flight Center	Susan L. Ustin University of California, Davis
Siegfried A.W. Gerstl Los Alamos National Laboratory	Ronald M. Welch South Dakota School of Mining and Technology
Alexander F.H. Goetz, team leader University of Colorado	Carol A. Wessman University of Colorado

Rationale for HIRIS

HIRIS will embody both high spatial resolution (30-m pixels) and contiguous spectral coverage in the region of 0.4–2.45 μm in 192 bands. In addition, HIRIS is designed to point ±45° crosstrack and +56 to −30° downtrack in order to provide coverage of every place on the globe, except the poles, within 2 days and to create bidirectional reflectance distribution functions. HIRIS is a sampling instrument and is not intended to provide global coverage.

HIRIS will operate at the intermediate scale between the human and the global, and thus it is essential for linking the studies of processes at the surface of the Earth to the global monitoring program that is a primary function of EOS. Some of the fundamental questions in Earth system science revolve around the scale dependence of some processes and the scale invariance of others, as well as the interactions of processes that occur at fundamentally different scales. Experimental measurements can investigate processes on the detailed level at which the transport of nutrients, sediments, gases, and solutes occurs, such as the uptake of carbon dioxide and nitrogen by plants, the release of water vapor in organic compounds by plants, the movement of sediment in rivers, and the elution of chemicals from the seasonal snowpack. At a scale of hundreds of meters to kilometers, we can examine the large-scale effect of some of these processes, but we cannot investigate scale dependency or address how results from field investigations can be extrapolated to the global scale. Experience has shown that it is logistically infeasible to mount

an aircraft program for acquiring large amounts of intermediate-scale data. Therefore, HIRIS is essential in order to understand the processes that are taking place within the coarser resolution elements of the Moderate Resolution Imaging Spectrometer (MODIS), another EOS–A instrument, and that are necessitated by the global monitoring function.

HIRIS will permit the detailed examination and monitoring of sensitive ecosystem interfaces where the rates of change are highest and, therefore, most easily detected. Changes are detected best at interfaces, such as the montane snowline, the savanna-woodland border, the wetland-upland edge, and the estuarine-oceanic zone. Many of the important fluxes occur at spatial scales that are far too small to be seen by the coarser resolution mapping instruments or that require high spectral resolution for their detection. Thus, a global sampling program employing HIRIS will be an essential component for a global mapping and modeling program that has instruments designed for large-scale monitoring.

HIRIS science requirements

The science requirements for HIRIS have been developed by the HIRIS science team since 1989 (Goetz and others, 1991). The science requirements have driven the instrument design, and the resulting major HIRIS parameters are given in table 2. Following is the underlying rationale for some of the major HIRIS functional instrument parameters.

As discussed above, HIRIS acts as an intermediate-level data collection system in a multistage sampling program. Keeping this mission in mind and basing our decisions on the experience of the Landsat TM, we chose a spatial resolution equivalent to that of TM, a ground instantaneous field of view of 30 m. The requirement for a 30-m or smaller pixel can be quantified in vegetation research. In forest ecosystems, successional changes in vegetation structure and function are linked to the size of the gaps that are created by tree death, windfall, and other forms of disturbance. Similarly, arguments can be made for the requirement for high spatial resolution in geological mapping because, in many regions, rock outcrops may have only a few square meters of surface exposure. Alternatively, studies of macrophytes in inland waters, as well as in coastal areas, may require higher spatial resolution than is provided by the 30-m pixel. However, the penalty paid for higher spatial resolution in the form of increased data rate and reduced number of spectral bands was too high, and the 30-m ground instantaneous field of view was established as a requirement.

Table 2.—HIRIS functional instrument parameters

Item	Performance
Design altitude	705 km
Ground instantaneous field of view	30 m
Swath width	24 km
Spectral coverage	0.4–2.45 μm
Average spectral sample interval	
0.4–1 μm	9.4 nm
1–2.45 μm	11.7 nm
Pointing	
Along-track	+56° to −30°
Crosstrack	+45° to −45°
Encoding	12 bits/pixel
Maximum internal data rate	405 Mbps
Maximum output data rate	100 Mbps
Image motion compensation	1 (off), 2, 3, 4, and 8

The choice of spectral coverage was dictated both by scientific requirements and technological capabilities. The 0.4–2.45 μm region contains all the information that can be derived by passive sensors from reflected solar energy. In the visible and near-infrared spectral region, diagnostic information is attainable for water, snow, and vegetation and for some minerals and soils. In the region beyond 1 μm, diagnostic spectral features are found for snow, clouds, vegetation, and minerals in soils.

The requirements for spectral resolution are driven by the water and vegetation studies in the visible and near-infrared region and by the needs for vegetation biochemistry and mineralogical mapping in the region beyond 1 μm. Deriving the biochemical constituents from vegetation also requires data over the full spectral range. One of the advances in our understanding biological activity in surface waters by the use of imaging spectrometry will be our ability to identify directly the constituents in their respective concentrations. Absorption spectra of algal pigments, such as phycoerthyrin and peridinin, exhibit features that have full-width, one-half-maximum values of 20 nm. Therefore, a 20-nm resolution and 10-nm sampling will be required in order to discern these features in the 0.4–0.7 μm region.

Requirements of the spectral resolution for vegetation research are being developed. The resolution offered by TM clearly has not proven sufficient for species identification or for measuring the biochemical state of terrestrial ecosystems beyond the general measurements of stress. One goal of imaging spectrometer research is to develop the capability to detect subtle changes in ecosystem biogeochemistry as precursor indicators of future changes in structure and function. This problem is being studied by the remote sensing of changes in the total canopy content of important constituents such as nitrogen and lignin (Wessman and others, 1988). Advances have been made in extracting spectral features that are associated with dry leaf matter from the spectra of healthy, turgid vegetation (Goetz and others, 1990). In both cases, an approximate 10-nm spectral sampling was adequate for resolving the relevant spectral features.

Spectral features for minerals are associated both with an electronic transition in transition elements, mainly iron, in the visible and near-infrared region and with vibrational modes in the region beyond 1.5 μm. Vibrational features, generally overtone bending-stretching vibrations, are exhibited by minerals bearing Al-OH, Mg-OH, CO_3, and H_2O constituents (fig. 2). These minerals have features in some cases as small as 10-nm full-width, one-half-maximum values that require 5-nm sampling for proper description. However, the majority of mineral features can be described completely by the use of 10-nm sampling. A significant degradation in identification, particularly in magnesium-bearing minerals, as well as in limestone and dolomite, is seen when the sampling interval is increased to 20 nm. In general, 10 nm is a critical sampling interval throughout the 0.4–2.45-μm wavelength region.

The frequency requirements of coverage are related directly to the dynamic nature of the problem to be studied. Water studies have the greatest need for high-frequency measurements, vegetation is next, and geological studies are a distant third. The geological requirements concern acquiring data at an optimum time of year for the proper lighting and vegetation cover in the absence of cloud cover. HIRIS will not acquire continuous coverage but rather will sample sites at high spatial and spectral resolution. By pointing crosstrack ±45°, the maximum time between acquisition for any point on the Earth, except the poles, is 2 days. In some cases, data acquisition is possible on subsequent days even at the Equator.

Pointing is, therefore, a necessary requirement. Not only is crosstrack pointing required, but an additional requirement exists for along-track pointing in order to develop bidirectional reflectance distribution functions for surfaces, to remove atmospheric absorption and path radiance components, to avoid sun glint on water targets,

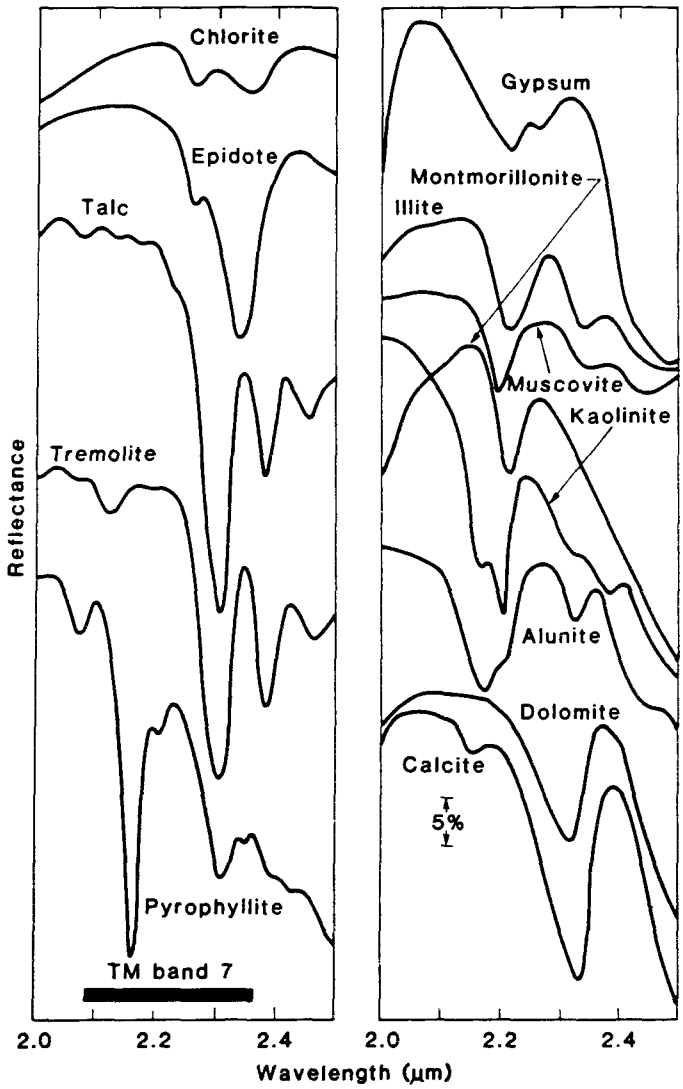

Figure 2.—Laboratory reflectance spectra of common minerals in the 2.0–2.5 μm region (taken from Goetz and Rowan, 1981).

and to facilitate target tracking in order to increase signal-to-noise performance for dark targets, such as water and any target in the longer wavelength part of the spectrum where the solar irradience is low.

Data analysis

Over 50 science data products, that is, biogeophysical parameters that can be derived from HIRIS data, have been identified by the HIRIS science team. Here are several examples of the kinds of information that can be derived from HIRIS data, as well as the techniques that are needed for analysis.

Atmospheric water vapor

HIRIS data will be acquired through the Earth's atmosphere, and because imaging spectrometry data have a much higher spectral resolution than multispectral data scanners such as TM have, much more effort must be applied in order for us to understand and compensate for atmospheric transmission and scattering. In the 0.4–2.5 μm region, water vapor absorption affects more than one-half the spectrum (fig. 3). Carbon dioxide, oxygen, and methane are additional absorbers that have a significant effect in this wavelength region. Initial work has been carried out in deriving column atmospheric water vapor amounts on a pixel by pixel basis, which is necessary in order to remove the variable amounts of water vapor over the scene.

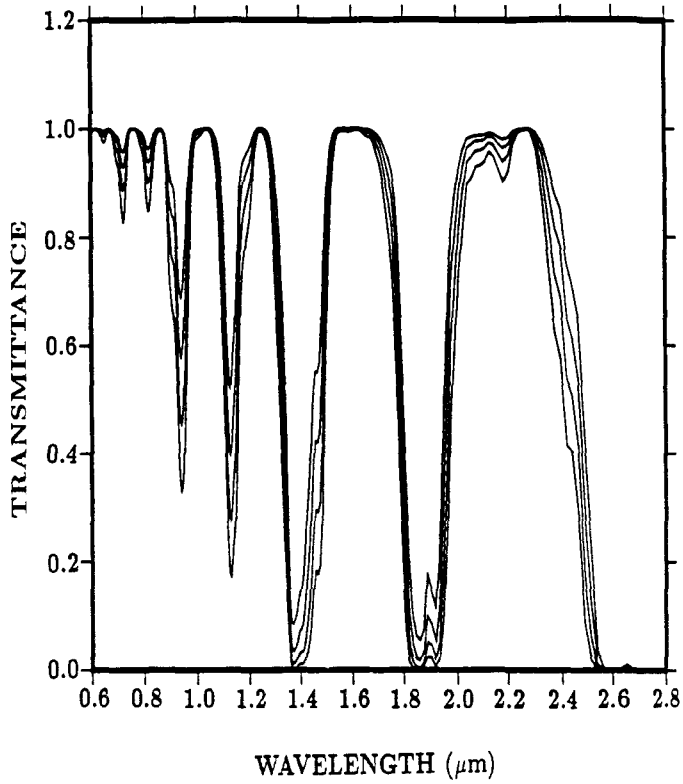

Figure 3.—Vertical atmospheric transmittance as a function of different water vapor amounts. The four curves from top to bottom correspond to column vapor amounts of 0.63, 1.3, 2.5, and 5.0 cm, respectively (taken from Gao and Goetz, 1990).

Column atmospheric water vapor amounts at high spatial resolution have been derived from spectral data that was collected by AVIRIS, which covers the spectral region from 0.4 to 2.5 μm in 10-nm bands and has a ground instantaneous field of view of 20×20 m from an altitude of 20 km (Gao and Goetz, 1990). The quantitative derivation is made by curve fitting the observed spectra with the calculated spectra in the 1.14-μm and 0.94-μm water vapor band spectral model by the use of a nonlinear least squares fitting technique. For this analysis, it is mandatory that data be collected in narrow, contiguous spectral bands throughout the region. Figure 4 shows an example of curve fitting of the spectra measured over an unvegetated area.

This spectral matching technique is directly applicable to retrieving column water vapor amounts from AVIRIS spectra, and from HIRIS as well, that are measured on clear days having a visibility of 20 km or greater. The precision of the retrieved column water vapor amounts from several data sets is 5 percent or better (Gao and Goetz, 1990). Column water vapor images can be constructed by this technique, and they show high variability in the

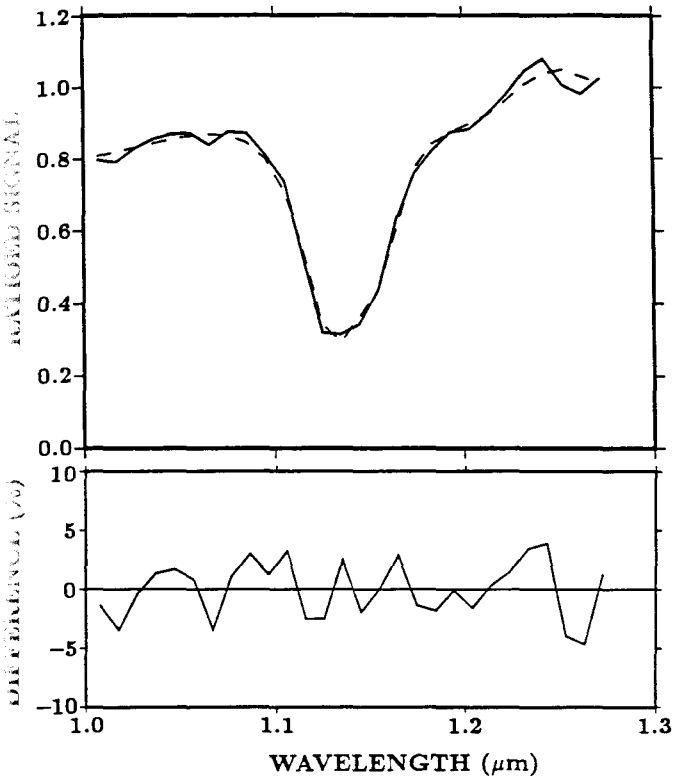

igure 4.—An example of curve fitting of spectra measured over a onvegetated surface. The top plot shows the observed spectrum olid) and the fitted spectrum (dashed). The bottom plot shows the ercent differences between the observed and fitted spectra (taken om Gao and Goetz, 1990).

uantity of water vapor, primarily because of altitude changes, cloud eight, and frontal activity (Gao and Goetz, 1991; Gao and others, in ress).

egetation

key contribution of imaging spectrometry to vegetation and ecol-gy studies is the quantification of vegetation biochemistry. Estima-on of biochemical constituents in vegetation, such as lignin, cellu-se, starch, sugar, and protein, by remote sensing methods is an nportant goal in ecological research. The spectral reflectances of ried leaves exhibit diagnostic absorption features that can be used to stimate the abundance of important constituents. Lignin and nitro-en concentrations have been obtained from canopies by the use of naging spectrometry and multiple linear regression techniques Wessman and others, 1988). The difficulty in identifying individual pectra of leaf constituents in the region beyond 1 μm is that liquid ater contained in the leaf dominates the spectral reflectance of eaves in this region. By means of spectral matching techniques, as iscussed above for determining atmospheric water vapor, we have een able to remove the liquid water contribution to the spectrum Goetz and others, 1990). The residual spectrum resembles spectra or cellulose in the 1.1 μm region, lignin in the 1.7 μm region, and ellulose plus starch in the 2.0–2.3 μm region (fig. 5). In the entire .0–2.3 μm region, each of the major constituents contributes to the pectrum. The quantitative estimates will require using unmixing echniques on the residual spectra.

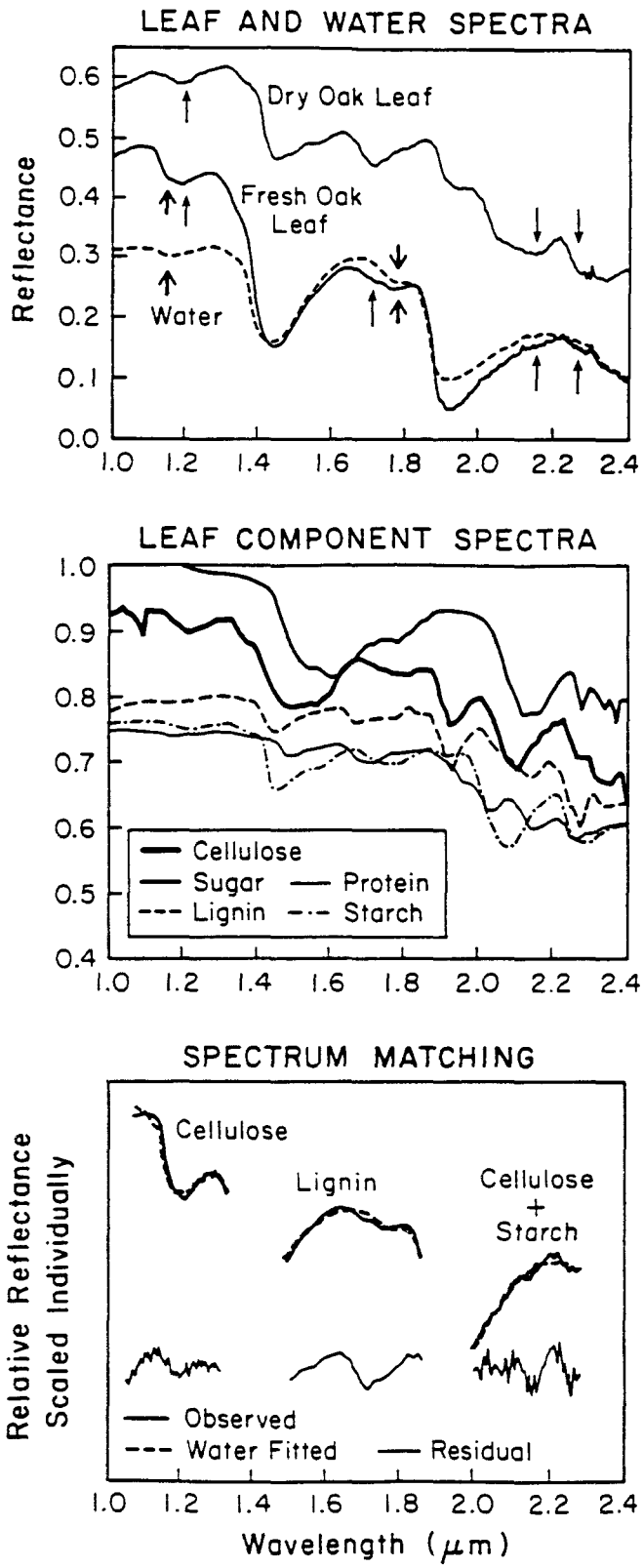

Figure 5.—Reflectance of dry and fresh oak leaves, spectra of leaf biochemical components, and water and residual spectra after water removal (taken from Goetz and others, 1990).

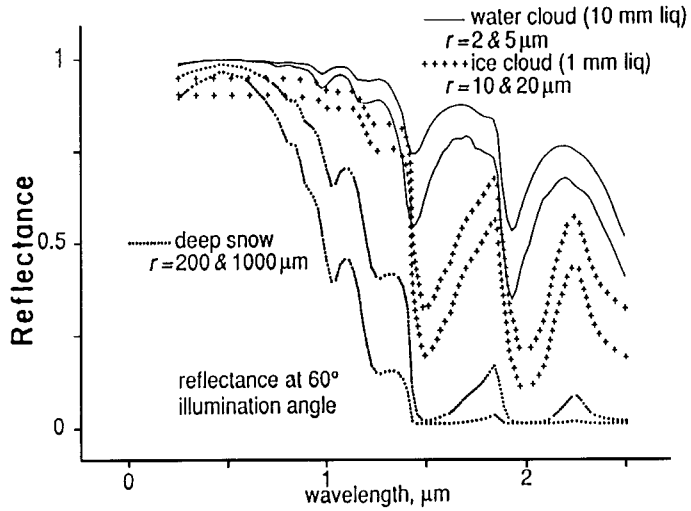

Figure 6.—Spectral signatures of snow, water clouds, and ice clouds. Increased absorption in the 1- to 2-μm range as grain size increases makes it possible to estimate the snow grain size and to separate snow from clouds. Abbreviations: r, reflectance; liq, liquid.

Snow and ice

The extent of snow and ice cover changes dramatically with the season, and as much as 30 percent of the Earth's surface is covered during the Northern Hemisphere's winter. Because snow is highly reflective in the visible and near-infrared region, this has a large effect on the Earth's albedo. Snow albedo depends on grain size, illumination angle, contaminants, and when the pack is thin, depth (Dozier, 1989). Grain size can be measured by using the full spectral resolution of HIRIS (fig. 6). In the near-infrared region, ice is moderately absorptive, and grain size has a large effect on albedo in the 1- to 1.3-μm range.

Contaminants increase absorption in the visible spectrum where snow is highly transparent. In fact, we may be able to identify the type of contaminant by its spectral signature in the visible region. Similarly in a thin snow pack, the spectral signature of the Earth beneath the snow will be observable in the visible region. Finally, the illumination angle is calculated from the solar zenith angle and the topography of the scene. Thus, HIRIS should be ideal for making detailed measurements of snow surface characteristics. A combination of these measurements and the large-scale measurements of MODIS should make it possible to track the energy balance of the snow pack through time.

A second reason for monitoring the snow pack is to estimate the snow melt for water supply and water chemistry properties. The water content is estimated from grain size, depth, and areal extent of the snow pack. The melt rate is estimated from these parameters and an estimate of the amount of energy absorbed by the snow pack. This can be calculated from the albedo measurements.

Image processing

The data sets produced by imaging spectrometry (fig. 7) are large and not easy to manipulate by using today's available software. Each 10×10-km AVIRIS image contains approximately 140 megabytes of data. However, new developments have made it possible to interact with AVIRIS data and to carry out analyses, such as those discussed above, on RISC work stations (F. Kruse, oral communication, 1991). The Spectral Image Processing System is now available from the University of Colorado, Boulder, Colorado, USA.

Summary

HIRIS is designed to acquire images in 192 spectral bands simultaneously throughout the solar-reflective part of the spectrum. It will provide the link between measurements of processes at the human scale and global monitoring by MODIS. HIRIS data are applicable to many disciplines in the earth sciences and will be particularly valuable in detecting change on land and in the bordering oceans.

Data analysis techniques include the powerful tools of spectrum matching, which so far have provided unique results in the determination of column atmospheric water vapor amounts at high spatial resolution, as well as in vegetation biochemistry. The data sets are large but rich in information.

Acknowledgments

The author wishes to thank Dave Norris of the Jet Propulsion Laboratory (JPL), HIRIS project manager during the design development phase, for his many ideas and innovations, including image motion compensation. Thanks also go to the many other JPL personnel, including Don Rockey, Deb Vane, Valerie Duval, Fred Vescelus, Terry Reilly, Mark Herring, and Teri Smith. At the University of Colorado, Bo-Cai Gao developed and applied the concepts of spectrum matching. Last but not least, the HIRIS science team members contributed to the wording for the justification in their various disciplines. The part of the research described in this article was carried out at the University of Colorado and was supported by contract number 958039 with the Jet Propulsion Laboratory and NAS5–30552 with the Goddard Space Flight Center, Greenbelt, Maryland, USA.

References

Abrams, M.J., Ashley, R.P., Rowan, L.C., Goetz, A.F.H., and Kahle, A.B., 1977, Mapping of hydrothermal alteration in the Cuprite mining district, Nevada, using aircraft scanner images for the spectral region 0.46 to 2.36 μm: Geology, v. 5, p. 713–718.

Collins, W., Chang, S.H., Raines, G., Canney, F., and Ashley, R., 1983, Airborne biogeophysical mapping of hidden mineral deposits: Economic Geology, v. 78, p. 737–749.

Dozier, J., 1989, Spectral signature of alpine snow cover from the Landsat Thematic Mapper: Remote Sensing of Environment, v. 28, p. 9–22.

Gao, B.C., and Goetz, A.F.H., 1990, Column atmospheric water vapor retrievals from airborne imaging spectrometer data: Journal of Geophysical Research, v. 95D, p. 3549–3564.

———1991, Cloud area determination from AVIRIS data using water vapor channels near 1 μm: Journal of Geophysical Research, v. 96D, p. 2857–2864.

Gao, B.C., Westwater, E.R., Stankov, B.B., Birkenheuer, D., and Goetz, A.F.H., in press, Comparison of column water vapor measurements using downward-looking optical and infrared imaging systems and upward-looking microwave radiometer: Journal of Applied Meteorology.

Goetz, A.F.H., 1987, The Portable Instant Display and Analysis Spectrometer (PIDAS), *in* Airborne Imaging Spectrometer Data Analysis Workshop, 3rd, Pasadena, California, USA, 1987, Proceedings: JPL Publication 87–30, p. 8–17.

Goetz, A.F.H., Billingsley, F.C., Elston, D., Lucchitta, I., Shoemaker, E.M., Abrams, M.J., Gillespie, A.R., and Squires, R.L., 1975, Application of ERTS images and image processing to regional geologic problems and geologic mapping in northern Arizona: JPL Technical Report TR–32–1597, 188 p.

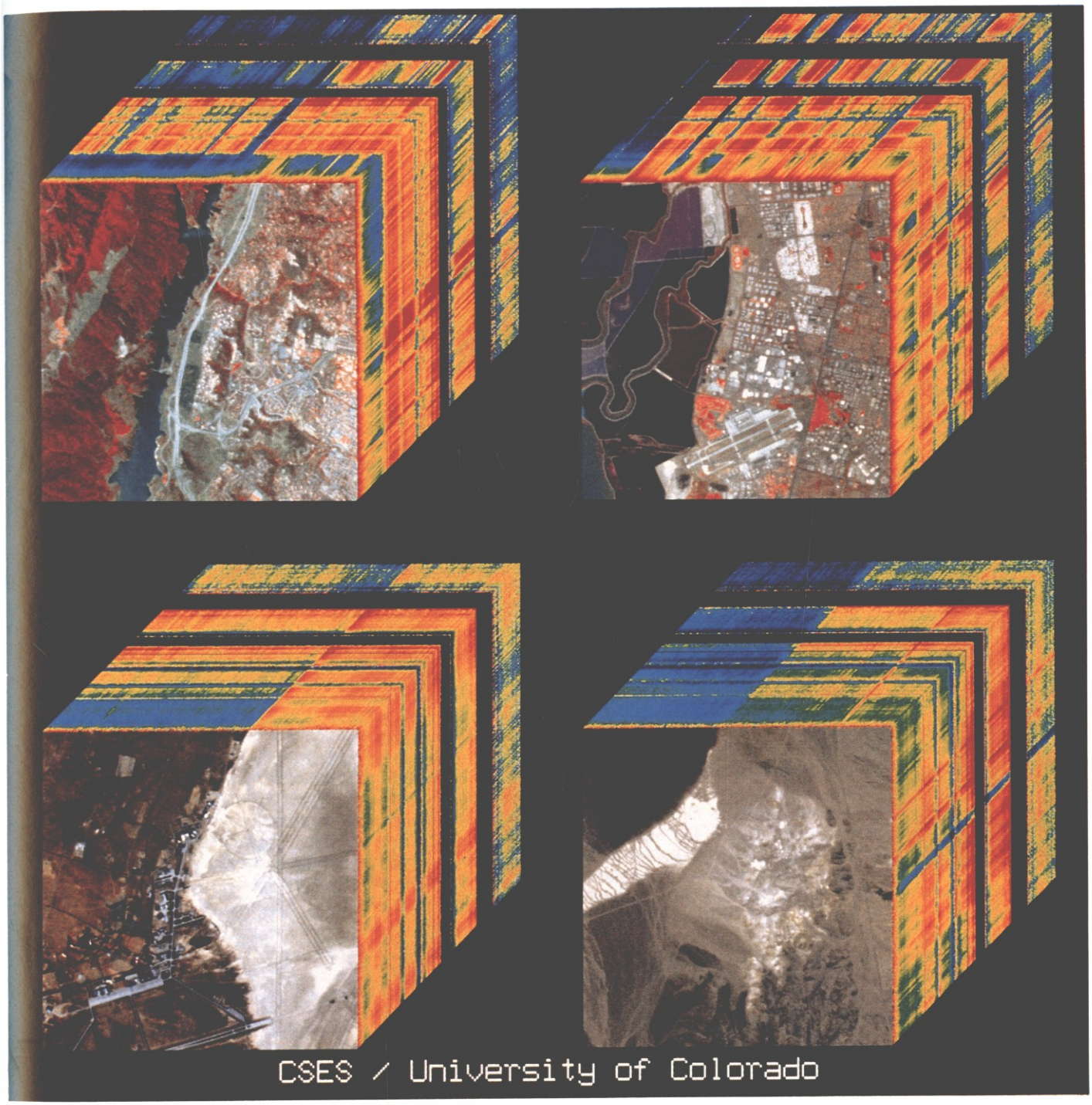

Figure 7.—AVIRIS image cubes. Each represents a stacked set of 224 spectral band images. The front face of the cube is a color infrared composite made from three spectral band images, and the sides of the cube represent the color-coded surface radiance of each of the edge pixels. The wavelength ranges from 0.4 μm at the front to 2.45 μm at the back. Red is high and blue is low, whereas the dark bands represent the atmospheric water vapor absorption bands at 1.4 and 1.9 μm.

Goetz, A.F.H., Gao, B.C., Wessman, C.A., and Bowman, W.D., 1990, Estimation of biochemical constituents from fresh, green leaves by spectrum matching techniques: International Geoscience and Remote Sensing Symposium, Remote Sensing Science for the Nineties (IGARSS '90), College Park, Maryland, USA, 1990, Proceedings, v. 2, p. 971–974.

Goetz, A.F.H., and others, 1991, HIRIS science requirements document: Pasadena, California, USA, Jet Propulsion Laboratory, JPL D–7843 (JPL internal document), 25 p.

Goetz, A.F.H., and Rowan, L.C., 1981, Geologic remote sensing: Science, v. 211, p. 781–791.

Goetz, A.F.H., Rowan, L.C., and Kingston, M.J., 1982, Mineral identification from orbit: Initial results from the Shuttle Multispectral Infrared Radiometer: Science, v. 218, p. 1020–1024.

Goetz, A.F.H., Vane, G., Solomon, J., and Rock, B.N., 1985, Imaging spectrometry for Earth remote sensing: Science, v. 228, p. 1147–1153.

Hunt, G.R., 1980, Electromagnetic radiation: The communication link in remote sensing, *in* Siegal, B.S., and Gillespie, A.R., eds., Remote sensing in geology: New York, John Wiley, p. 5–45.

Porter, W.M., and Enmark, H.T., 1988, System overview of the Airborne Visible/Infrared Imaging Spectrometer (AVIRIS), *in* Vane, Gregg, ed., Imaging Spectroscopy II, San Diego, California, USA, 1987: SPIE [Society of Photo-Optical Instrumentation Engineers] Proceedings, v. 834, p. 22–31.

Vane, G., and Goetz, A.F.H., 1988, Terrestrial imaging spectroscopy: Remote Sensing of Environment, v. 24, p. 1–29.

Wessman, C.A., Aber, J.D., Peterson, D.L., and Melillo, J.M., 1988, Remote sensing of canopy chemistry and nitrogen cycling in temperate forest ecosystems: Nature (London), v. 335, p. 154–156.□

Dr. Alexander F.H. Goetz *is a Professor of Geological Sciences and Director of the Center for the Study of Earth from Space (CSES) within the Cooperative Institute for Research in Environmental Sciences (CIRES). He received his degrees from the California Institute of Technology in the USA. Prior to joining the University of Colorado in 1985, he spent 15 years at the NASA Jet Propulsion Laboratory, where he was a Senior Research Scientist and Manager of the Imaging Spectrometer Program. Since 1989 he has been Team Leader for NASA's Earth Observing System (EOS), High Resolution Imaging Spectrometer (HIRIS) facility.*

by Vernon H. Singhroy

Radar geology: Techniques and results

Radar images are a valuable source of information for the study of global geoscience processes. Synthetic Aperture Radar data have been used increasingly in support of geological mapping and in studies related to the investigations of structural geology and geologic hazards.

Introduction

The decade of the 1990s is the decade for radar remote sensing. The European Space Agency (ESA) has recently launched a European Remote Sensing satellite (ERS–1) that will provide multilook C-band (5.66-cm) images. Other planned programs will be the Japanese Earth Resources Satellite (JERS–1) L-band system and the Canadian Radarsat multilook, high-resolution C-band system. In addition, several airborne radar systems, commercial and experimental, are available in Canada and the United States.

In preparation for Radarsat, the Canada Centre for Remote Sensing (CCRS) has flown over 50 geological test sites between 1987 and 1992. CCRS's main objective is to determine what geological information can be extracted from Synthetic Aperture Radar (SAR) images or from its combination with other data sets. The radar data were flown in support of (1) geological mapping in glaciated and vegetated terrain, (2) structural geology investigations that are searching for mineral deposits and hydrocarbon traps, and (3) studies of geologic hazards including seismic hazards. The results of the airborne SAR campaign are encouraging for a number of multidisciplinary geological programs (summarized in table 1) and have led to the increased use of radar imagery in recent years. This article discusses the techniques and results of radar imagery in order to evaluate the contribution of SAR images to the study of global geoscience processes.

Geological mapping

Several studies have shown that SAR imagery is useful for geological mapping. For example, in glaciated and vegetated Quaternary terrains having flat areas and exposed soil, Singhroy and others (1992) have shown that the tonal differences on springtime radar imagery can help to detect the variability of soil moisture, which corresponds to the distribution of surficial materials. However, in rough or undulating terrain, the slope has a stronger influence on radar backscatter than the soil moisture has. Further research needs to be done in order to understand the relationship between radar backscatter and the porosity, texture, and moisture content of the underlying surficial materials. The potential of springtime radar imagery in revising and aiding ongoing, detailed Quaternary and engineering geology mapping will be realized in the near future. Several radar image-enhancement techniques have been used to delineate surficial materials. In relatively flat terrain without vegetation, a simple stretched image and a 5×5 directional filter provide an effective tool for discriminating materials. In areas that have a mix of exposed soil, vegetation, and moderately rolling relief, combinations of the Landsat Thematic Mapper (TM) bands, particularly TM bands 3 and 5, and the stretched and filtered C-band radar image were useful. In areas where surficial materials are covered by natural vegetation (as in the case of most of northern Canada), the recommended technique for the delineation of surficial materials is to use a combination of the radar-landform and geobotanical relationships. More research needs to be conducted in order to understand fully these relationships and the influence of vegetation distribution on radar texture. However, where a close relationship exists between the distribution of surficial materials and the type and density of vegetation, a radar plus TM composite image provides a useful technique for Quaternary mapping.

Radar images also provide valuable information on landforms and terrain roughness. Because landforms provide clues to surficial materials, the radar images are, therefore, a useful and practical tool for Quaternary mapping. Kenny and others (1991) also have shown that enhanced springtime airborne SAR (C–HH and X–HH; HH, horizontally transmitted-horizontally received waves) combined with multispectral data are more suited to our interpreting landforms and surficial materials than are the existing 1:15,840-scale black and white aerial photographs. In other areas, Graham and Grant (1990) have interpreted C-band SAR prints having a 45° incidence angle for reconnaissance surficial mapping. They easily identified major new lineaments, fold pattern, morainal topography, hummocky and ribbed moraines, grained tills, and surface erratics.

SAR, TM, and other geologic data have been integrated in multidisciplinary geological mapping programs. Mussakowski and others (1991) have produced customized sets of enhanced multiple data that consisted of the integration of SAR, magnetic data, and geology. Bowie and others (in press) have digitally integrated digital terrain models (DTM), lithology, and SAR data to produce a composite image map that facilitated interpretation of the Sudbury impact structure in central Ontario, Canada. They used an intensity, hue, saturation (IHS) transform in the integration process that produced the composite image map.

Lowman (1991), in evaluating the geological value of orbital radar and airborne C-band SAR in the Canadian Shield area, has focused on the Sudbury impact structure. He has noted that topography and the bedrock geology expressed by topography are well displayed on the airborne SAR and that little azimuth biasing is evident compared to that in orbital radar. This appears to be the result of a combination of the higher resolution in range and azimuth of the airborne SAR and C-band wavelength, as well as the 45° incident angle, which is well suited for Canadian Shield terrain.

Structural investigations

SAR images have been used for structural geology investigations in support of mineral and hydrocarbon exploration. Image maps have been produced by the integration of SAR (C–HH), magnetic vertical gradient, and color and texture transforms (Rheault and others, 1991, and Harris, 1991). Figure 1 shows a C-band airborne SAR of the

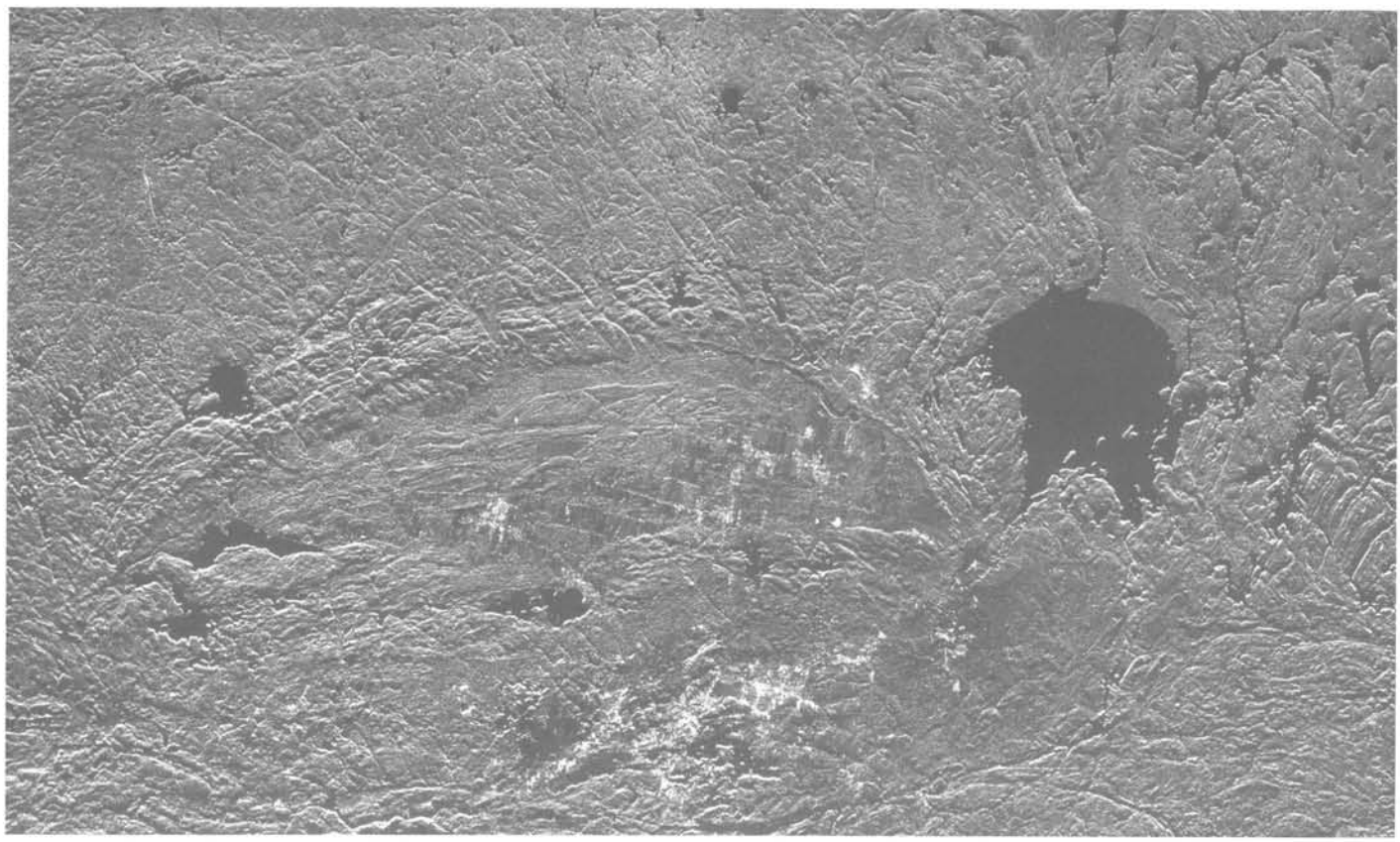

Figure 1.—Airborne radar image of the Sudbury structure in central Ontario, Canada, was recorded digitally by the use of the CCRS's C-band SAR operating in wide-swath mode. In this mode, the image represents a path about 60 km wide and has a resolution of 20 m in the crosstrack (range) direction and 10 m in the along-track (azimuth) direction. The image provides a good representation of the topography and can be used by a geologist to map faults and layering trends and to recognize folds within many rock units. The Sudbury structure is considered generally to be the largest meteorite-impact site on Earth, and the area is the world's largest producer of nickel-copper ores. In addition, the boundaries of three of the structural provinces that make up the Canadian Shield (Superior, Southern, and Grenville) intersect close to Sudbury, and each of these three structural provinces can be identified by differences in structural style. Because the image is stored in digital format, it can be manipulated on an image analysis system. Provided by Canada Centre for Remote Sensing.

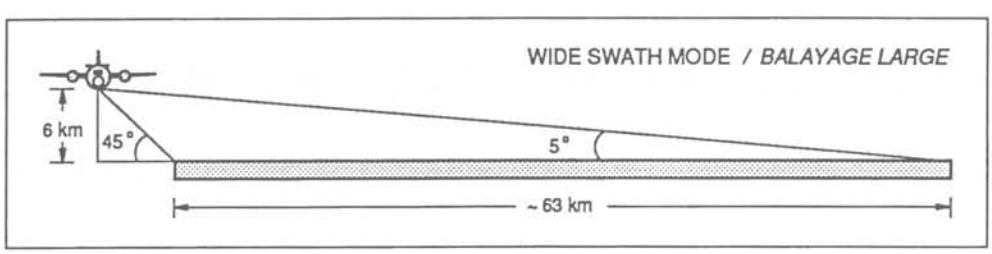

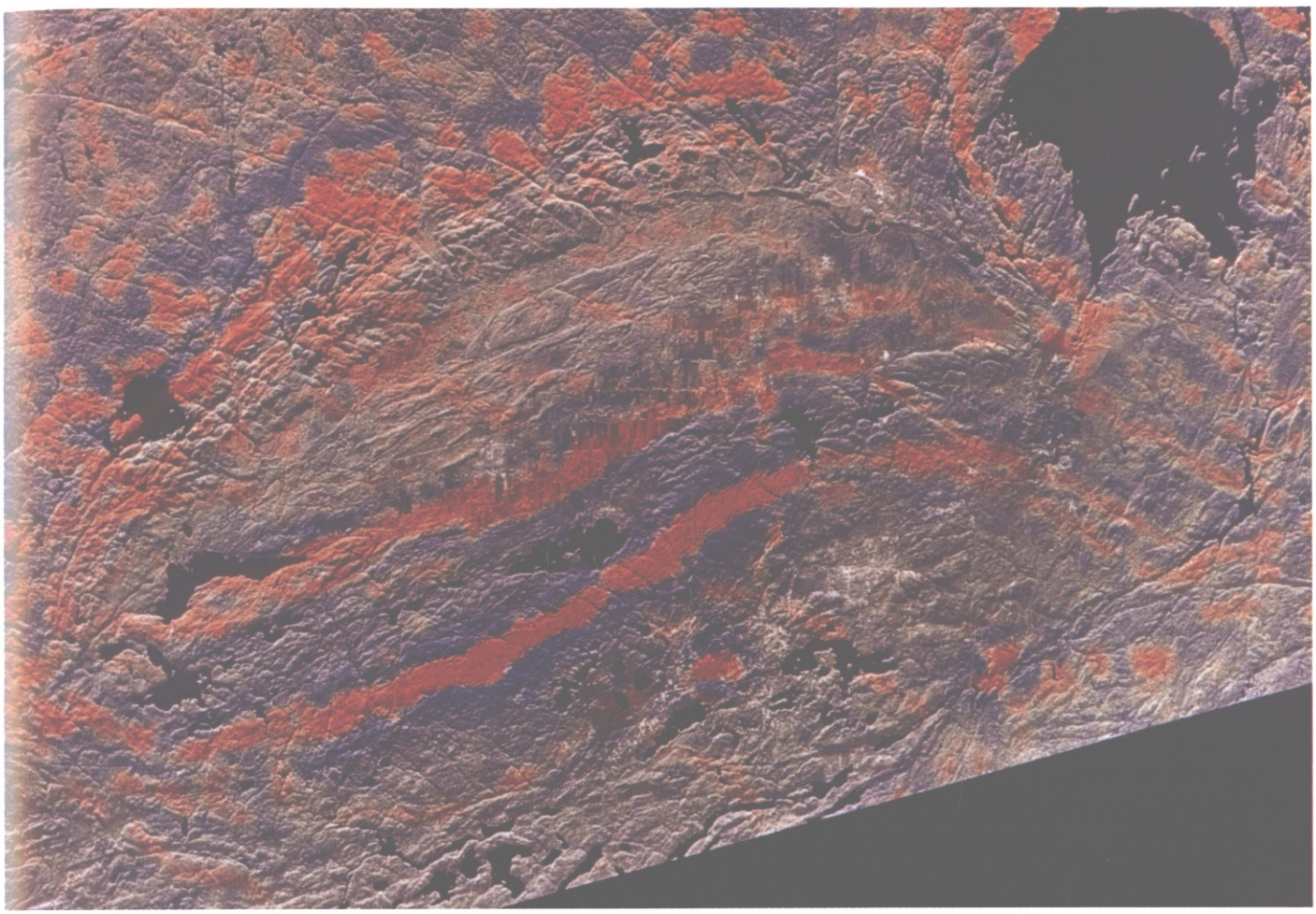

Figure 2.—An enhanced image of the Sudbury structure, Ontario, Canada. The image combines magnetic vertical gradient, C-band SAR, and TM band 4 by using an IHS color display transform. As a result, faults, dikes, and the Sudbury ring structure are clearly visible from this enhancement. Taken from Rheault and others (1991).

Sudbury basin, and figure 2 shows the same area enhanced by a combination of the SAR image, magnetic data, and a TM image. The enhancement included filtering, contrast stretching, and color transformation performed on each data set. To reduce the speckle in the SAR images, a 3×3 medium filter was used. A 9×9 high-pass filter and a 25×25 low-pass filter were convolved over the medium filter. This enhances the fracture systems. IHS color transformation was applied to the three stretched images (high-pass SAR, Landsat TM band 4, and magnetic vertical gradient) in order to produce the enhanced image shown in figure 2 (Rheault and others, 1991). Harris (1991) also found the combined IHS transform SAR and magnetic images to be a useful product for structural and lithologic mapping in support of gold-exploration programs in Nova Scotia.

Other techniques combining Seasat SAR and geophysical data have been used for structural interpretation in support of hydrocarbon exploration in the western sedimentary basin of Canada. A combination of SAR, TM, and magnetic vertical gradient data created an enhanced structural image that was used to produce lineament density maps (Misra and others, 1991).

Geologic hazards

Data integration techniques and the visual interpretation of SAR data are as important to geologic hazards studies as they are to geological mapping and exploration programs. McFall and Singhroy (1989) have combined SAR and TM images to create image maps that were used to delineate local fracture systems and "pop ups" for seismic hazard studies in southern Ontario. In other areas, Roy (1991) has used SAR mosaicked images to interpret geologic structures and types of motion associated with the Charlevoix seismic zone in Quebec. Also, Li and others (1989) have combined SAR and SPOT data to study regional tectonic activity that was associated with the Nahanni earthquakes of 1985 and 1988 in the Northwest Territories.

Table 1.—Summary of results of radar geology studies in Canada

[See text for explanation of acronyms]

Category and study (reference)	Objective	Techniques and results
Geological mapping		
Wawa, Ontario (Mussakowski and others, 1991).	To integrate remote sensing and geoscience data in support of multidisciplinary geological mapping program.	A coregistered digital geoscience and remote sensing data base was created.
		Customized set of enhanced multiple data products was used for visual interpretation (for example, composite of SAR, magnetic data, and geology).
		Integration process involved selective uses of bedrock and surficial geology, aeromagnetic data, Landsat TM, and airborne SAR.
		Relationships were established among vegetation, surficial material, lithology, and structure.
Sudbury, Ontario (Lowman, 1991).	To evaluate simulated orbital SAR for geological mapping.	Visual interpretation of wide-swath image (60 km) to determine size and ellipticity of Sudbury structure.
	To interpret shape of Sudbury structure.	Narrow-swath image (18 km) was useful in mapping detailed structures and unmapped basaltic dikes.
Sudbury, Ontario (Bowie and others, 1992).	To integrate digitally DTM, geological map of Sudbury region, SAR wide swath, and geology derived from SAR.	Image map of 1:250,000-scale lithology and wide-swath SAR was produced as a standard product for regional geological mapping.
		IHS transform was used for data integration.
Cape Breton Island, Nova Scotia (Prince and Akhavi, 1990).	To correlate and integrate airborne SAR, Landsat TM, DTM, geological, and geophysical data sets.	Two look directions were necessary to map multidirection lineaments, which facilitated structural interpretation of sedimentary basin in southwestern Cape Breton Island.
		SAR and DTM show poor correlation with lithology and geophysical units.
Bathhurst Inlet, Northwest Territories (He and Wang, 1990).	To use textural analysis for automatic identification of lithologic units from airborne SAR images.	Textural measures of SAR data produced enhanced images that assisted in lithologic discrimination and in planning of geological mapping survey.
Sudbury and southern Ontario (Singhroy and others, 1992).	To use airborne SAR images for Quaternary mapping of several different glaciated terrains in Ontario and Manitoba.	In flat areas, variability in soil moisture interpreted from springtime SAR corresponds to different textures (grain size) of glacial sediments and thereby aided in surficial mapping.
		A 5×5 filter and stretched springtime SAR combined with TM bands 3 and 5 produced an image that enabled the delineation of glacial materials and landforms.
		In Boreal forest areas (for example, northern Manitoba), a TM and SAR composite image provided both textural and spectral data that facilitated the mapping of engineering-terrain units.
Port Stanley, Ontario (Kenny and others, 1991).	To update Quaternary mapping from airborne SAR and multispectral data.	Images produced from springtime airborne SAR (C–HH and X–HH) and multispectral data are more suited for interpretation of .landforms and surficial materials than are existing black and white 1:15,840-scale aerial photographs. The composites produced are the result of principal components 1 and 3 (blue and red) of the airborne SAR and multispectral data and a stretched band 7 of the multispectral image.
Nelson front, Manitoba (Rao and others, 1989).	To develop integrated remote sensing technique for mapping low-relief structures across the Nelson front.	C-band SAR combined with TM was interpreted to provide information on deformational patterns in low-relief Precambrian terrains. The glacial overburden cover was reduced by using a simple geographic information system and Bayesian statistical integration.
Central Newfoundland (Graham and Grant, 1990).	To show the applicability of SAR as a geological reconnaissance tool.	Visual interpretation of wide-swath C-band SAR. The large depression angle in the far range enhanced small relief features and surface textures. Major new lineaments, fold pattern, and foliation were mapped. Morainal topography, hummocky and ribbed moraines, coarsely textured tills, and surface erratics were identified easily.
Mineral exploration		
Sudbury Basin, Ontario (Rheault and others, 1991).	To develop techniques for combining SAR and geophysical data in support of mineral exploration in the nickel-copper Sudbury mining district.	An image was produced from airborne SAR (C–HH) and magnetic vertical gradient by the use of color and texture IHS transform to map dikes and faults.
		An image was produced from a 9×9 high-pass SAR and was combined with TM band 4 in a color and texture transform to map faults.

Table 1.—Summary of results of radar geology studies in Canada—Continued

[See text for explanation of acronyms]

Category and study (reference)	Objective	Techniques and results
Mineral exploration—Continued		
Eastern Nova Scotia (Harris, 1991).	To produce a map of geologic structure based on photogeologic and computer-assisted analysis of remotely sensed data and a limited field program. To evaluate the interpreted structural map with respect to regional tectonic framework and known gold occurrences.	Enhanced SAR and magnetic data were useful in mapping regional structure. IHS transform radar and geophysical images provided a useful visual product for structural and lithological mapping. East-west- and northwest-southeast-trending faults were interpreted from the remotely sensed data and from geological maps and then were correlated with gold occurrences.
Hydrocarbon exploration		
Peace River district, Alberta, Canada (Rheault and others, 1991).	To develop techniques for combining SAR and geophysical data in support of hydrocarbon exploration in the Peace River district.	Color composite image of combined SAR and TM bands 3, 5, and 4 (BGR, blue, green, red) was produced to map tonal anomalies and faults.
Western sedimentary basin, Canada (Misra and others, 1991).	To use SAR and TM data to map lineaments for the entire sedimentary basin. To integrate satellite lineaments and magnetic, geological, and oil and gas well data to search for additional hydrocarbon traps.	Seasat SAR and TM images reflect basement faulting beneath 1,000 m of glacial and Paleozoic sediments. The faults influence the sedimentation patterns, differential compaction of sediments, location of carbonate reefs, and dolomitization processes. Lineament density maps show good correlation with oil and gas fields and were used to search for new traps. Northeast and northwest sets of lineaments transect the entire western sedimentary basin.
Geologic hazards		
Prince Edward County, Ontario (McFall and Singhroy, 1989).	To use airborne SAR, TM, and springtime infrared photographs for mapping neotectonic features and their drift cover in flat terrain.	TM bands 4, 5, and 7 composite and springtime SAR image provided enhancement for locating local fracture systems and large "pop ups." However, because of very flat terrain, large-scale infrared photographs were more useful for mapping fracture systems and small "pop ups."
Seismic hazard in Charlevoix impact structure, Quebec (Roy, 1991).	To map from airborne SAR intersecting faults in the Charlevoix seismic zone.	SAR digital mosaicked images were interpreted to produce a structural model of the Charlevoix seismic zone. North-south lineaments further north along the Saguenay River, lineaments parallel to the Saguenay graben and St. Lawrence River, and fine intersecting lineaments in the area were significant in terms of types of motion.
Nahanni earthquakes, Northwest Territories (Li and others, 1989).	To use C-band SAR and SPOT for studying regional tectonic activity associated with Nahanni earthquakes of 1985 and 1988.	Integrated C-band SAR, SPOT, and earthquake epicenter data were used to map fracture systems associated with the Nahanni earthquakes. Low scan angle of wide swath (60 km). C-band SAR enhanced lineaments and different sun angle of SPOT complemented shadow areas of SAR data.

Conclusion

The summary of techniques and results in table 1 and the above descriptions demonstrate the potential of SAR in multidisciplinary geological investigations. Although these early results are encouraging, more techniques need to be developed for different areas, particularly in arid and tropical terrains. It is evident, however, that SAR data will be a valuable source of information in the study of global geoscience processes.

References

Bowie, C., Huppe P., and Glynn, J.E., in press, Experiment in combining geology maps with terrain relief data, *in* GIS 92, Surveys, Mapping and Remote Sensing Sector, Ottawa, Ontario, Canada, 1992: Canada Department of Energy, Mines and Resources.

Graham, D.F., and Grant, D.R., 1990, A test of airborne side-looking Synthetic Aperture Radar in central Newfoundland for geological reconnaissance: Canadian Journal of Earth Sciences, v. 28, p. 257–265.

Harris, J.R., 1991, Mapping of regional structure of eastern Nova Scotia using remotely sensed imagery: Implications for regional tectonics and

gold exploration: Canadian Journal of Remote Sensing, v. 17, no. 2, p. 122–136.

He, Doug-Chen, and Wang, Li, 1990, Recognition of lithologic units in airborne SAR images using new texture features: International Journal of Remote Sensing, v. 11, no. 12, p. 2337–2344.

Kenny, F.M., Singhroy, V.H., and Barnett, P., 1991, Application of airborne multispectral and SAR images for Quaternary mapping, *in* Thematic Conference on Geologic Remote Sensing, 8th, Denver, Colorado, USA, 1991, Proceedings: Ann Arbor, Michigan, USA, Environmental Research Institute of Michigan, p. 1449–1461.

Li, B., Moon, W.M., Won, J.S., Lamontagne, M., Slaney, V.R., and Graham, D., 1989, Application of satellite remote sensing technique in the geological investigation of Nahanni earthquake area, *in* Thematic Conference on Remote Sensing for Exploration Geology, 7th, Calgary, Alberta, Canada, 1989, Proceedings: Ann Arbor, Michigan, USA, Environmental Research Institute of Michigan, p. 615–626.

Lowman, P.D., 1991, Original shape of the Sudbury structure, Canada: A study with airborne imaging radar: Canadian Journal of Remote Sensing, v. 17, no. 2, p. 152–161.

McFall, G., and Singhroy, V.H., 1989, Remote sensing applications to neotectonics studies in southern Ontario, *in* Thematic Conference on Remote Sensing for Exploration Geology, 7th, Calgary, Alberta, Canada, 1989, Proceedings: Ann Arbor, Michigan, USA, Environmental Research Institute of Michigan, p. 533–546.

Misra, K.S., Slaney, V.R., Graham, D., and Harris, J., 1991, Mapping of basement and other tectonic features using Seasat and Thematic Mapper in hydrocarbon-producing areas of the western sedimentary basin of Canada: Canadian Journal of Remote Sensing, v. 17, no. 2, p. 137–151.

Mussakowski R., Trowell, N.F., and Heather, K.B., 1991, Digital integration of remote sensing and geoscience data for the Goudreau-Lochalsh area, Wawa, Ontario: Canadian Journal of Remote Sensing, v. 17, no. 2, p. 162–173.

Prince, J.D., and Akhavi, M.S., 1990, Integration of C-band imagery with TM, geophysical and geological data, Cape Breton Island: Program summaries: Nova Scotia Department of Mines and Energy Report no. 90–3, p. 44.

Rao, G.S.K., Won, J.S., Moon, W.M., Slaney, V.R., Graham, D.F., and Lowman, P.D., 1989, Integrated imaging experiment with C–SAR and other geological image data across the Nelson front, northern Manitoba, *in* Thematic Conference on Remote Sensing for Exploration Geology, 7th, Calgary, Alberta, Canada, 1989, Proceedings: Ann Arbor, Michigan, USA, Environmental Research Institute of Michigan, p. 579–590.

Rheault, M., Simard, R., Garneau, C., and Slaney, V.R., 1991, SAR Landsat TM-geophysical data integration utility of value-added products in geological exploration: Canadian Journal of Remote Sensing, v. 17, no. 2, p. 185–190.

Roy, D., 1991, Intersecting faults at the NE tip of Jacques Cartier horst, *in* Multi-Agency Group for Neotectonics in Eastern Canada Annual Meeting, Ottawa, Ontario, Canada, 1991, Summary of MAGNEC annual meeting: Atomic Energy Control Board, AECB Open-File 34–5–4–0, p. 18–20.

Singhroy, V.H., Kenny, F.M., and Barnett, P.J., 1992, Radar imagery for Quaternary geological mapping in glaciated terrains: Canadian Journal of Remote Sensing, v. 18, no. 2, p. 117–123.□

Dr. V.H. Singhroy *is Chairman of the Advisory Board on Remote Sensing of the International Union of Geological Sciences, Research Scientist in geological remote sensing, and Scientific Advisor at the Canada Centre for Remote Sensing in Ottawa, Ontario, Canada.*

by Diane L. Evans

Geologic process studies using Synthetic Aperture Radar (SAR) data

Numerical models of climatic processes offer the promise of simulating future global trends; however, it is crucial for us to understand how changes in climate are manifested locally before we can evaluate the true impact of climate change. Thus, increased awareness and concern about global climate change have led to an equal interest in remote sensing as a tool for mapping and monitoring changes in the land surface and cover.

Geologic processes, such as soil erosion, transportation, deposition, and degradation, affect not only the amount of arable land available for cultivation but also have an impact on sedimentation in estuaries, deltas, and other coastal environments. Additional geologic processes, such as tectonism and volcanism, have a profound impact on human life as well. These additional processes become modulators of global climate not only through destructive seismic activity but also through the influence of volcanoes on the chemistry of the oceans and atmosphere and through eruptions of gases and particulates into the stratosphere.

Synthetic Aperture Radar plays an important role in landform mapping and structural interpretation because viewing geometries can be optimized for different terrain types in a way similar to that used for low sun-angle aerial photography. In addition, radar data are important for geologic process studies because unique quantitative information about surface roughness, vegetation extent, soil moisture, topography, and topographic change can be extracted from calibrated data sets.

Introduction

The image brightness of Synthetic Aperture Radar (SAR) is related to radar backscatter at the pixel level, and it is a function of slope, surface roughness, dielectric constant, and subsurface discontinuities. Therefore, it provides intrinsic physical information about surfaces and volumes that complement measurements made by sensors operating in the visible, shortwave infrared, and thermal infrared parts of the electromagnetic spectrum.

Radar sensors provide their own illumination and, as a result, can provide reliable multitemporal data that are independent of weather or sun illumination through all seasons and at all latitudes. Radar waves penetrate through clouds and, under certain conditions, through vegetation canopies and thin veneers of alluvial overburden, which makes it possible to explore regions of the Earth's surface that are not accessible by the use of other remote sensing techniques.

Geologic processes that are particularly amenable to studies employing SAR data include volcanism; soil erosion, degradation, and redistribution; coastal erosion and inundation; glacier fluctuations; permafrost; and crustal motions. Such process studies are critical not only to our understanding of recent tectonic activity and climate change but also to the mitigation of geologic hazards and to exploration for nonrenewable resources.

Sensors flying now, as well as those planned for flight in the 1990s, provide an opportunity to develop models and test methods for large-scale mapping, geophysical processing, and the generation of high-resolution digital elevation models that will make it possible to use SAR data routinely for global process studies. Data acquired from airborne sensors such as the Airborne Imaging Radar (AIR-SAR), which was developed by the National Aeronautics and Space Administration's Jet Propulsion Laboratory (JPL), are being used for investigations that focus on fairly small test sites (figs. 1–3). Data from the Shuttle Imaging Radars (SIR–C and X–SAR), scheduled for flights in 1993, 1994, and 1996, will expand these studies to regional scales; and the Earth Observing System (EOS) SAR, planned later in the decade, will provide both global coverage and a monitoring capability.

When data from these systems are combined with data from other planned spaceborne sensors, such as the European Space Agency's (ESA) European Remote Sensing satellites (ERS–1 and ERS–2), the Japanese Earth Resources Satellite (JERS–1), and the Canadian Radarsat, it will be possible to build a time-series view of temporal changes over many regions of the Earth. Operating parameters for these SAR systems are given in table 1. Key geophysical products that will be derived in support of geologic process studies from the resulting data are given in table 2. The status of our current capability to generate these geophysical products is described below.

Landform mapping

Exploitation of radar data for geological studies has advanced most in the area of landform mapping. Several studies have shown the value of SAR images for mapping structures in volcanic and sedimentary terranes (Greeley and Martel, 1988; Campbell and others, 1989; Gaddis and others, 1989; Sabins, 1983; Wadge and Dixon, 1984; Lynne and Taylor, 1986) and for studying the processes of erosion, weathering, and deposition (see Blom and Daily, 1982; Evans, 1988; Arvidson and others, in press).

Images from the Shuttle Imaging Radars (SIR–A and SIR–B) of the eastern Sahara in northern Africa revealed the capability of spaceborne radars' providing insight into the geologic record that is

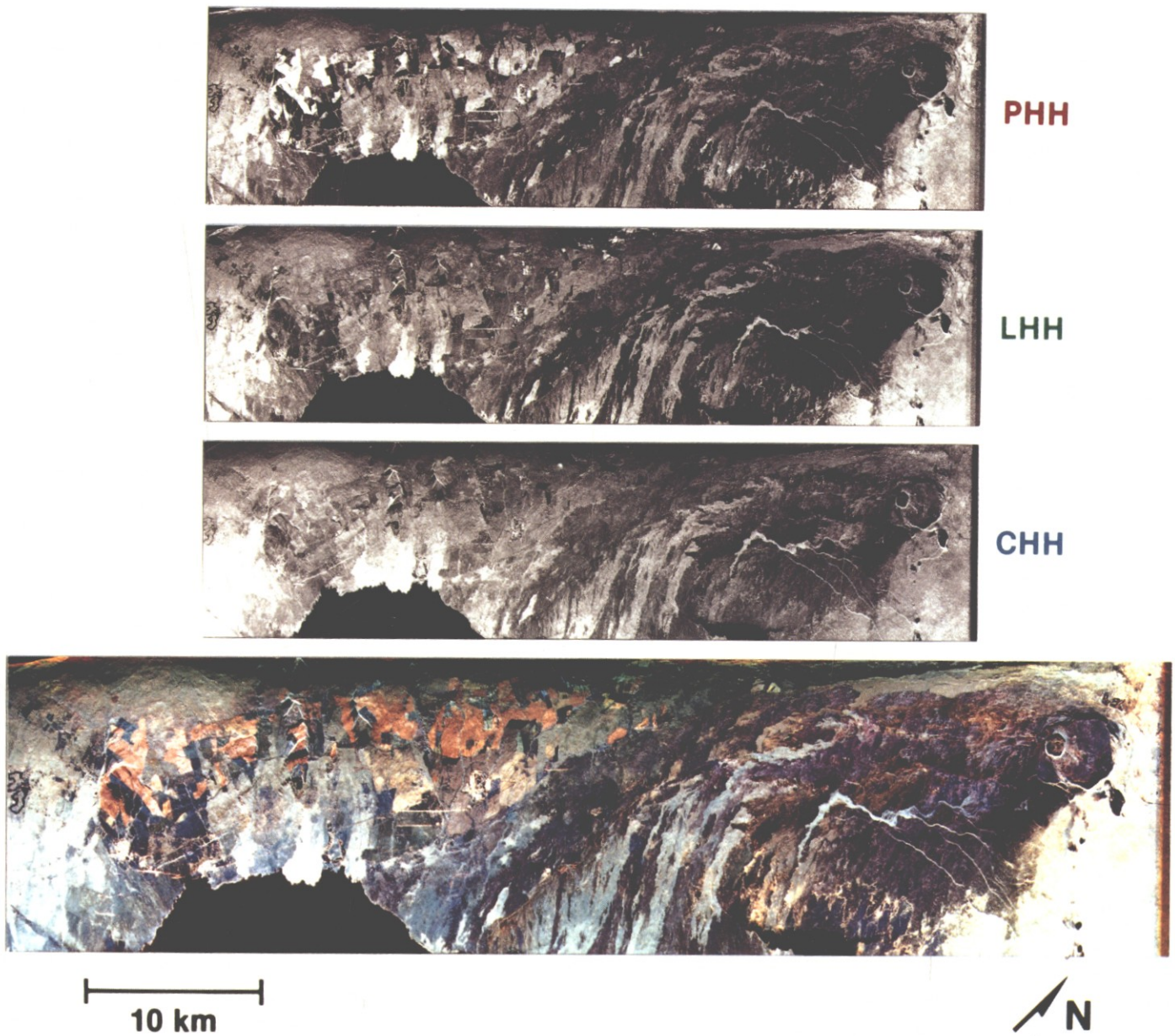

Figure 1.—Multifrequency AIRSAR images of Kilauea Crater, Hawaii, USA, showing lava flows of varying ages and surface roughness. Images such as these will be used to support the Earth Observing System's (EOS) volcanology investigation (for example, see Mouginis-Mark and others, 1991). See table 1 for explanation of abbreviations.

buried beneath thin deposits of windblown sand and is masked from sensors that operate in the visible part of the spectrum (McCauley and others, 1982; McCauley and others, 1986; Schaber and others, 1986). Subsequent reexamination of data acquired in 1978 from the Seasat satellite and in 1988 from AIRSAR showed that significant penetration also occurred in the Mojave Desert of southern California, USA, which indicates that subsurface features of potential tectonic significance may be revealed in radar images of semiarid terranes (Blom and others, 1984) (fig. 4).

Several techniques have been developed that may result in automated landform mapping. For example, a technique that can be used to map textural variations was described by Blom and Daily (1982) and was used by Stromberg and Farr (1986). The technique involves the production of images that represent only certain scales of texture. This is accomplished first by filtering the Fourier transform of an area into several spatial frequency bands and then by producing an image for each of these bands. These bandpass images are used next in a standard, unsupervised classification algorithm in order to produce a map, the units of which represent unique textural signatures. One also could use images in which pixels represent local variance, or other statistical quantities, in different sized boxes in the classification algorithm. These techniques not only discriminate units that are based on texture, but they produce a spatial frequency signature for the units as well. These signatures allow the comparison

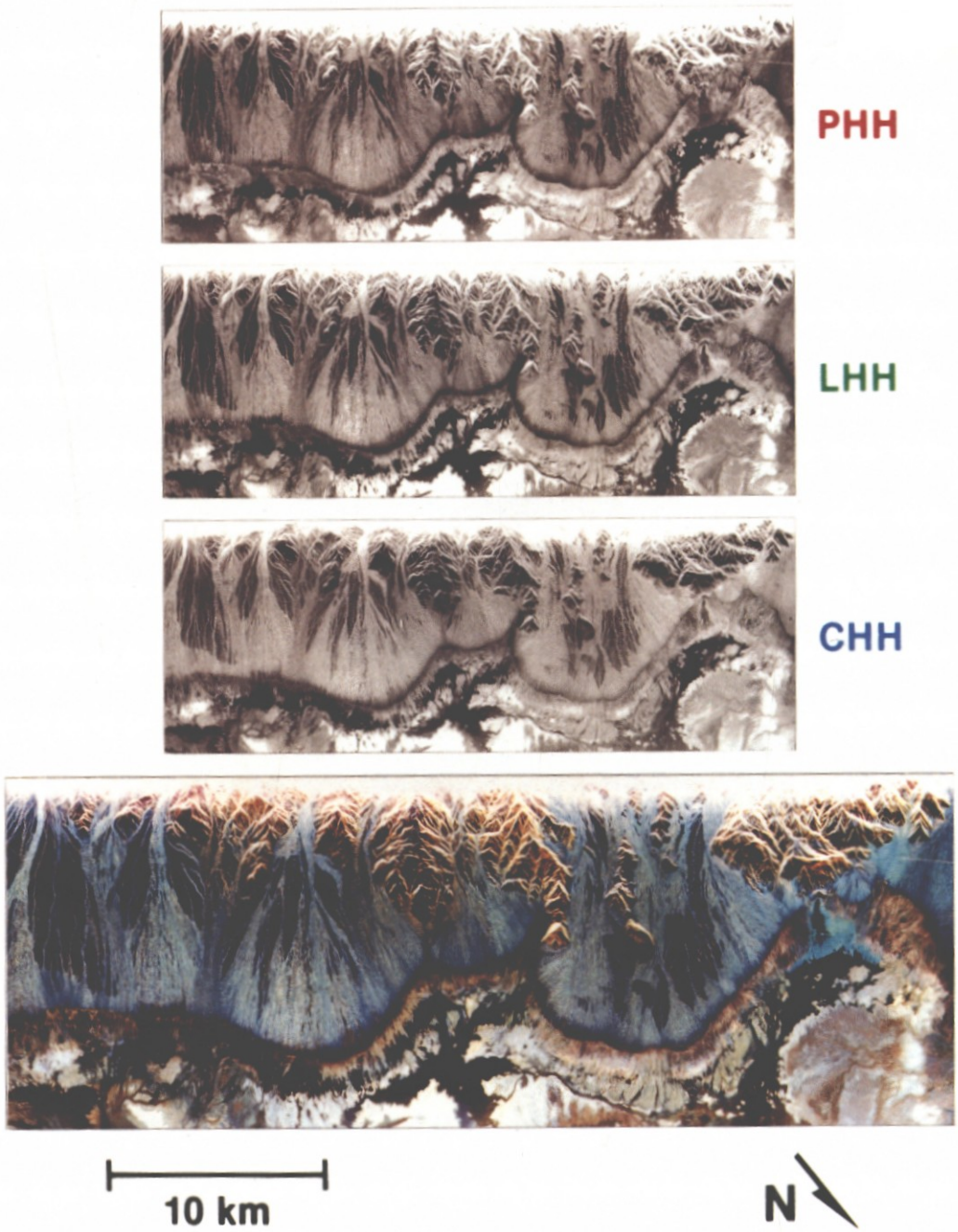

Figure 2.—Multifrequency AIRSAR images of Death Valley, California, USA, showing alluvial fan units of varying ages and surface roughness. Such images will be used to determine the relative ages of geomorphic surfaces, information that is required for studies of modern erosion rates, past climate fluctuations, and dating of young faults.

of units between maps and may allow the identification of rock types if adequate knowledge exists about the climate, tectonic history, and response of different rock types to these factors.

Surface roughness

Weathering and depositional processes generally cause surfaces to smooth as they age, whereas erosional processes can cause a roughening of surfaces. The scales of these processes are different, and their rates vary as a result of climate, rock type, and geologic structure. However, their effects can be used to date surfaces relatively for studies of climatic change and tectonic history. In cases where numerical ages exist, average process rates over time also may be derived.

Microtopography or surface roughness is the link between weathering and depositional processes and radar remote sensing data.

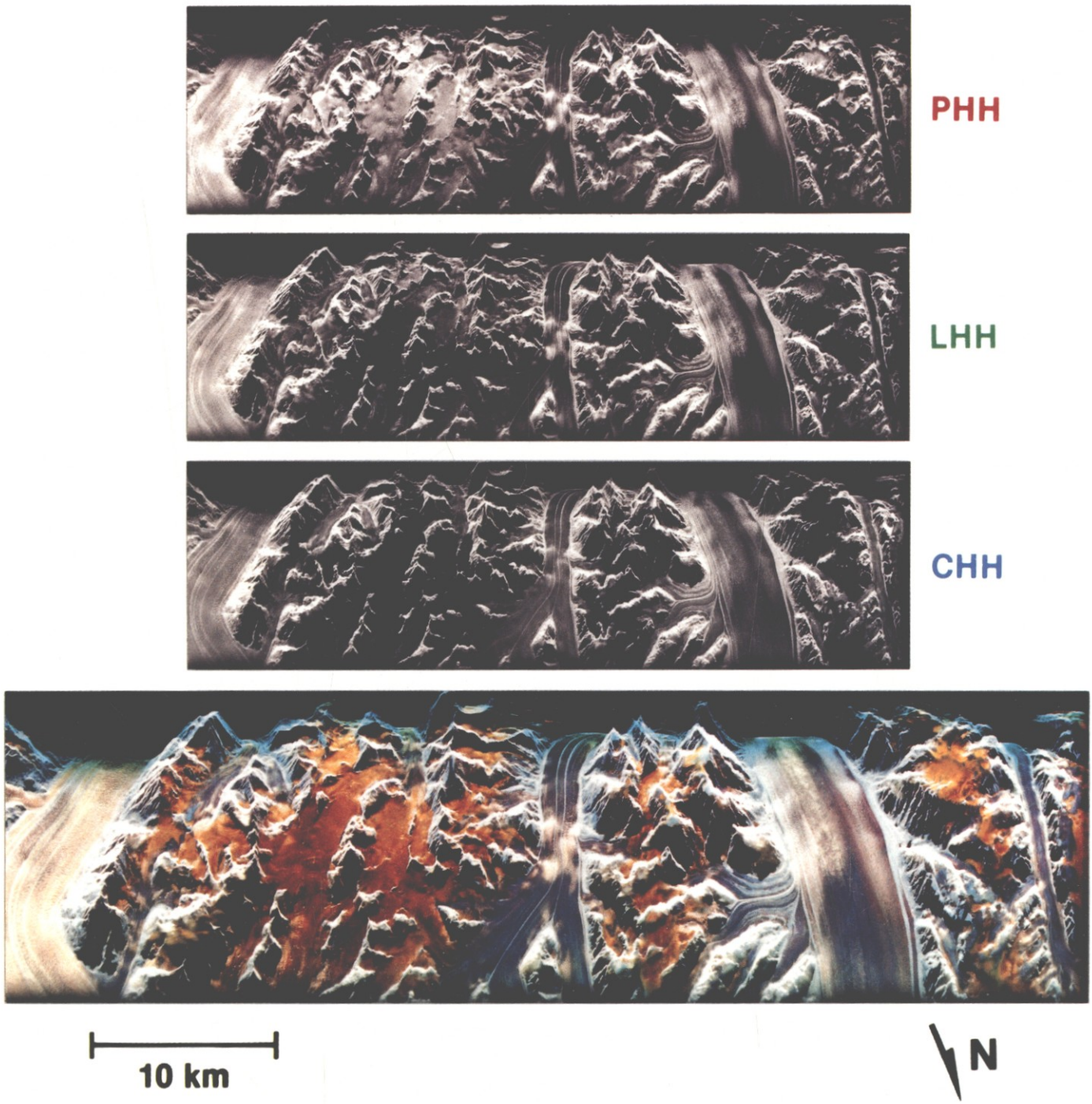

Figure 3.—Multifrequency AIRSAR images of glaciers near the southwest coast of Greenland showing variations in both surface and subsurface structure. Images such as these will be used in order to study changes in glacier mass balance (see Rott, 1990; Jezek and others, 1991).

Work by van Zyl and others (1991) showed that surface microtopography could be inferred from multifrequency SAR data by the inversion of a radar backscatter model. In that study, physical properties were measured at three different 10 m by 10 m sites representing surfaces that had root mean square (rms) heights varying from less than 1 cm to tens of centimeters. Ground measurements included soil moisture content, dielectric constant, and microtopographic profiles. The profiles were generated from helicopter photography using twin metric framing cameras that was reduced later to profiles covering 10–30 m at 1-cm spacing, which allowed the estimation of the power spectrum, rms height, and correlation length of the surfaces (Wall and others, 1991). AIRSAR data acquired at three different incidence

Table 1.—Operating parameters of examples of current and future SAR systems

[Abbreviation: N/A, not applicable]

	AIRSAR	ERS-1	SIR-C/X-SAR	JERS-1	RADARSAT	EOS SAR
Spectral coverage[1]	P,L,C	C	L,C,X	L	C	L,C,X
Polarization[2]	Quad	VV	Quad (C,L) VV (X)	HH	HH	Quad (L) Dual (C,X)
Look angle (degrees)	15–60	23	15–60	35	20–50	15–40
Resolution (m)	10	30	25	30	10–100	20–250
Swath coverage (km)	12	100	10–150	80	50, 500	30–500
Orbit altitude (km)	10	800	215	568	792	620
Orbit inclination (degrees)	N/A	98	57	98	98.6	98
Launch date	N/A	1991	1993 1994 1996	1992	1994	1999

[1] X-band wavelength is ~3 cm
C-band wavelength is ~5.6 cm
L-band wavelength is ~ 24 cm
P-band wavelength is ~68 cm

[2] HH, horizontally transmitted, horizontally received wave
VV, vertically transmitted, vertically received wave
Quad = amplitude and phase of returned wave are both recorded so that any combination of transmit and receive polarization can be synthesized through ground processing

Table 2.—Examples of solid Earth products that are required from EOS SAR data

[Abbreviation: res, resolution, —, not applicable]

Products	Units	Accuracy	Horizontal res	Temporal res
Geologic feature distribution	m	30	30 m	3 months, once
Surface roughness, high res	cm	5–10%	30 m	1 year, once
Surface roughness, low res	cm	10	25 km	1–2 weeks
Vegetation extent, high res	—	10%	30 m	1 season, 1 year
Land topography, high res	m	5–10, vertical	30 m	Once
Topographic change	cm	10, vertical	30 m	After event
Soil moisture	—	10–25	60–100 m	1 week

angles and three wavelengths over the test site were calibrated by using trihedral corner reflectors that were deployed in the area prior to obtaining the images in order to provide radar backscatter values (σ^0) for each resolution element in the scenes (van Zyl, 1990). The radar backscatter model was used next in order to infer the power spectra of surface microtopography for the three surfaces, and the power spectra were compared to the field measurements. The result was that van Zyl and others (1991) found a close match between the estimated and measured surface microtopography.

Evans and others (in press) extended this work to the Cima volcanic field in California and the Lunar volcanic field in Nevada, USA. They not only found a close match between the estimated and measured surface microtopography, but they also confirmed work by Farr (in press) that showed that surface roughness changes can be correlated with age.

In order to determine the areas of an image for which the radar backscatter model is valid, van Zyl (1989) described an unsupervised classification technique that provides a means to segment images into classes displaying different types of scattering. The algorithm classifies scatterers into one of three types on the basis of the polarization characteristics of the transmitted and received waves. The three scattering classes are single reflection, double bounce, and diffuse scattering. For single reflection from a slightly rough dielectric surface, the incident wave will experience little multiple scatter. A dihedral reflection exhibits a double-bounce geometry and results in a 180-degree phase shift between horizontally transmitted-horizontally received (HH) waves and vertically transmitted-vertically received (VV) waves. For diffuse scattering, highly varying phase differences of HH to VV exhibit a noiselike character. The orientation angle of the average scattered wave tracks that of the transmitted wave, a behavior that is similar to the behavior observed for the single-reflection case. However, the sense of rotation of the scattered wave is the same as that of the transmitted wave polarization, which is more consistent with a double-bounce mechanism. Papers by van Zyl (1989) and Evans and others (1988) noted that this behavior is generated by a class of "three-layer" vegetation models, such as the one discussed in van Zyl (1985), Richards and others (1987), and Durden and others (1989). The classification technique was used by Evans and others (1988) in order to map clearcut areas in a Maine, USA, forest that were not discernable in L-band HH and VV images. Evans and van Zyl (1990) also used this technique for differentiating areas that had been burned recently near Mt. Shasta in California, USA, as did Evans and others (1988) and Evans and Smith (1991) for differentiating areas having less than 10 percent vegetation cover in a semiarid region in Wyoming, USA. Figure 5 shows these two examples and a classification map for the area around Kilauea Crater, Hawaii, USA. In each of these examples, the radar backscatter model is valid for roughness scales on the order of one-half the radar wavelength for areas that are classified as single reflections for all three frequencies.

Soil moisture

Soil moisture is a hydrologic storage variable, as well as an indicator of moisture fluxes, and is, therefore, a critical parameter for many earth science investigations. SAR images have been applied successfully to map saturated soils in temperate regions (Waite and others, 1981; Krohn and others, 1983; Ormsby and others, 1985; Evans and others, 1986; Imhoff and others, 1986, 1987). This success largely

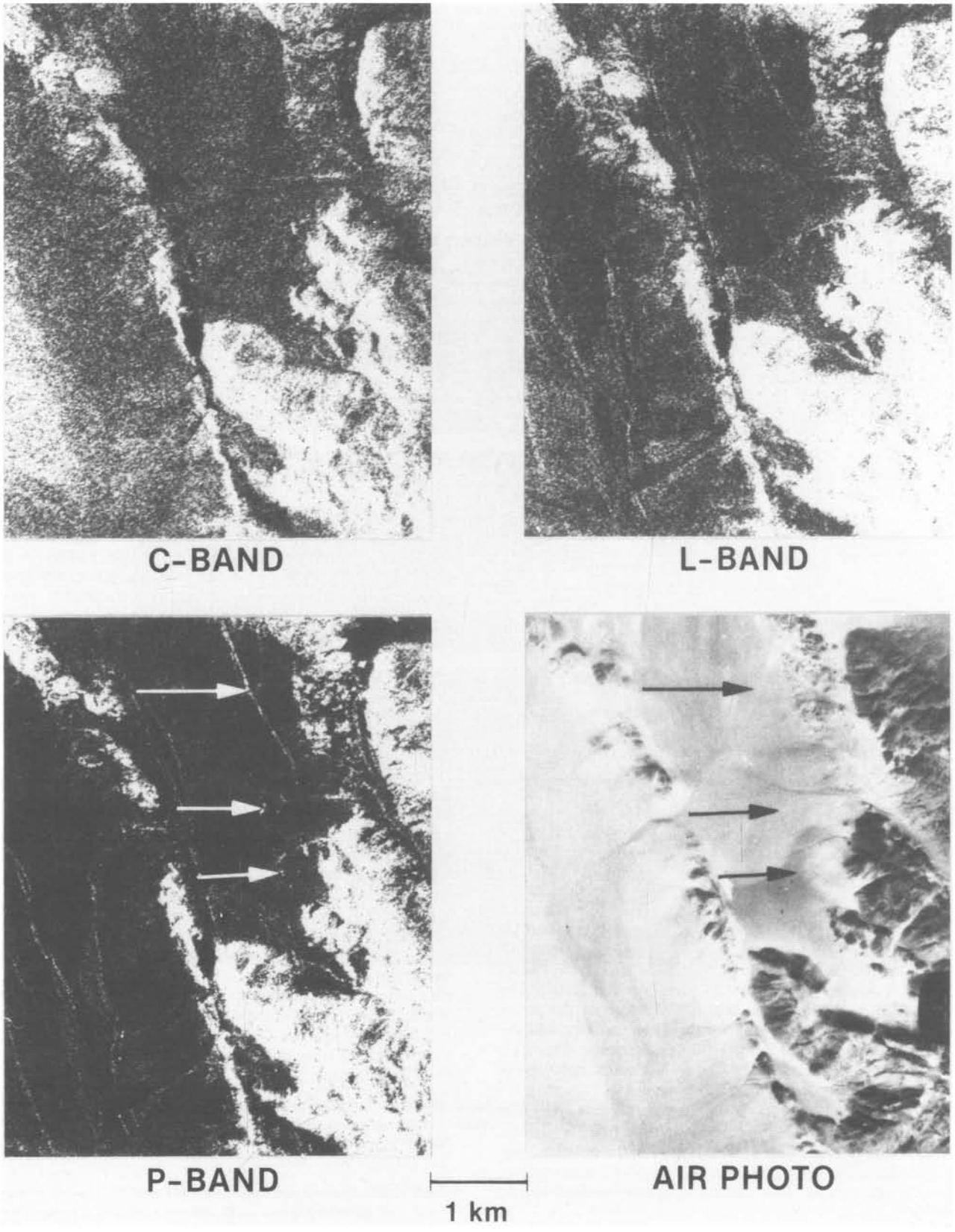

Figure 4.—Comparison of multifrequency AIRSAR images over Means valley in the Mojave Desert of California, USA. Features at arrows in P-band image, which are seen to some extent in the L-band, are shallow subcrops and a dike.

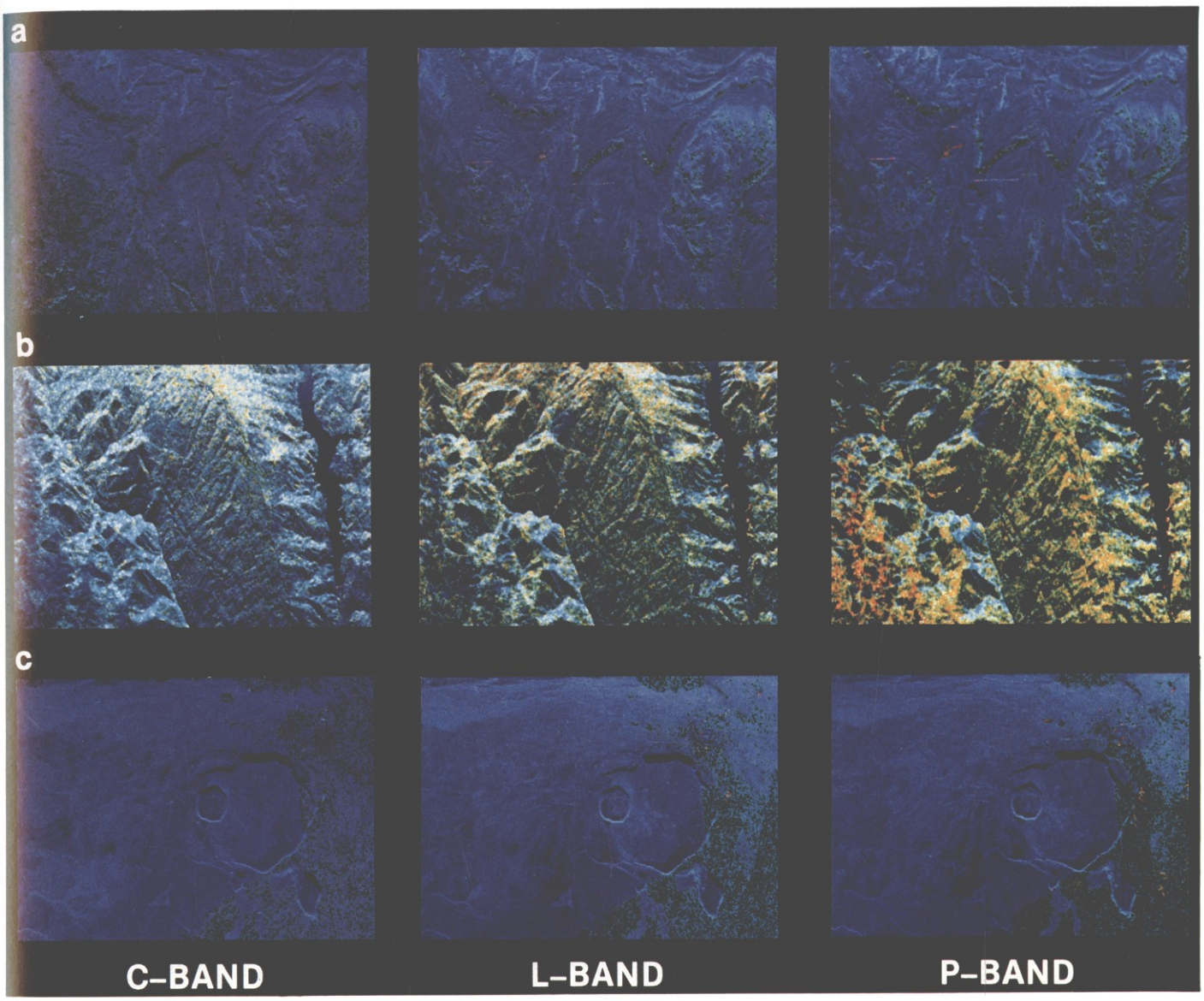

Figure 5.—Classification results based on C-, L-, and P-band polarimetric AIRSAR data of (a) Wind River basin of Wyoming; (b) Mt. Shasta, California; and (c) Kilauea Crater, Hawaii, USA. Pixels classified in red are consistent with a double bounce; in blue, with a single reflection; and in green, with diffuse scattering. According to Evans and others (1988) and Evans and Smith (1991), areas having less than 10 percent vegetation cover in the Wind River example are classified as single reflection. In the Mt. Shasta example, Evans and van Zyl (1990) found that areas that had been burned recently allowed additional penetration into the canopy, which results in the increased double bounce at the P-band in the lower left of the image. In the Kilauea example, the forest canopy is so dense on the right edge of the image that very little return resulted from the ground under the vegetation.

results from the cloud penetration capabilities of radar and the enhanced backscatter that results from standing water beneath vegetation canopies. This backscatter enhancement, modeled by Engheta and Elachi (1982), is caused by forward scattering of waves from stems (or trunks) and the flooded surface (double bounce). L-band backscatter enhancement from flooded vegetation also has been noted in the Tropics from 12.5-m-high mangroves in Bangladesh (Imhoff and others, 1986, 1987), from 10–12-m-high swamp forests in Guatemala (K.O. Pope, written communication, 1987), and from 7–10-m-high swamp forests in Borneo (Ford and Casey, 1988).

Change detection techniques are being investigated in order to assess their applicability to monitoring changes in soil moisture in less humid environments by the use of the ratios of images. An example of the detection of soil moisture change from multitemporal coverage (fig. 6) was described in Evans (in press).

Multitemporal SAR data were acquired in support of soil moisture studies at Mahantango Creek, Pennsylvania (Engman and others, 1991), and Walnut Gulch, Arizona (Dubois and others, 1991), in the USA in the summer of 1990. Results of these experiments were incorporated into the planning for additional SAR soil moisture experiments flown in Europe in 1991. Multitemporal aircraft data and correlative field measurements were acquired at Slapton Wood, UK; Orgeval, France; Montespertoli, Italy; and Castilla La Mancha, Spain, as part of the deployment.

Topography and topographic change

Topography is required in order to complete the three-dimensional view of surface properties and to correct the distortions that are inherent in SAR images. Active microwave techniques that use interferometry may provide a feasible method for acquiring these data. Zebker and Goldstein (1986) showed the feasibility of generating topographic data bases through the use of radar interferometry. Mission studies and the development of aircraft prototypes are underway for the purpose of investigating a variety of methods for the acquisition of a global topographic data base from space (Cumming and others, 1990; Goldstein and others, 1988).

NASA's JPL has implemented an aircraft interferometer that is similar to the one described by Zebker and Goldstein (1986). For the JPL system, the phase difference image that results from combining the two complex data sets has been used to generate topographic data having an rms error of typically 2–5 m for a 10 m by 10 m pixel (Zebker and others, in press). These data are acquired in a single polarization state at C-band simultaneously along with standard L- and P-band polarimeter data so that the data are registered automatically.

In order to address problems at the global scale, discussions are taking place about the generation of a high-resolution digital elevation model of the entire globe, which could serve as a topographic data base for all remote sensors. Among possible options for spaceborne interferometry is the use of subsequent passes of the EOS SAR or two antennas separated on a single structure or by a tether on a dedicated spacecraft. Once the baseline topography is determined, a third interferometric pass can be used to determine what, if any, topographic change has occurred in the intervening time between SAR overpasses (Gabriel and others, 1989). The near cancellation of systematic errors is possible, and sensitivity to topographic change on the order of tens of centimeters is attainable (fig. 7). The extreme sensitivity of this technique to elevation changes, its high spatial resolution (typically 10–30 m), and its broad swath coverage mean that it could be used to monitor erosion, sand encroachment, and soil shrinking and swelling (Gabriel and others, 1989). It also may be used to make extensive, accurate measurements of geophysical phenomena, including warping and buckling in fault zones, plate motions, and residual displacements from seismic events.

The use of SAR interferometry will be tested extensively for geological studies as part of the ERS–1 mission. Current plans are to monitor changes in surface topography due to eruptions (either

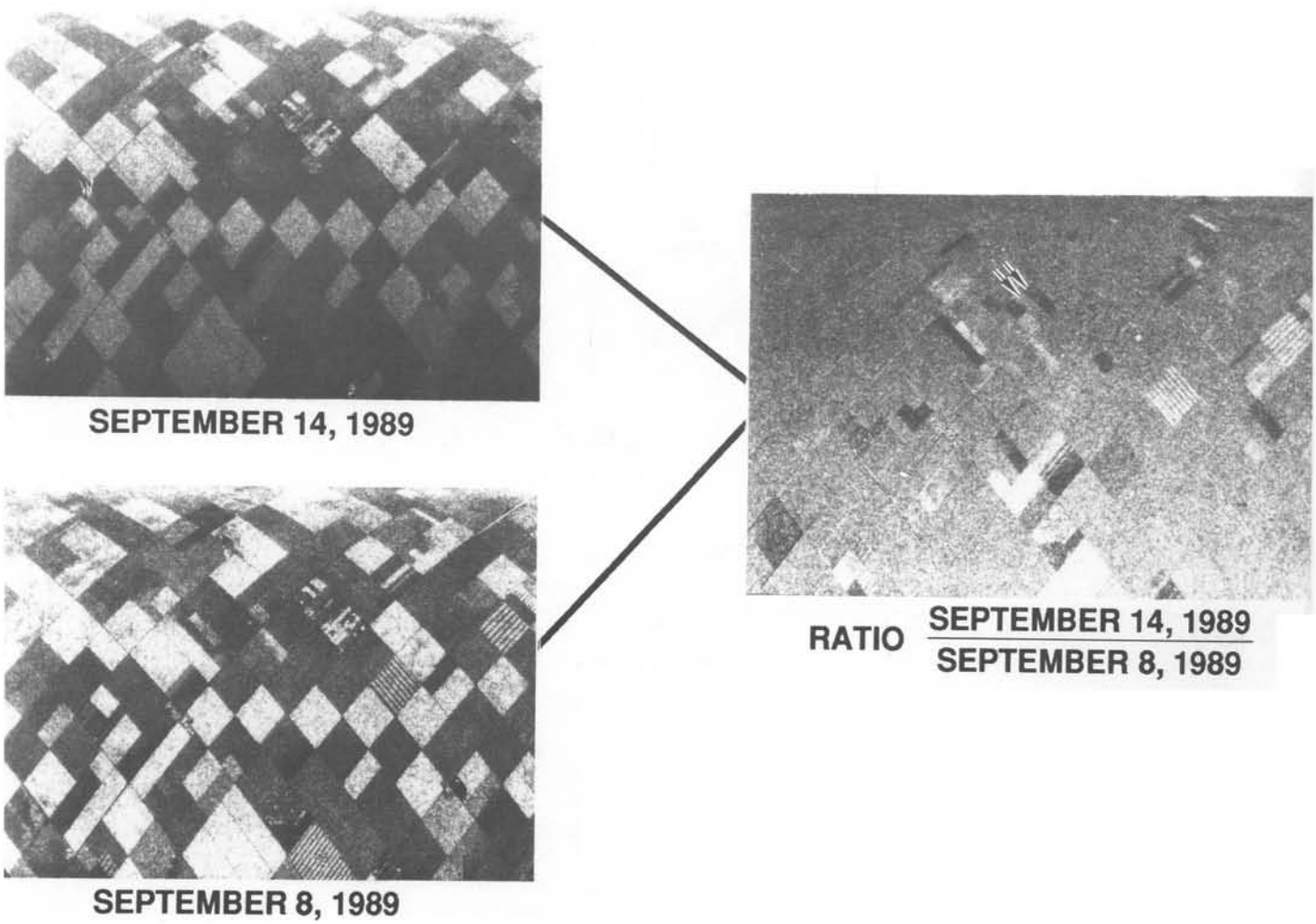

Figure 6.—Example of the ratio of multitemporal images for a soil moisture study area near Fresno, California, USA. Gray field (left arrow) showed no apparent difference in moisture between the 2 days in this CVV image. Dark field (right arrow) was drier on the second day. Courtesy of E. Engman and J.J. van Zyl, modified from Evans (in press).

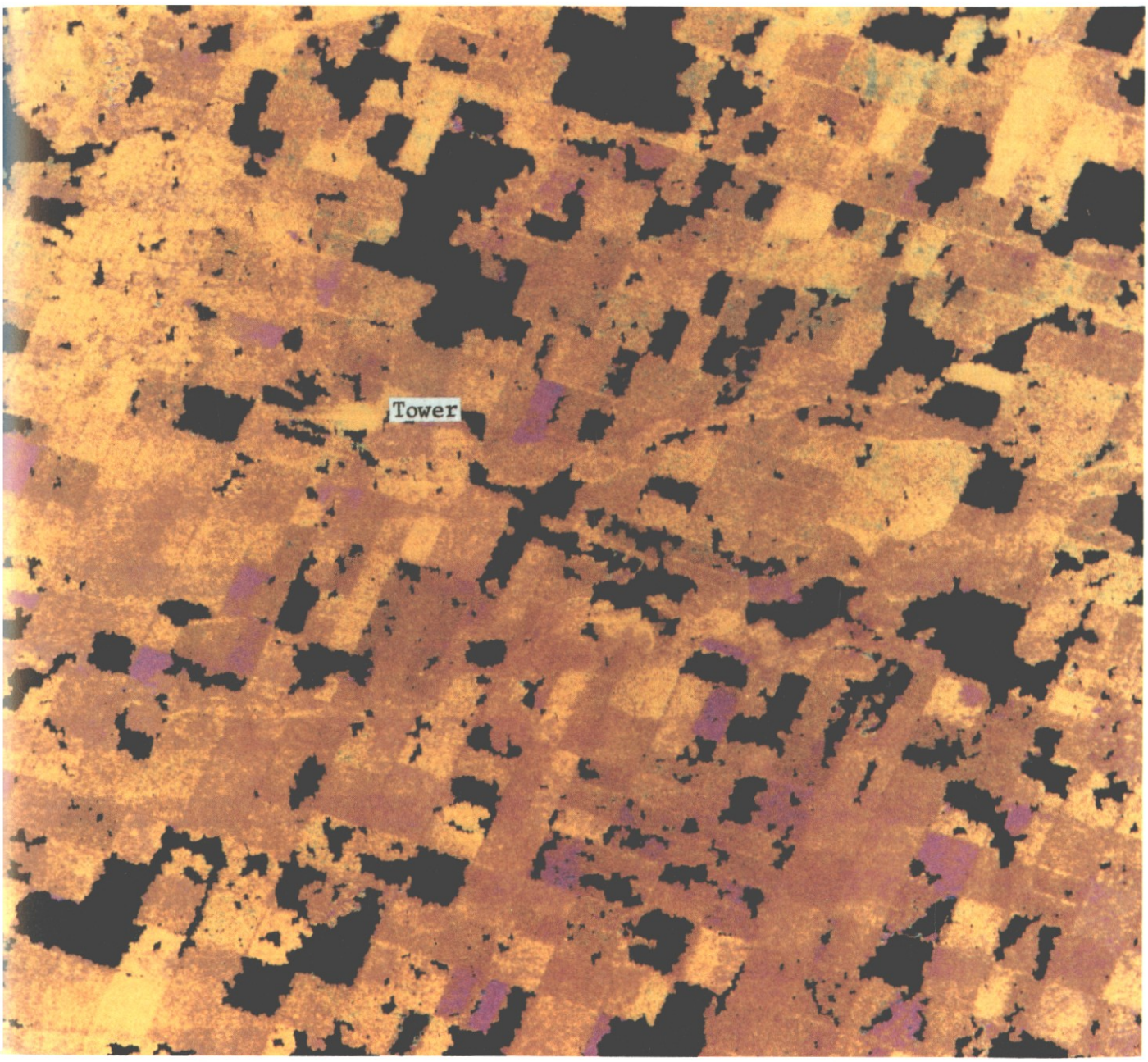

Figure 7.—Image showing topographic changes derived from Seasat SAR data over an area in the Imperial Valley of California, USA. Yellow represents no change, black represents loss of phase coherence between the data sets, and red and blue represent changes in topography on the order of 2–3 cm. These changes were interpreted to be related to soil swelling as a result of irrigation. Taken from Gabriel and others (1989).

explosive activity or events that produce lava flows) and to swelling of the flanks of volcanos because of the intrusion of magma at a shallow depth; frost-heave displacement in regions of both continuous and discontinuous permafrost; and the topography, motion, and disturbances of glaciers.

A look to the future

Major challenges in the future include the development of strategies that will allow us to extrapolate from regional to global scales (for example, the validation of geophysical products and the reconciliation between scales of radar backscatter models and atmospheric general circulation models) and the development of new technology that will result in additional sensor capabilities (for example, 35- and 90-GHz systems and lightweight electronics). Along with these advances will come many new applications of active microwave remote sensing (for example, precipitation mapping and subsurface mapping) that, in turn, will require new techniques for data processing and analysis.

In addition, several strategies are being pursued for the synthesis of other data sets and the geophysical information derived from SAR data. For example, multisensor classifications, which have included radar images as adjunct bandpasses to optical or infrared sensor systems (Blom and Daily, 1982; Rebillard and Evans, 1983; Evans, 1988), have reported improved classification accuracies over visible and infrared data alone. These studies, however, did not exploit the full diversity of the SAR sensors available at this time (for example, Evans and others, 1990). A different approach being investigated is to derive geophysical parameters from sensor systems independently and then do a combined interpretation on the derived geophysical products (Srinivasan and Richards, 1990; Evans, in press).

Finally, new data handling and analysis tools will be required in order to handle the enormous increase in SAR data that are expected over the next decade. The Magellan mission to Venus provided the first planetary-scale data base using SAR. Although complex in itself, future Earth-orbiting missions will acquire this same amount of data routinely so that changes can be monitored and possibly can be predicted.

Acknowledgments

This work was performed at the Jet Propulsion Laboratory, California Institute of Technology, and was sponsored by the National Aeronautics and Space Administration.

References

Arvidson, R.E., Evans, D.L., Farr, T.G., and others, in press, Characterization of lava flow degradation in the Pisgah and Cima volcanic fields, California, using remote sensing data: Geological Society of America Bulletin.

Blom, R.G., Crippen, R.J., and Elachi, Charles, 1984, Detection of subsurface features in Seasat radar images of Means Valley, Mojave Desert, California: Geology, v. 12, no. 6, p. 346–349.

Blom, R.G., and Daily, Michael, 1982, Radar image processing for rock-type discrimination: IEEE [Institute of Electrical and Electronics Engineers] Transactions on Geoscience and Remote Sensing, v. GE–20, no. 3, p. 343–351.

Campbell, B.A., Zisk, S.H., and Mouginis-Mark, P.J., 1989, A quad-pol radar scattering model for use in remote sensing of lava flow morphology: Remote Sensing of Environment, v. 30, p. 227–237.

Cumming, Ian, Hawkins, David, and Gray, Laurence, 1990, All-weather mapping with interferometric radar: International Symposium on Remote Sensing of Environment, 23rd, Bangkok, 1990.

Dubois, P., Kustas, B., Sorooshian, S., Guerra, A., and van Zyl, J.J., 1991, Monsoon '90 SAR results: JPL Airborne Geoscience Workshop, 2nd, Pasadena, California, USA, 1991.

Durden, S.L., van Zyl, J.J., and Zebker, H.A., 1989, Modelling and observation of the radar polarization signature of forested areas: IEEE Transactions on Geoscience and Remote Sensing, v. 27, no. 3, p. 290–301.

Engheta, N., and Elachi, C., 1982, Radar scattering from a diffuse vegetation layer over a smooth surface: IEEE Transactions on Geoscience and Remote Sensing, v. GE–20, p. 212–216.

Engman, E., Saatchi, S., and van Zyl, J.J., 1991, MACHYDRO '90 results: JPL Airborne Geoscience Workshop, 2nd, Pasadena, California, USA, 1991.

Evans, D.L., 1988, Multisensor classification of sedimentary rocks: Remote Sensing of Environment, v. 25, no. 2, p. 129–144.

———in press, Current status and future developments in radar remote sensing: ISPRS [International Society for Photogrammetry and Remote Sensing] Journal of Photogrammetry and Remote Sensing.

Evans, D.L., Farr, T.G., Ford, J.P., Thompson, T.W., and Werner, C.L., 1986, Multipolarization radar images for geologic mapping and vegetation discrimination: IEEE Transactions on Geoscience and Remote Sensing, v. GE–24, no. 2, p. 246–257.

Evans, D.L., Farr, T.G., and van Zyl, J.J., in press, Estimates of surface roughness derived from Synthetic Aperture Radar data: IEEE Transactions on Geoscience and Remote Sensing.

Evans, D.L., Farr, T.G., van Zyl, J.J., and Zebker, H.A., 1988, Radar polarimetry: Analysis tools and applications: IEEE Transactions on Geoscience and Remote Sensing, v. 26, no. 6, p. 774–789.

Evans, D.L., and Smith, M.O., 1991, Separation of vegetation and rock signatures in Thematic Mapper and polarimetric SAR images: Remote Sensing of Environment, v. 37, p. 63–75.

Evans, D.L., and van Zyl, J.J., 1990, Polarimetric imaging radar: Analysis tools and applications, *in* Kong, J.A., ed., Radar polarimetry, v. 3 *of* Progress in electromagnetic research: New York, Elsevier Science Publishers, p. 371–389.

Evans, D.L., van Zyl, J.J., and Burnette, C.F., 1990, Incorporation of polarimetric radar images into multisensor data sets: IEEE Transactions on Geoscience and Remote Sensing, v. 28, no. 5, p. 932–939.

Farr, T.G., in press, Microtopographic evolution of lava flows at Cima volcanic field, Mojave Desert, California: Journal of Geophysical Research.

Ford, J.P., and Casey, D.J., 1988, Shuttle radar mapping with diverse incidence angles in the rainforests of Borneo: International Journal of Remote Sensing, v. 9, p. 927–943.

Gabriel, A.K., Goldstein, R.M., and Zebker, H.A., 1989, Mapping small elevation changes over large areas: Differential radar interferometry: Journal of Geophysical Research, v. 94, no. B7, p. 9183–9191.

Gaddis, L., Mouginis-Mark, P.J., Singer, R.B., and Kaupp, V., 1989, Geologic analysis of Shuttle Imaging Radar (SIR–B) data of Kilauea Volcano, Hawaii: Geological Society of America Bulletin, v. 101, no. 3, p. 317–332.

Goldstein, R.M., Zebker, H.A., and Werner, C.L., 1988, Satellite radar interferometry: Two dimensional phase unwrapping: Radio Science, v. 23, no. 4, p. 713–720.

Greeley, R., and Martel, L., 1988, Radar observations of basaltic lava flows: International Journal of Remote Sensing, v. 9, no. 6, p. 1071–1085.

Imhoff, M., Story, M., Vermillion, C., Khan, F., and Polcyn, F., 1986, Forest canopy characterization and vegetation penetration assessment with spaceborne radar: IEEE Transactions on Geoscience and Remote Sensing, v. GE–24, p. 535–542.

Imhoff, M.L., Vermillion, C., Story, M., Choudhury, A.M., Gafoor, A., and Polcyn, F., 1987, Monsoon flood boundary delineation and damage assessment with spaceborne radar: IEEE Transactions on Geoscience and Remote Sensing, v. GE–25, p. 405–413.

Jezek, K., Crawford, J.P., Bindschadler, R., Drinkwater, M.R., and Kwok, R., 1991, Synthetic aperture radar observations of the Greenland ice sheets, *in* Airborne Synthetic Aperture Radar (AIRSAR) Workshop, 2nd, Pasadena, California, USA, Proceedings: JPL Publication 90–56, 57 p.

Krohn, M.D., Milton, N.M., and Segal, D.B., 1983, SEASAT synthetic aperture radar (SAR) response to lowland vegetation types in eastern Maryland and Virginia: Journal of Geophysical Research, v. 88, no. C3, p. 1937–1952.

Lynne, G.J., and Taylor, G.R., 1986, Geological assessment of SIR-B imagery of the Amadeus Basin, N.T., Australia: IEEE Transactions on Geoscience and Remote Sensing, v. GE–24, no. 41, p. 575–581.

McCauley, J.F., Breed, C.S., Schaber, G.G., McHugh, W.P., Issawi, B., Haynes, C.V., Grolier, M.J., and El Kilani, A., 1986, Paleodrainages of the eastern Sahara—The radar rivers revisited (SIR–A/B implications for a mid-Tertiary trans-African drainage system): IEEE Transactions on Geoscience and Remote Sensing, v. GE–24, no. 4, p. 624–648.

McCauley, J.F., Schaber, G.G., Breed, C.S., Grolier, M.J., Haynes, C.V., Issawi, B., Elachi, C., and Blom, R., 1982, Subsurface valleys and geoarchaeology of the eastern Sahara revealed by Shuttle Radar: Science, v. 218, no. 4576, p. 1004–1020.

Mouginis-Mark, P.J., Rowland, S., Francis, P., and others, 1991, Analysis of active volcanoes from the Earth Observing System: Remote Sensing of Environment, v. 36, p. 1–12.

Ormsby, J.P., Blanchard, B.J., and Blanchard, A.J., 1985, Detection of lowland flooding using active microwave systems: Photogrammetric Engineering and Remote Sensing, v. 51, no. 3, p. 317–328.

Rebillard, P., and Evans, D.L., 1983, Analysis of coregistered Landsat, Seasat and SIR–A images of varied terrain types: Geophysical Research Letters, v. 10, no. 4, p. 277–280.

Richards, J.A., Sun, G., and Simonett, D., 1987, L-band radar backscatter modeling of forest stands: IEEE Transactions on Geoscience and Remote Sensing, v. GE–25, p. 487–498.

Rott, H., 1990, Snow and land ice in the climate system: Research problems and possibilities of remote sensing: Remote Sensing and the Earth's Environment, ESA [European Space Agency] SP–301, p. 61–75.

Sabins, F., 1983, Geologic interpretation of space shuttle radar images of Indonesia: American Association of Petroleum Geologists Bulletin, v. 67, p. 2076–2099.

Schaber, G.G., McCauley, J.F., Breed, C.S., and Olhoeft, R.R., 1986, Physical controls on signal penetration and subsurface scattering in the Eastern Sahara: IEEE Transactions on Geoscience and Remote Sensing, v. GE–24, no. 4, p. 603–623.

Srinivasan, A., and Richards, J.A., 1990, Knowledge-based techniques for multi-source classification: International Journal of Remote Sensing, v. 11, no. 3, p. 505–525.

Stromberg, W.D., and Farr, T.G., 1986, A Fourier-based textural feature extraction procedure: IEEE Transactions on Geoscience and Remote Sensing, v. GE–24, no. 5, p. 722–731.

van Zyl, J.J., 1985, On the importance of polarization in radar scattering problems: Pasadena, California, USA, Ph.D. thesis, California Institute of Technology Antenna Lab Report no. 120, p. 32–33.

———1989, Unsupervised classification of scattering behavior using radar polarimetry data: IEEE Transactions on Geoscience and Remote Sensing, v. 27, no. 1, p. 36–45.

———1990, Calibration of polarimetric radar images using only image parameters and trihedral corner reflector responses: IEEE Transactions on Geoscience and Remote Sensing, v. 28, no. 3, p. 337–348.

van Zyl, J.J., Burnette, C.F., and Farr, T.G., 1991, Inference of surface power spectra from inversion of multifrequency polarimetric radar data: Geophysical Research Letters, v. 18, no. 9, p. 1787–1790.

Wadge, G., and Dixon, T.H., 1984, A geological interpretation of Seasat SAR imagery of Jamaica: Journal of Geology, v. 92, p. 561–581.

Waite, W.P., MacDonald, H.C., Kaupp, V.H., and Demarke, J.S., 1981, Wetland mapping with imaging radar: IGARSS [International Geoscience and Remote Sensing Symposium] Digest 2, p. 794–799.

Wall, S.D., Farr, T.G., Muller, J.P., Lewis, P., and Leberl, F.W., 1991, Measurement of surface microtopography: Photogrammetric Engineering and Remote Sensing, v. 57, no. 8, p. 1075–1078.

Zebker, H.A., and Goldstein, R.M., 1986, Topographic mapping from interferometric synthetic aperture radar observations: Journal of Geophysical Research, v. 91, no. B5, p. 4993–4999.

Zebker, H.A., Madsen, S.N., Martin, J., Wheeler, K.B., Miller, T., Lou, Y., Alberti, G., Vetrella, S., and Cucci, A., in press, The TOPSAR interferometric radar topographic mapping instrument: IEEE Transactions on Geoscience and Remote Sensing.□

Diane L. Evans *received her bachelor's degree in geology from Occidental College, Los Angeles, California, USA, in 1976 and her master's and doctoral degrees in 1978 and 1981, respectively, in geological sciences from the University of Washington, Seattle, Washington, USA. She is Program Manager for the Earth Science Program and the Project Scientist for the Spaceborne Imaging Radar (SIR) projects at the Jet Propulsion Laboratory in Pasadena, California. She is also Principal Investigator for studies emphasizing the characterization of geologic surfaces by the use of multiparameter radar data and for the development of techniques for quantitative analysis of SAR images, as well as being a member of the ERS–1 and EOS SAR science team.*

by E. Leroi, O. Rouzeau, J.-Y. Scanvic, C.C. Weber, and G. Vargas C.

Remote sensing and GIS technology in landslide hazard mapping in the Colombian Andes

Methods of mapping zones that are susceptible to landslides have been based in the past upon interpretation of aerial photographs in combination with field surveys. Prior to the launching of the United States' Landsat satellite and, especially, France's SPOT satellite, remote sensing was used very little for landslide susceptibility mapping as its characteristics have been unsuitable until now.

The Geological Application of Remote Sensing project in the Chicamocha valley of Colombia demonstrates the use of remote sensing in mapping the zones that are susceptible to landslides. The mapping is based on the interpretation of a hybrid SPOT and Landsat stereopair, calculation of a digital elevation model from the remotely sensed data, production of quantitative geomorphologic information, and digital classification of the types of land use. Finally, the various map files—geomorphology (slope, exposure, and drainage), lithology, land use, and faults—are combined by the use of a geographic information system in order to produce the final product.

This experiment shows that, provided stereoscopy can be obtained, remote sensing from space forms a complement to field surveys and is a highly effective tool for this type of mapping at scales ranging from 1:25,000 to 1:50,000.

Introduction

Among natural hazards, landslides present a major danger for most Latin American countries, especially in areas of the Andes where the risk is increased by human settlement. Research is being conducted in order to improve the methods of mapping the areas that are vulnerable to landslides, and current approaches are based on geological and structural studies, geomorphology, and modeling.

Aerial photographs, because of their excellent spatial resolution and stereoscopic capacity, have been regarded as an extremely important tool that is complementary to field surveys in compiling landslide inventories. However, they are often old, and for economic or administrative reasons, new photography is not feasible everywhere. In addition, although aerial photographs are a valuable statement of previous conditions, they tend to be somewhat ineffective for identifying and mapping susceptible areas on a regional scale. This is due to their analogic character and to the fact that the photographs provide limited access to the large variety of triggering factors.

Given this situation, we have studied a new approach to mapping landslides that is based upon available satellite products. By using digital images provided by the French SPOT satellite's High Resolution Visible (HRV) instrument, we first applied this method in the area of La Paz, western Bolivia (Scanvic, 1990), which was surveyed earlier in great detail in 1976. After this first application, we realized the need to improve the method, and a second experiment was initiated in a similar Andean area in Colombia. This study is being carried out under the auspices of the Geological Application of Remote Sensing (GARS) project. It is sponsored internationally by the United Nations Educational, Scientific, and Cultural Organization (UNESCO) and by the International Union of Geological Sciences (IUGS) with the participation of the French Centre National d'Etudes Spatiales (CNES), the French Bureau de Recherches Géologiques et Minières (BRGM), the French UPCM, the Colombian Instituto de Investigaciones en Geociencias, Minería y Química (INGEOMINAS), and the Netherlands International Institute for Aerial Survey and Earth Sciences (ITC).

The GARS project

The GARS project in Colombia is conducting landslide susceptibility mapping in the upper Rio Chicamocha valley. The area includes a considerable number of large landslides, particularly debris flows, some of which are active today. These threaten the town of Paz del Rio and the railway line that transports coal and iron from the mines to be used in the manufacturing of steel in Belencito. In a preliminary study (see Guillande and others, 1991), the method used a digital elevation model that was compiled from topographical maps, field observations, and field mapping.

In the second phase, new developments in BRGM have made it possible to carry out the landslide susceptibility mapping by using a geographic information system (GIS) that is based only on remote sensing data. The GIS operates by means of specific raster-mode software, Synergis, that was developed by BRGM. The sequence of processes enabling the assessment and mapping of potentially hazardous zones is as follows:

(1) Acquisition of remote sensing data. Because of weather problems, only one image of the stereo SPOT XS pair (right view) has been acquired. A Landsat Thematic Mapper (TM) vertical image (left view) of 30-m resolution has been substituted for the second image of the SPOT pair.

(2) Calculation of a digital elevation model from combined SPOT and Landsat data. The model has an accuracy of 40 m in the X and Y axes and 20 m in Z.

(3) Data processing and color-composite restitution at a scale of 1:50,000.

(4) Visual interpretation. Lithology, faults, landslides, and head scarps of debris flows are extracted from the landscape and are restored by stereoscopy.

All this information has been digitized, geocoded, and, when necessary, transformed into raster mode. The Chicamocha valley is underlain by north-south-striking, generally well exposed sedimentary rocks, and the lithological map based on remote sensing is of better quality than the previous map that was based on field observations. The fault pattern appears to be more complex than expected, particularly with respect to the east-west fractures, which are represented poorly on existing documents but are a normal consequence of the compression of the Nazca plate. For convenience, the fault map was transformed into fault density in raster mode.

Particular attention has been paid to mapping the head scarps of debris flows, as these are considered to be indicators of ground instability and can be used in determining, by the use of statistical methods, the critical conditions of the various permanent hazard factors. Digital classification of the SPOT image has distinguished seven classes of land use, four for vegetation and three for bare soil and human settlements. By applying three-dimensional software to the SPOT and Landsat digital elevation model, we have produced images that provide basic quantitative geomorphologic information, that is slope, exposure, and drainage, the last of these being transformed into drainage density in raster mode. Lastly, panoramic views have been created by combining the digital elevation model and the corresponding SPOT orthoimage. Processing is based on a specific software, Vue 3D, developed in France by ISTAR. This software makes it possible to select the different parameters such as azimuth, look direction, and altitude, for example.

Statistical analysis

At this stage, the five raster-mode files that correspond to the permanent hazard factors (lithology, slope, land use, faults, and drainage) were put into the Synergis GIS data base, and an analysis was performed by using these multiple variables. First, head scarps of debris flows were transformed into a surface by giving the same thickness of one pixel to each observed feature. These were then used to pilot a statistical method that determined separately, for each of the hazard factors, the critical conditions of relative landslide susceptibility. The statistical results show that the most effective parameters are lithology, slope, and land use. According to the results, the image pixels were characterized next in terms of the landslide susceptibility value for each of the five hazard factors, the sum making it possible to map the total relative susceptibility (see figure).

This method allows us to combine the different factors easily into a GIS and to compare each one directly with all the others. It is possible, for instance, to classify each factor as a function of its respective susceptibility independently from the group. For example, the susceptibility of one lithologic unit can be compared to the susceptibility of a certain slope class, and their relative weight in landslide dynamics can be calculated. This method has been applied systematically to single pixels, and the susceptibility map was drawn. This map is, naturally, adjusted to known landslides; susceptibility is defined on the basis of head-scarp criteria; and its purpose is prediction. If we assume that the same phenomena produce the same results, susceptibility mapping delineates potentially unstable zones that are not yet disturbed by landslides. Such mapping can be regarded as a land-monitoring document, particularly in terms of planning for possible hazards.

Conclusions

Although improvement is still possible in the methods of evaluating the weight of certain factors such as faults and drainage, the objectives of the project have been reached for the Chicamocha valley test site. We have demonstrated that the processing and interpretation of remote sensing data make it possible to map landslide hazards at scales that range from 1:25,000 to 1:50,000. In order to do this, a stereopair of images is vital, but only limited field control is necessary.

The document resulting from this initial study has been assessed by comparison with published maps and by field control in selected areas. This assessment has shown the validity of this type of mapping in the conditions of the Andean region.

On the basis of these results, a similar method of mapping has been applied with success in northwestern Taiwan. In addition, the assessment of radar capacity for improving landslide identification and mapping is planned.

References

Guillande, R., Caro, P., and Chorowicz, J., 1991, A first approach to digital mapping of landslide hazards in the Andes of Colombia using remote sensing techniques (GARS project): Episodes, v. 14, no. 4, p. 364–367.

Scanvic, J.Y., 1990, Mapping the vulnerability of ground to landslides: Potential use of SPOT stereoscopic data for La Paz (Bolivia): International Symposium on Remote Sensing of Environment, 23rd, Bangkok, Thailand, 1990, Proceedings, p. 703–708.□

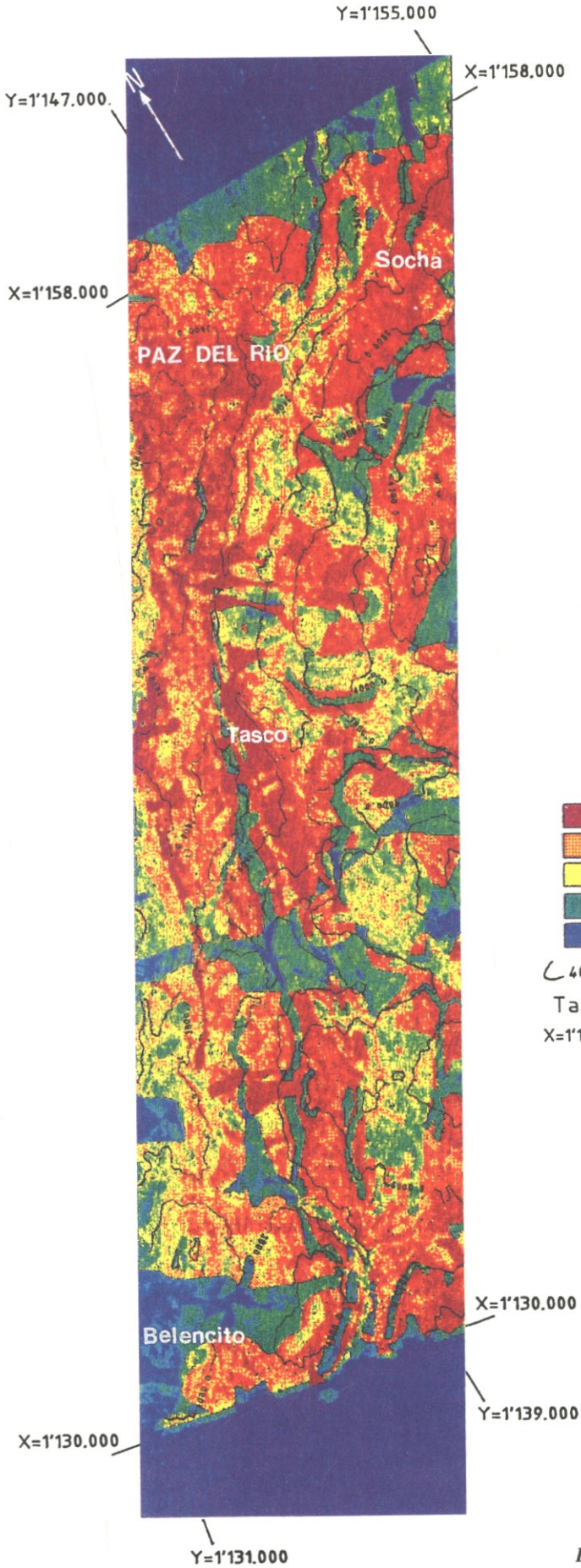

LANDSLIDE SUSCEPTIBILITY MAP

Paz del Rio (Colombia)

Location map

Very high susceptibility
High susceptibility
Medium susceptibility
Low susceptibility
Very low susceptibility
4000 Contour lines and elevation
Tasco Town, village
X=1'130.000 Geographic coordinate

0 5 km

Map computed by BRGM

Landslide susceptibility in the vicinity of Paz del Rio, Colombia.

March 1992

Dr. Olivier Rouzeau *has worked in the Remote Sensing Department of the French Bureau de Recherches Géologiques et Minières (BRGM) since 1986. A geologist and image processing and GIS specialist, he dedicates most of his work to the development of new methodologies for environmental studies (hazard maps, erosion maps).*

Dr. Jean-Yves Scanvic *is a geologist and the deputy to the head of the Remote Sensing Department of BGRM. He participated early in the development of earth resources satellite applications in 1968 with the French Spatial Agency (CNES). He is the author of a book in French on the geological applications of remote sensing.*

Dr. C.C. Weber *is a past Secretary General of the International Union of Geological Sciences (IUGS), and as such, he coordinated the activities of numerous multinational scientific commissions. In particular from 1980 to 1984, he presented to UNESCO the International Geological Correlation Programmes, many of which have an environmental component such as sea-level variations. He is Chairman of the IUGS-UNESCO program on the geological applications of remote sensing. In addition, Dr. Weber has lectured at the universities of Rennes and Paris VI and has published 97 papers and books, most of which have appeared in international scientific publications.*

Germán Vargas Cuervo *is a geologist and remote sensing expert with the Colombian Instituto de Investigaciones en Geociencias, Minería y Química (INGEOMINAS, Diagonal 53 No. 34-53, Bogotá, D.C., Colombia). His main field of interest has been environmental geology, primarily mass movement hazards in the eastern Colombian Andes. He is working now at Université Pierre et Marie Curie in Paris, France, on a doctoral thesis that involves remote sensing and GIS applications for the study of these phenomena.*

by Nick Rengers, Robert Soeters, and Cees J. van Westen

Remote sensing and GIS applied to mountain hazard mapping

Airborne and satellite remote sensing techniques, such as photography, imaging radar, and multispectral scanning, provide imagery of the Earth's surface that is a valuable tool for the inventory and monitoring of mountain hazard phenomena. When this imagery is processed by the use of computer-based geographic information systems, spatially distributed geographic data can be combined with information derived from digital processing and visual interpretation of remote sensing imagery. This combination of data enables us to analyze the influence of terrain factors upon the occurrence of mountain hazard processes.

Special emphasis is given to the importance of the scale (regional, medium, and large) at which hazard maps are prepared for regional, local, and site-planning purposes. In addition, the number of ground resolution cells that are necessary to detect, recognize, or identify objects in photographic or other types of remote sensing imagery provide us with information about the dimensions of features needed in order to determine the existence of mass-movement processes.

Introduction

For the past two decades, nonphotographic remote sensing has undergone enormous development and has found widespread applications. However, in many cases, strong overselling of the potentials of remote sensing has created disappointment for its users. At the same time, we have seen the development of the applications of geographic information systems (GIS) in the earth sciences.

Although the integration of remote sensing and GIS offers very interesting opportunities (Ehlers and others, 1989), we will review critically herein the possibilities and limitations of this integration as it applies specifically to mountain hazard mapping.

The authors are involved in a research program that is sponsored by the United Nations Educational, Scientific, and Cultural Organization (UNESCO), the European Economic Community, and the Netherlands Government. This research program, within the framework of the International Decade for Natural Disaster Reduction, aims to develop mountain hazard mapping methods that use GIS based on personal computers (PC). Further, we intend to transfer these methods to hazard mapping specialists in the Andean countries of Bolivia, Colombia, Ecuador, Peru, and Venezuela. In the methods that we have developed, remote sensing imagery plays a large role.

Remote sensing and GIS

Both digital remote sensing and GIS are based on assigning numerical values to well-defined areas (scene elements) of the Earth's surface in order to produce a numerical image of this surface. Through a process of image correction and resampling, the remote sensing data coded by geology can be matched with the raster cells of the GIS. This opens many possibilities for correlation studies between basic remote sensing data and the thematic information derived from the introduction of maps digitized in GIS.

In order to determine the limitations of these correlations, we must define both the type of data that are available from digital remote sensing and its resolution, as well as how these data fit with the thematic information introduced into GIS from other sources. Figure 1 shows the relationship between GIS and remote sensing in general terms, remote sensing being one of several possible types of data put into a GIS.

Figure 2 shows in more detail the possibilities that exist for the input of remote sensing data or information derived from remote sensing data into the GIS. These include (1) direct inputting of raw remote sensing data into the data base of a GIS; (2) digital image processing of the raw remote sensing data (this may include geometric correction, image enhancement and resampling procedures, and subsequent input of calibrated and (or) data coded by geology into the GIS); and (3) digital image processing of the raw remote sensing data, preparation of a picture, visual interpretation of the picture, and input of the thematic interpretation into the GIS by digitization of the thematic interpretation map. The dashed line in figure 2 encloses a GIS in which the digital image processing capabilities are integrated. An example of such a GIS is the PC-based Integrated Land and Watershed Management Information System (ILWIS) that has been developed at the International Institute for Aerial Survey and Earth Sciences (Netherlands) (Valenzuela, 1988) and that was used in a hazard assessment analysis described by the authors (Soeters and others, 1991). A schematic representation of ILWIS is given in figure 3.

The introduction of the capability of digital image processing in GIS results in important advantages. For instance, the ILWIS software allows the display of geometrically corrected images (orthophotography, Landsat Thematic Mapper (TM), and SPOT imagery) and overlaying of thematic information from other sources; screen digitizing over displayed raster imagery; display of individual bands or color composites that use tools such as linear stretching, histogram equalization, and filtering; and supervised classification in the imagery.

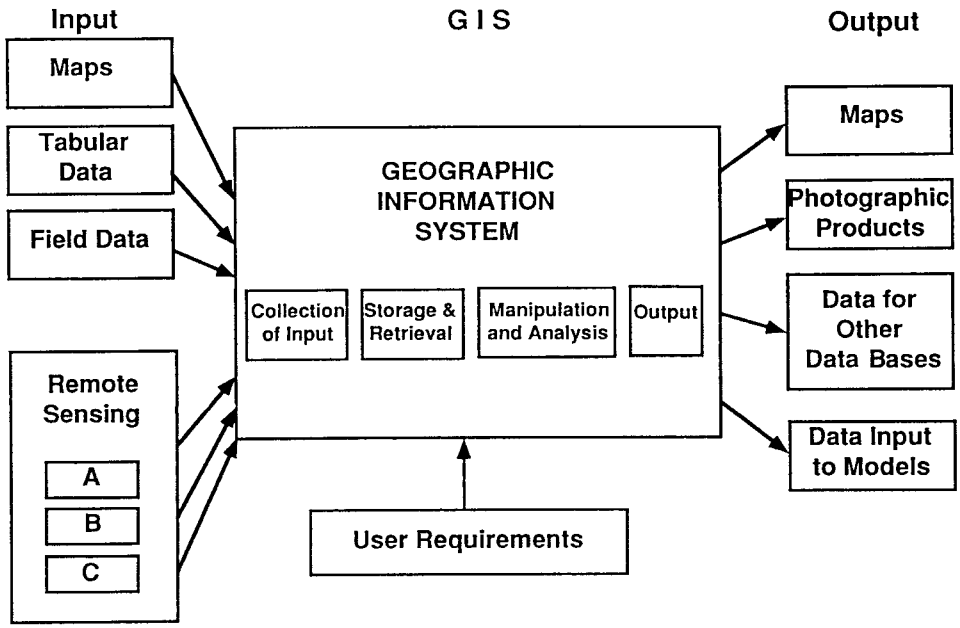

Figure 1.—Relationships between GIS and remote sensing.

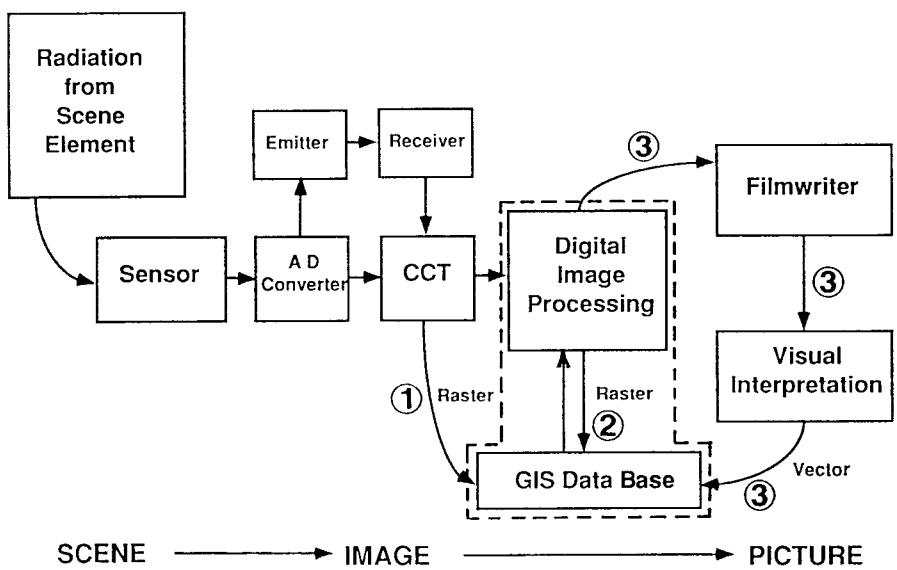

Figure 2.—Input of remote sensing data into a GIS. The interrupted line encloses a GIS in which digital image processing has been integrated. For explanation of numbers, see text. Abbreviations: AD, analog-digital; CCT, computer compatible tape.

Mountain hazard mapping at various scales

Natural hazard mapping is not restricted to the delineation of occurrences of phenomena such as mass movement, flooding, earthquakes, and volcanism in the past, but it is focused on making predictions about the occurrences of such phenomena in the future (Varnes, 1984). Hazard maps outline zones that are defined in terms of the probability of occurrence of potentially damaging phenomena within a certain span of time.

During the preparation of such maps, the influence of a number of factors must be assessed on the likelihood of occurrence. The more detailed the resulting map should be, the more factors will have to be studied. Therefore, the methodology that has to be followed depends upon the scale of the map to be prepared, the purpose for which it is to be made, and the amount of information that is available for the area concerned.

The following section gives an overview of the various scales of maps showing mass-movement hazards. These were prepared in the mountain hazard mapping research project described by Soeters and others (1991). We will describe the purpose for which the maps are

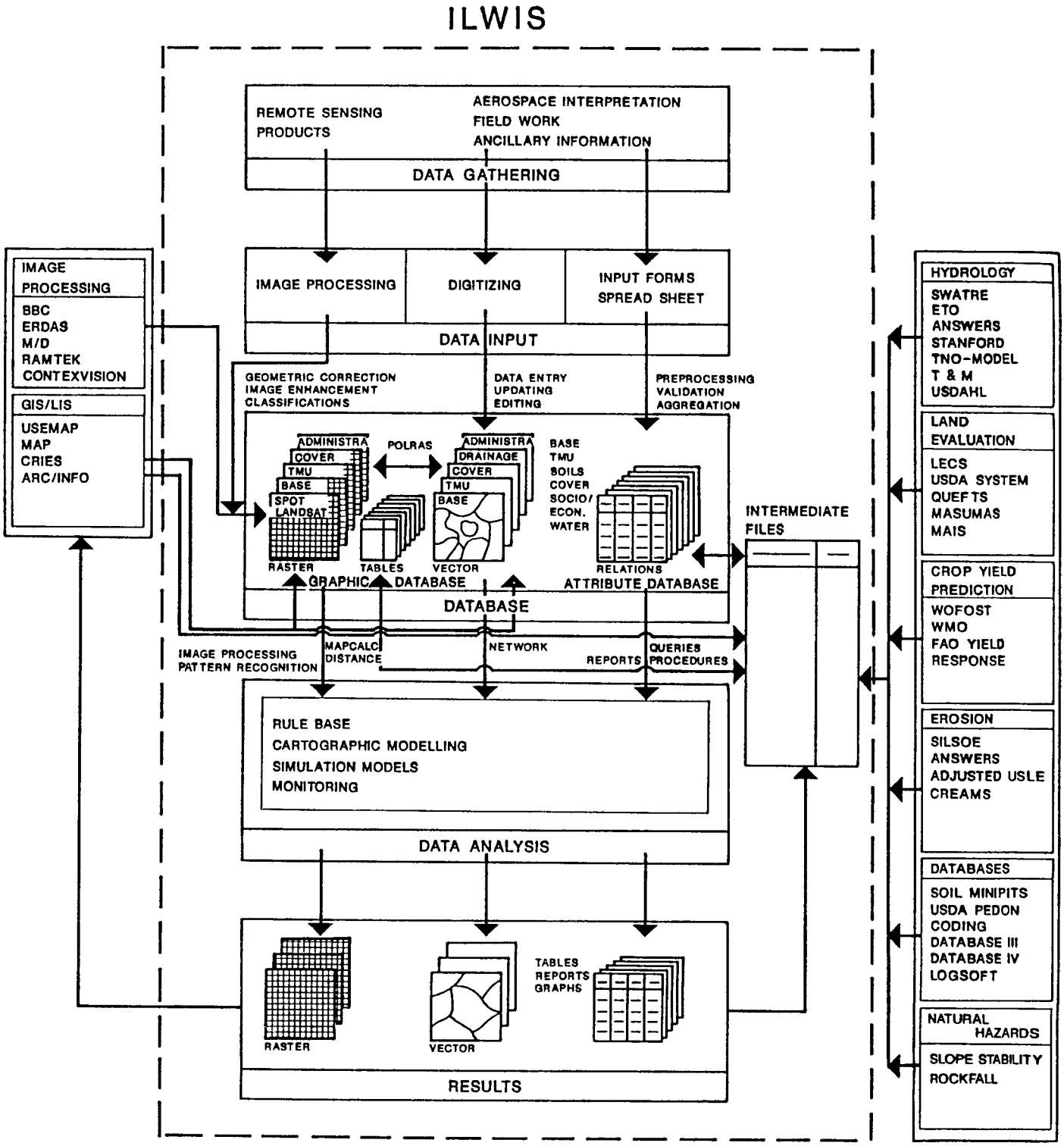

Figure 3.—Schematic representation of ILWIS (taken from Valenzuela, 1988).

used, the methodology that is applied, the input information that is necessary, and the type of remote sensing imagery that can be used.

Regional scale hazard mapping

Regional scale hazard mapping (1:100,000 to 1:250,000) is applied in the early planning stages of regional (infrastructural) development and uses a semiquantitative methodology that includes map overlays. This mapping requires information from thematic maps on the geology, geomorphology, land use, topography, and drainage network of the area at a regional (small) scale. Often, such information is not available, and the delineation of terrain mapping units (see Meijerink, 1988) can be followed instead. A terrain mapping unit is a zone that has a unique combination of morphology, soil, and bedrock and can be outlined in stereo imagery at a small scale. Mapping of individual mass-movement phenomena is not possible in this stage, except for some sample areas. Available records and data bases on landslide occurrences may help if they are available.

As terrain zoning at this scale is based primarily on the morphological characteristics of the terrain, use can be made of stereo imagery at a small scale (1:60,000 to 1:150,000). This imagery is either panchromatic black and white or multispectral and can be combined into a color composite picture. Radar imagery may be useful at this stage if the ground resolution is sufficient to delineate terrain mapping units.

Medium-scale hazard mapping

Medium-scale hazard mapping (1:25,000 to 1:50,000) is used to determine hazard zones that are better defined for the location of engineering structures of various kinds including, for instance, road location and urban planning. The methodology employs a variety of analytical methods, mostly statistical, in order to determine hazard zones by multivariate analysis and weighing of the different factors that contribute to the development of potentially damaging phenomena. This mapping calls for detailed topographic information in the form of digital elevation models and various types of thematical maps, such as maps showing lithology, geological structure, geomorphological processes, and occurrences of slope processes of different types.

Remote sensing stereo imagery of medium scale (1:15,000 to 1:25,000) is required, and it may be either panchromatic black and white or multispectral. The spatial resolution must allow for the identification of individual mass-movement phenomena that are larger than 10 m in dimension.

Large-scale hazard mapping

Large-scale hazard mapping (1:5,000 to 1:15,000) is needed in the early stages of site investigation in order to determine quantitatively the hazard for a particular civil engineering work. Quantitative analytical methods are used that include multivariate statistical and numerical slope stability analyses. This mapping requires very detailed topographic information from a good-quality 1:5,000- or 1:10,000-scale topographic base map. In addition, detailed information is needed on geology, geomorphology, land use, and slope instability processes, as well as on the hydrogeological and geotechnical characteristics of the geological units.

Large-scale (1:5,000 to 1:10,000) black and white or color stereo imagery is necessary. It must have sufficient resolution to identify the elements of mass-movement phenomena that are smaller than 5 m in dimension.

All scales

In conclusion for all scales of hazard mapping, stereo imagery is of the utmost importance because the zones into which the terrain is divided are distinguished primarily on the basis of morphology, rocks, and soils. For hazard mapping at scales more detailed than the regional mapping, the resolution of the imagery is of greater importance. At these larger scales, the occurrence of individual mass movements becomes important input information in the analytical methods we use for hazard assessment. In the following section, we will discuss resolution and its relationship to the size of objects that can be detected, recognized, or identified.

Resolution of remote sensing imagery

The word "resolution" causes confusion as it has different meanings in photography and in nonphotographic remote sensing. In aerial photography, "ground resolution" is defined usually (see fig. 4) as the minimum number of meters required per line pair on the ground in order to be visible as two distinct lines of different color or grey tone in the picture. In nonphotographic remote sensing, the expression "ground resolution" is used mostly to indicate the size of the area on the ground ("scene element" or "instantaneous field of view") for which the radiation is integrated in order to give one radiation value in the image. When the image is presented as a picture without data reduction, then the ground resolution area will form the basic element (pixel) of the picture.

In order to prevent confusion, we prefer to use the expression "ground resolution cell," which is equal to the scene element in nonphotographic remote sensing. Furthermore, the resolution in terms of meters per ground resolution cell ($R_{m/grc}$) is related to photographic resolution in terms of meters per line pair ($R_{m/lp}$) in the following way (taken from Naithani, 1990):

$$R_{m/grc} = \frac{1}{2\sqrt{2}} \times R_{m/lp}$$

For simplicity reasons in the following text and tables, the size of a ground resolution cell in aerial photography will be rounded off to 1/2.5 times the value for the resolution in meters per line pair, as presented by Naithani (1990).

Figure 4B shows that only line pairs that are wider than one ground resolution cell per line are detectable on an image by their contrast in grey tone or color. Objects that are not lines but that are

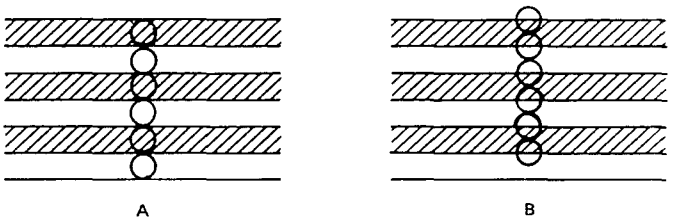

Figure 4.—Line pairs and ground resolution cells (circles) used to define resolution in aerial photography (taken from Naithani, 1990).* A, *Six ground resolution cells resolve three line pairs;* B, *more than six ground resolution cells are needed in order to resolve three line pairs.* B *is the general case, and* A *is a very special case where lines of one ground resolution cell width would be just recognizable because they coincide in position.

Table 1.—Number of ground resolution cells needed to detect, recognize, or identify an object of varying contrast in relation to its background

[In parentheses are given the minimum dimensions of a nonelongated object counted in numbers of ground resolution cells]

	Detection	Recog-nition	Identification
EXTREME CONTRAST white or black object in variable grey tone background	5 - 8 (2 x 3)	10-15 (3 x 4)	20 - 30 (5 x 6)
HIGH CONTRAST dark or light object in grey tone background	10 - 15 (3 x 4)	30-40 (5 x 7)	80 - 100 (8 x 10)
LOW CONTRAST grey tone feature in grey tone background	200 - 250 (10 x 20)	400-600 (20 x 30)	1000 - 1500 (30 x 40)

Table 2.—Minimum sizes needed for an object to be detected, recognized, or identified depending upon the conditions of contrast between the object and its background for various types of imagery

[Values should be used only as an indication of relative size. For a detailed explanation on the determination of size, see the text. Abbreviation: A.P., aerial photography]

		Landsat MSS	Landsat TM	Spot XS	Spot Pan	A.P.* 1:100.000	A.P.* 1:50.000	A.P.* 1:25.000	A.P.* 1:10.000
GROUND RESOLUTION CELL SIZE		80m	30m	20m	10m	1m	0.5m	0.25m	0.1m
HIGH CONTRAST feature-background	Detection	320m	120m	80m	40m	4m	2m	1 m	0.4m
	Recognition	560m	210m	140m	70m	7m	3.5m	1.8m	0.7m
	Identifica-tion	800m	300m	200m	100m	10m	5m	2.5m	1 m
LOW CONTRAST feature-background	Detection	1600m	600m	400m	200m	20m	10m	5m	2m
	Recognition	2400m	900m	600m	300m	30m	15m	7.5m	3m
	Identifica-tion	3200m	1200m	800m	400m	40m	20m	10 m	4m

*Without Forward Movement Correction

irregular in form need a minimum size of 2×3 ground resolution cells (see also table 1) in order to be detectable on the basis of their known spectral characteristics against a contrasting background.

We should define some more terms at this time. "Detection" means that it is possible to decide if an object of known spectral characteristics is present or absent at a defined geographic location. "Recognition" means that it is possible to decide if an object of known form and spectral characteristics is present anywhere in the picture. "Identification" means that it is possible to identify objects of variable forms and spectral characteristics on the basis of their characteristic forms and context within the background.

On the basis of our experience in visually interpreting remote sensing imagery, we have concluded that, for various contrasts in grey tones between an object and a background, the numbers of ground resolution cells needed to detect, recognize, or identify objects in a picture are as listed in the table 1. In addition, we give in parentheses an indication of the size (expressed in number of ground resolution cells) needed for objects of nonelongated shape, as is usually the case for mass-movement phenomena. The larger dimension of an object is used in table 2 in order to indicate the minimum size needed for a mass-movement feature to be detectable, recognizable, or identifiable in photographic or other types of remote sensing imagery.

In terms of contrast, "extreme contrast" exists when a completely white or black object is present against a variable grey tone background. "High contrast" indicates a dark or light object against a grey tone background. "Low contrast" indicates that the spectral characteristics of an object do not differ significantly from the background and that objects can be identified or recognized only on the basis of their characteristic forms. These contrasts are illustrated by figures 5 and 6, which were derived from a large-scale aerial photograph that was digitized having a raster size as if the original ground

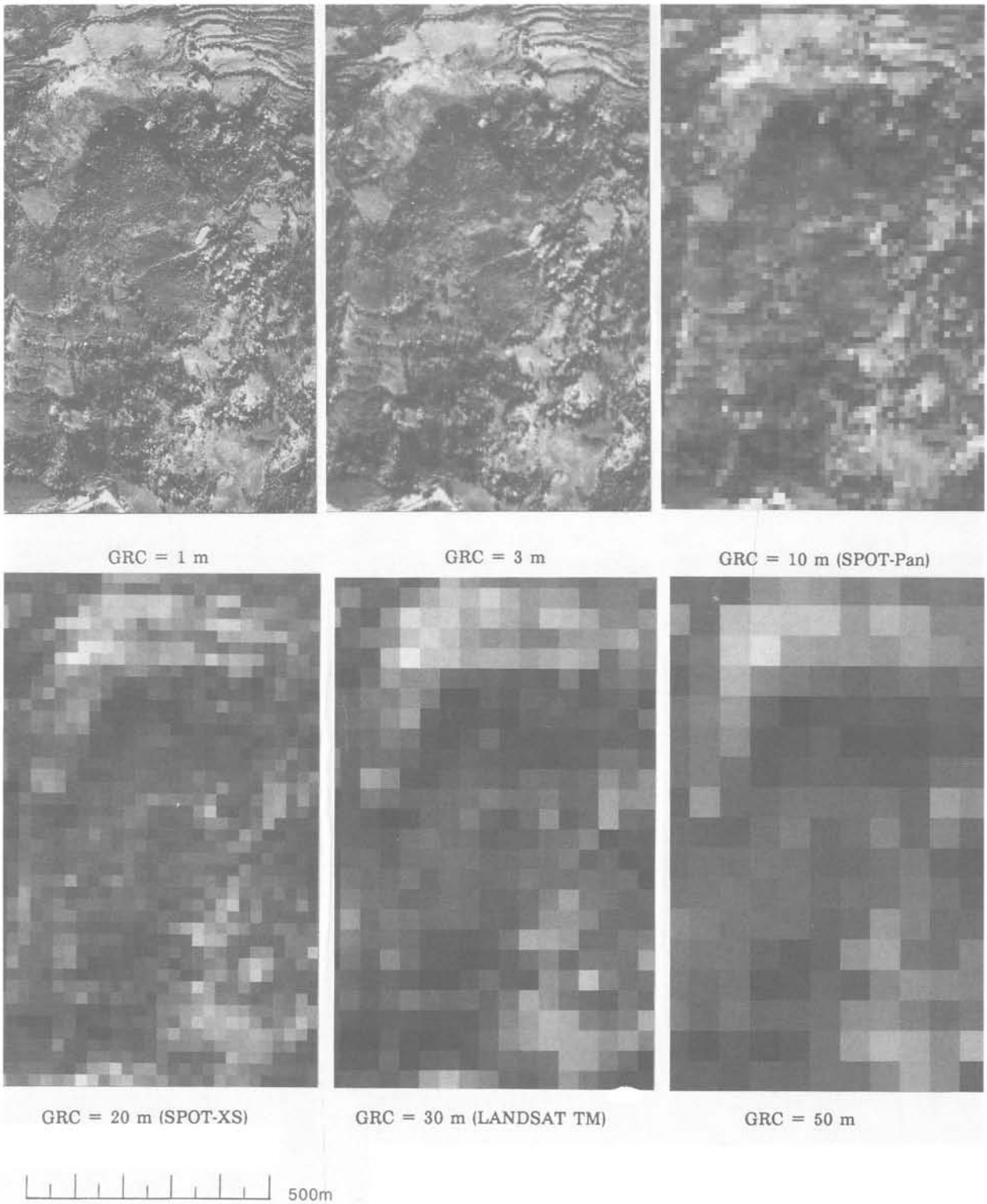

Figure 5.—An area in the Spanish central Pyrenees showing a landslide scar that is in shadow (high contrast) in the central upper part of the picture and a depositional area of landslide debris (low contrast) in the central to lower part of the picture. The pictures were derived from a digitized large-scale aerial photograph and have artificially aggregated pixel sizes determined as if the ground resolution cell (GRC) size of the pictures were 1, 3, 10, 20, 30, and 50 m.

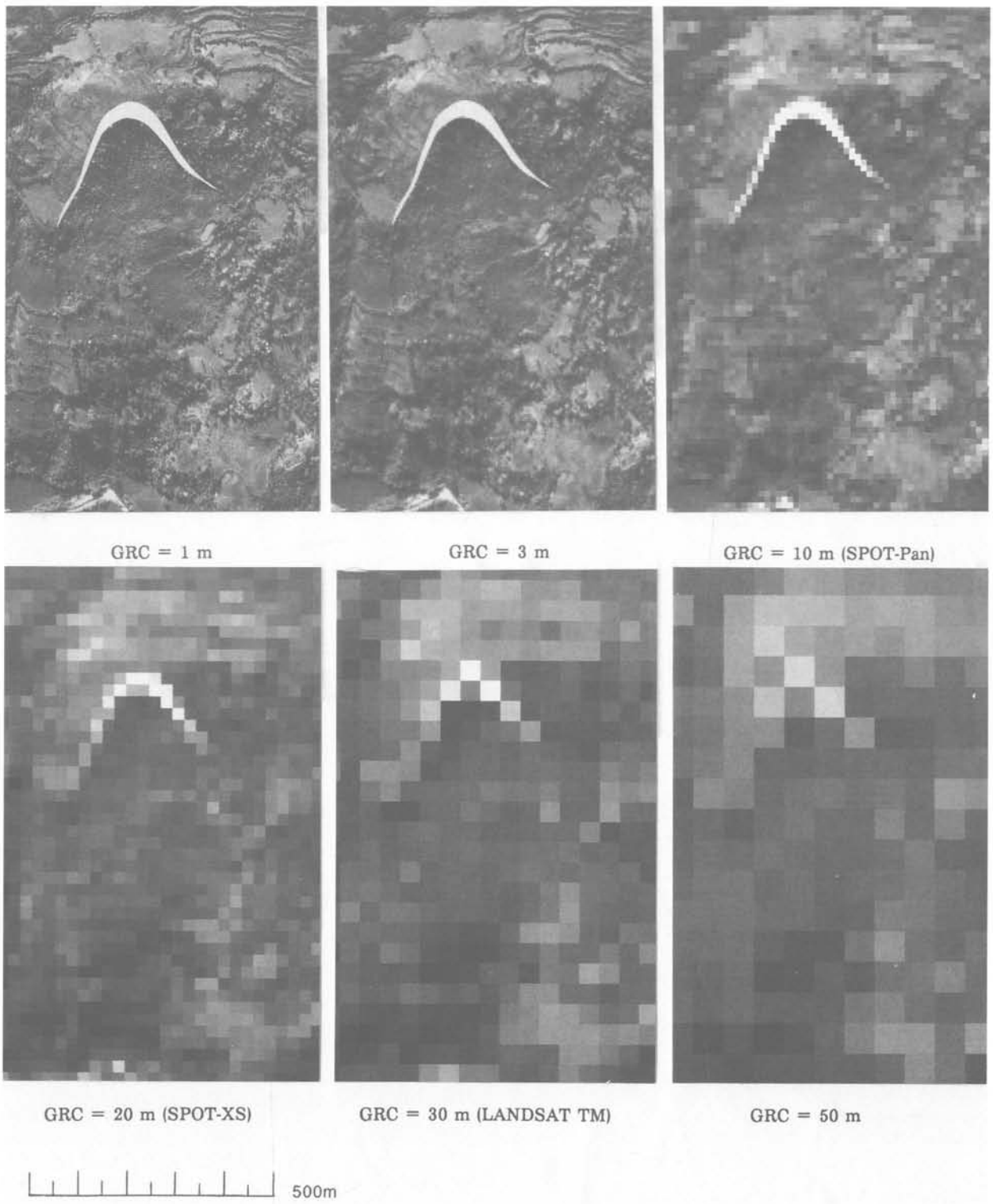

Figure 6.—The same area and the same ground resolution cell sizes as in figure 5, but here an artificially enhanced landslide scar is depicted completely in white in order to show the influence of extreme contrast on the resolution characteristics of pictures having various ground resolution cell (GRC) sizes. Such extreme contrasts rarely are encountered in imagery of parts of the continental Earth that are not covered by snow.

Table 3.—Current high-resolution satellite remote sensing missions suitable for GIS applications (taken from Ehlers and others, 1989)

Platform	Year	Spectral Bands	Spectral Range	Stereo	Ground Resolution Cell Size	Country
Shuttle	1983	1	Radar	No	17-58 m	U.S.A.
		2	VIS/NIR	No	20 m	W. GERMANY
Landsat-4/-5	1982/84	4	VIS/NIR	No *	80 m	U.S.A.
		7	VIS/NIR	No *	30 m	
			MIR/TIR	No	(TIR:120 m)	
SPOT	1986	1	Pan(VIS)	Yes	10 m	FRANCE
		3	VIS/NIR	Yes	20 m	
MOS	1987	4	VIS/NIR	No	50 m	JAPAN
IRS-1A	1988	4	VIS/NIR	No	36.5 m	INDIA

VIS = visible ; NIR = Near Infrared ; MIR = Middle Infrared ; TIR = Thermal Infrared
*Stereo can be produced using a good quality Digital Elevation Model

resolution cell had been 0.3 m. The individual pictures then were printed with artificially aggregated pixels as if the ground resolution cell size had been 1, 3, 10, 20, 30, and 50 m.

Figure 5 shows pictures of various ground resolution cell sizes for an area in the Spanish central Pyrenees (Sissakian and others, 1983). We see a landslide scar that is in shadow, which gives a high contrast in the upper middle part of the picture, and a depositional area of landslide debris, which has a low contrast in the central to lower part of the picture. The depositional area is recognizable by a characteristic surface texture (low contrast) and by a surrounding line of higher vegetation that has small-sized ground resolution cells. Figure 6 shows the same photograph, but here an artificially enhanced landslide scar is depicted completely in white in order to show the effect of extreme contrast on detectability.

Table 2 shows the minimum sizes of objects that can be detected, recognized, or identified in aerial photography of various scales and in various types of nonphotographic remote sensing imagery. The sizes were determined by multiplying the ground resolution cell size for the type of imagery by the larger of the two dimensions of the object given in table 1. The ground resolution cell size for aerial photography was determined by dividing the values for resolution in meters per line pair by a factor of 2.5, as given by Naithani (1990). The values in table 2 give only an indication of the order of magnitude of the relative size of the objects, as differences in form and contrast relationships will influence the resolution.

Possibilities for today

Satellite remote sensing can be a useful source of data when GIS is used for landslide hazard assessment if the GIS incorporates digital image processing. However, the application of both currently available satellite remote sensing and remote sensing planned in the near future is limited because of its spatial resolution (see tables 3 and 4). This resolution does not allow the identification of landslide features that are smaller than 100 m in conditions of high contrast between the feature to be mapped and the surrounding background. If contrast conditions are less favorable, identification is limited to features that are larger than an order of magnitude of 400 m.

Because of the spatial resolution limitations of most remote sensing, we need stereoscopic vision in order to recognize landforms. This requires stereo imagery, which enhances the applicability of currently available SPOT imagery. Therefore, SPOT imagery can be used for regional scale landslide hazard mapping that outlines terrain mapping units. Landsat TM images can be used as well if stereomates for stereoscopic vision are prepared with help of a detailed digital elevation model of the terrain. For larger scale hazard mapping at the medium and large scales, inventories of existing landslide phenomena are necessary, and to make these inventories, we need aerial photography that has good spatial resolution characteristics.

The potential use of radar imagery for landslide hazard mapping needs further investigation. Results of work on the classification of terrain roughness (Singhroy, Radar geology, this issue) seem encouraging, but problems are associated still with the production of calibrated and geometrically corrected radar imagery. Such corrected imagery is absolutely indispensable before the data can be introduced in the GIS for correlation with other thematic information on terrain characteristics.

European Remote Sensing satellite number 1 (ERS-1) radar imagery data will be used by the authors in the near future in a research project on mountain hazard mapping (Soeters and others, 1991), and we will evaluate the potential of its application to the classification of terrain roughness. We find it especially interesting that the application of radar imagery in tropical, mountainous areas is not dependent upon weather conditions for the collection of data.

Hopes for the future

Hopes for the future have emerged from our work on hazard mapping, including our use of remote sensing data in a GIS environment. Although space will not allow a full treatment of the history behind these hopes, we will express them here as suggestions to those who are involved in the development of GIS and in the planning for future remote sensing missions.

(1) The long-term availability of remote sensing imagery of the types now used widely (such as TM and SPOT) is essential for long-term monitoring of changes in the Earth's surface.

(2) For radar imagery, we need high-quality geometrical correction procedures that can produce radar imagery usable for input into GIS. Improvements in resolution may lead to wider applications of radar imagery in landslide hazard mapping, if the imagery yields suitable information on terrain roughness characteristics.

Table 4.—Planned satellite remote sensing missions suitable for GIS applications (taken from Ehlers and others, 1989)

[Abbreviation: ESA, European Space Agency]

Platform	Year	Spectral Bands	Spectral Range	Ground Resolution Cell Size	Country
Landsat 6	1991	8	Pan	15 m	U.S.A.
			VIS/NIR	30 m	U.S.A.
			MIR/TIR	120 m	U.S.A.
MOS 2	1991	4	VIS/NIR	50 m	JAPAN
ERS 1	1991	1	Radar	30 m	ESA
Shuttle	1992	2	Radar (SIR-C)	25 m	U.S.A.
		1	Radar (X-SAR)	25 m	GERMANY
JERS 1	1992	1	Radar (SAR)	20 m	JAPAN
SROSS-1	1992	1	Pan	52x80m	INDIA, GERMANY
SPOT-3	1993	1	Pan	10 m	FRANCE
		3	VIS/NIR	20 m	FRANCE
Radarsat	1994	1	Radar (SAR)	30 m	CANADA
EOS	1997	196	VIS/NIR	30 m	U.S.A.
		64	VIS/NIR	800 m	ESA, JAPAN
		1	Radar (SAR)	30 m	ESA, JAPAN

(3) For optical remote sensing, improvements would be welcomed in ground resolution. Ground resolution cell sizes on the order of 0.5 to 1 m would be necessary in order to be able to use satellite remote sensing for the inventory of landslide phenomena. Zooming into areas of particular interest would be an interesting approach.

(4) For the optimal integration of remote sensing and GIS, we should try to achieve a standardization in remote sensing of ground resolution cell sizes and systems for coding by geology. This would improve our possibilities of comparing and integrating data sets of different sources and scales, and it could reduce the volume of data sets with a quadtree approach, in which the ground resolution cell sizes are quartered in size in those areas where more detailed ground data are available.

(5) In order to improve the applications of geology information systems to the applied earth sciences, the following improvements to such systems will be indispensable. We need to develop better models and rules of general applicability in order to describe geological and hazard-causing processes. We need to develop three- and four-dimensional (including the time factor) GIS systems for more detailed analysis of landslide hazards at a large scale. And we need to improve the user friendliness of GIS systems in order to benefit the general public.

(6) A strong need exists for the education of earth scientists in the applications of remote sensing and geology information systems. Not only should training in these fields be included in all university curriculums, but provisions also should be made for experienced earth scientists to take courses that teach applications of remote sensing and GIS in their work. We see a gap at this time not just between earth scientists in the developed world and Third World but also in the developed world between scientists who have and have not had the opportunity to work with remote sensing and GIS.

References

Ehlers, M., Edwards, G., and Bédard, Y., 1989, Integration of remote sensing with geographic information systems: A necessary evolution: Photogrammetric Engineering and Remote Sensing, v. 55, no. 11, p. 1619–1627.

Meijerink, A.M.J., 1988, Data acquisition and data capture through mapping units: ITC [International Institute for Aerial Survey and Earth Sciences] Journal 1988–1, p. 23–44.

Naithani, K.K., 1990, Can satellite images replace aerial photographs? A photogrammetrist's view: ITC Journal 1990–1, p. 29–31.

Sissakian, V., Soeters, R., and Rengers, N., 1983, Engineering geological mapping from aerial photographs: The influence of photo scale on map quality and the use of stereo-orthophotographs: ITC Journal 1983–2, p. 109–118.

Soeters, R., Rengers, N., and Westen, C.J. van, 1991, Remote sensing and geographical information systems as applied to mountain hazard analysis and environmental monitoring, *in* Thematic Conference on Geologic Remote Sensing, 8th, Denver, Colorado, USA, 1991, Proceedings: An Arbor, Michigan, USA, Environmental Research Institute of Michigan, p. 1389–1403.

Valenzuela, C.R., 1988, ILWIS overview: ITC Journal 1988–1, p. 3–14.

Varnes, D.J., 1984, Landslide hazard zonation: A review of principles and practice: Paris, UNESCO, International Association of Engineering Geology, Commission on Landslides and Other Mass Movements on Slopes, Natural Hazards, v. 3, 176 p.□

Dr. Niek Rengers *graduated in 1965 from the Department of Geology at Leiden University in The Netherlands and obtained his doctorate from the Department of Civil Engineering in Karlsruhe, West Germany, in 1971. Since then he has worked at the International Institute for Aerospace Survey and Earth Sciences (ITC) in Enschede and Delft, The Netherlands, and he is now Associate Professor responsible for the Engineering Geology Branch of ITC. He also has held an appointment since 1980 as Associate Professor at the Faculty of Mining and Petroleum Engineering at the University of Technology in Delft, where he is responsible for remote sensing and engineering geological mapping. Recently he has devoted himself to the application of geographic information systems to natural hazard zonation and geotechnical site mapping.*

Ir. Robert Soeters *graduated in 1965 from the University of Technology in Delft, The Netherlands, and obtained a degree in mining engineering with specialization in geology. He has been working since 1967 at the International Institute for Aerospace Survey and Earth Sciences in Enschede, The Netherlands, as a Senior Lecturer in Engineering Geology. He is responsible for the course management of applied geomorphology and engineering geology at the postgraduate level. He also acts as Project Supervisor in consulting projects. Since 1984 he also has held an appointment as Senior Lecturer in Engineering Geology at the University of Technology in Delft, where he has responsibility for subjects on Quaternary geology and engineering geomorphology.*

Drs. Cees J. van Westen *graduated in 1987 from the Department of Physical Geography at the University of Amsterdam in The Netherlands. Since 1988 he has worked at the International Institute for Aerospace Survey and Earth Sciences in Enschede, The Netherlands, as a Researcher preparing a doctoral thesis on the use of geographic information systems (GIS) for landslide hazard assessment. He is participating in projects on the use of GIS for hazard zonation and engineering geological mapping.*

by Peter J. Mouginis-Mark and Peter W. Francis

Satellite observations of active volcanoes: Prospects for the 1990s

Observations of volcanoes and volcanic eruptions worldwide are being made increasingly often by the use of sensors that are flown upon Earth-orbiting spacecraft. Particularly exciting are the new capabilities that enable remote measurements of the temperatures of lava flows and volcanic domes, the regional dispersal of eruption plumes, and the topography and structure of cloud-covered volcanoes in areas such as Indonesia, Central America, and the Aleutian Islands. These measurements will become an integral component of observations made by the National Aeronautics and Space Administration's Earth Observing System, due for launch in 1998, and will present new challenges in terms of data handling and the political aspects of volcano-hazard monitoring.

Introduction

The 1990s will see the use of many new remote sensing instruments in studies of volcanoes and volcanic eruptions. By providing access to a completely new range of observations, the instruments flown on satellites and aircraft will contribute significantly to our knowledge of both eruption processes and the impact of eruptions on the environment. By providing views of so many volcanoes so often, remote sensing techniques also provide entirely new means for monitoring volcanoes worldwide and thus of contributing to the mitigation of volcanic hazards. Space-based instruments provide a unique synoptic perspective on the massive perturbations to the atmosphere that are caused by large volcanic eruptions. Thus, in the decade ahead, the interaction between volcanism and the atmosphere will be one of several interdisciplinary studies that will draw geologists and other earth scientists into closer collaborations. Specifically, the monitoring of the dispersion of stratospheric aerosols from large eruptions will provide an important means of testing and refining the global circulation models that are critical to the current debates about atmospheric evolution and global climatic change.

This article reviews some of the satellite systems that are being used to study volcanoes, provides a summary of planned missions that will have a strong volcanology component, and discusses the implications of using remote sensing in order to identify and monitor volcanic hazards. A list of acronyms is provided in table 1.

Current capabilities

Mouginis-Mark and others (1989) reviewed the applications of many remote sensing techniques as they are applied to the analysis of volcanoes and volcanic terranes. Briefly, satellite and airborne sensors have been used already in the following types of volcanology investigations:

(1) Mapping the distribution of volcanic lithologies in remote areas (for example, Landsat TM studies of the central Andes: Francis and de Silva, 1989; de Silva and Francis, 1990);
(2) Identifying potentially active volcanoes and characterizing their styles of activity (de Silva and Francis, 1990);

Table 1.—Acronyms

Acronym	Full name
ADEOS	Advanced Earth Observing Satellite
ARGOS	Data storage and forward channel on European satellites
ASTER	Advanced Spaceborne Thermal Emission and Reflection radiometer
AVHRR	Advanced Very High Resolution Radiometer
AVO	Alaskan Volcano Observatory
CVO	Cascades Volcano Observatory
EOS	Earth Observing System
EOSP	Earth Observing Scanning Polarimeter
ERS–1	European Remote Sensing satellite #1
GOES	Geostationary Operational Environmental Satellite
GSFC	Goddard Space Flight Center
GVN	Global Volcanism Network
HVO	Hawaiian Volcano Observatory
IAVCEI	International Association of Volcanology and Chemistry of the Earth's Interior
IDNDR	International Decade for Natural Disaster Reduction
IGBP	International Geosphere-Biosphere Programme
JERS–1	Japanese Earth Resources Satellite #1
MISR	Multiangle Imaging SpectroRadiometer
MLS	Microwave Limb Sounder
MODIS	Moderate Resolution Imaging Spectrometer
NASA	National Aeronautics and Space Administration
NOAA	National Oceanic and Atmospheric Administration
RIDGE	Ridge InterDisciplinary Global Experiment
SAGE III	Stratospheric Aerosol and Gas Experiment #3
SAR	Synthetic Aperture Radar
SeaWIFS	Sea-viewing Wide Field Sensor
SIR–A	Shuttle Imaging Radar experiment A
SIR–B	Shuttle Imaging Radar experiment B
SIR–C	Shuttle Imaging Radar experiment C
SPOT	Systeme Probatoire d'Observation de la Terre
TES	Tropospheric Emission Spectrometer
TIMS	Thermal Infrared Multispectral Scanner
TM	Thematic Mapper (Landsat)
TOMS	Total Ozone Mapping Spectrometers

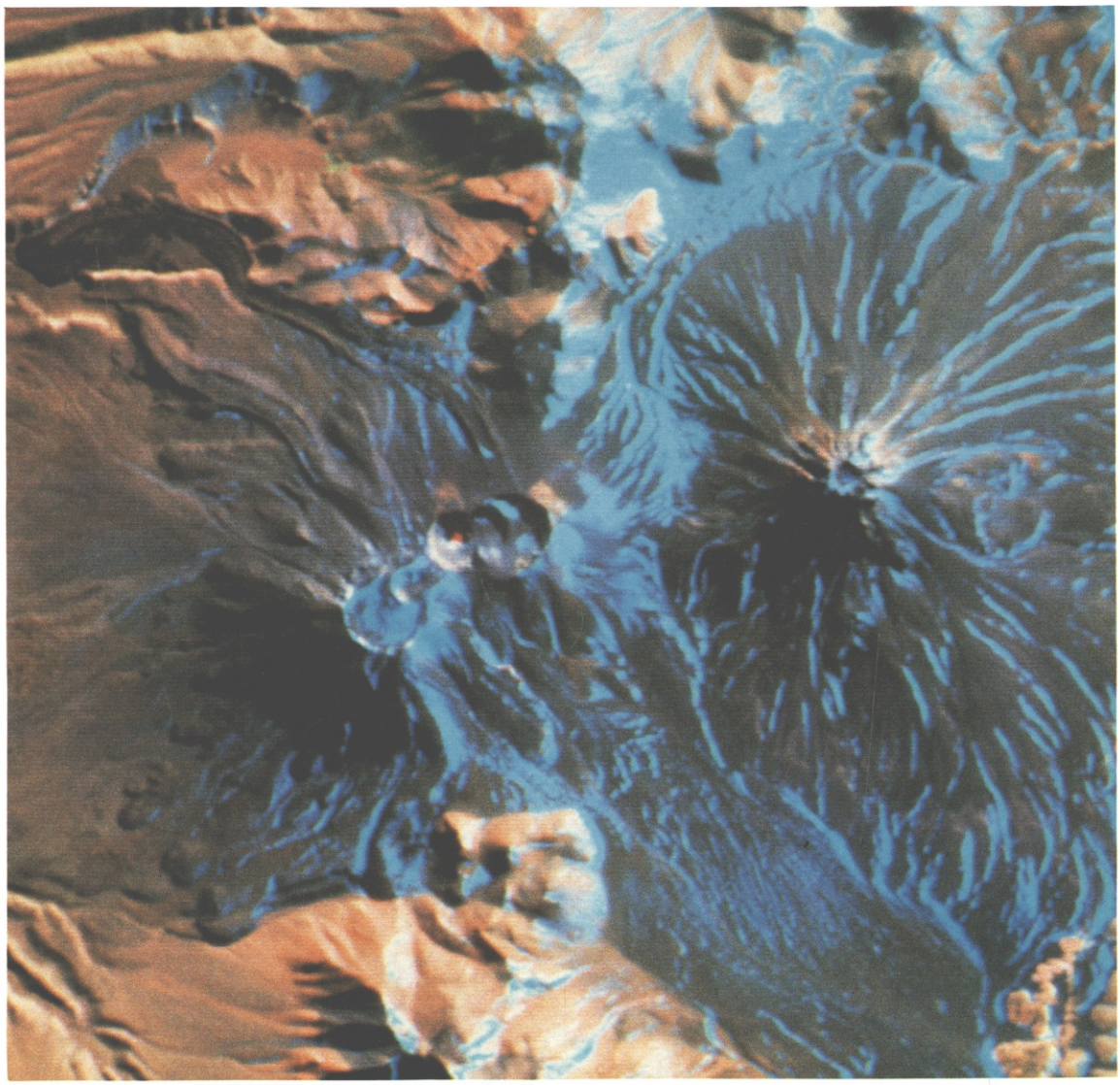

Figure 1.—Landsat 4 TM image of Lascar volcano, northern Chile, acquired March 11, 1985. TM bands 7, 5, and 2 are displayed in red, green, and blue, respectively. Active crater is at center of nested crater chain; thermal anomaly is observed in this image as a bright red spot. Prominent lava flow northwest of Lascar is thought to have erupted in the 19th century. Image width is equivalent to 15 km. Volcano on the right is Cerro Aguas Calientes (inactive).

(3) Identifying large volcanic debris avalanche deposits and the factors rendering volcanoes prone to collapse (Francis and Wells, 1988);
(4) Tracking the dispersal of major eruption plumes (AVHRR, TOMS: Matson, 1984; Krueger and others, 1990);
(5) Monitoring the thermal characteristics of lava flows, lava tubes, and volcanic domes (Landsat TM, TIMS, and AVHRR: Glaze, Francis, and Rothery, 1989; Pieri and others, 1990; S.K. Rowland and others, unpublished data, 1991);
(6) Investigating the spatial distribution of lava morphologies (SIR–B and aircraft radar) in order to aid rheological studies of the flows (Gaddis and others, 1990).

Volcanological applications of remote sensing techniques

Observations of Lascar volcano, northern Chile, provide instructive examples of volcanological applications of remote sensing techniques. Lascar is a 5,641-m-high volcano on the crest of the Andean chain in northern Chile (fig. 1). It has shown minor fumarolic activity throughout historic times, but no records of major eruptions exist. Because it is located at high altitude in a remote desert region, it has been difficult to obtain useful information on the condition of the volcano. When a powerful explosive eruption took place on September 16, 1986, the first reports reached the scientific commu-

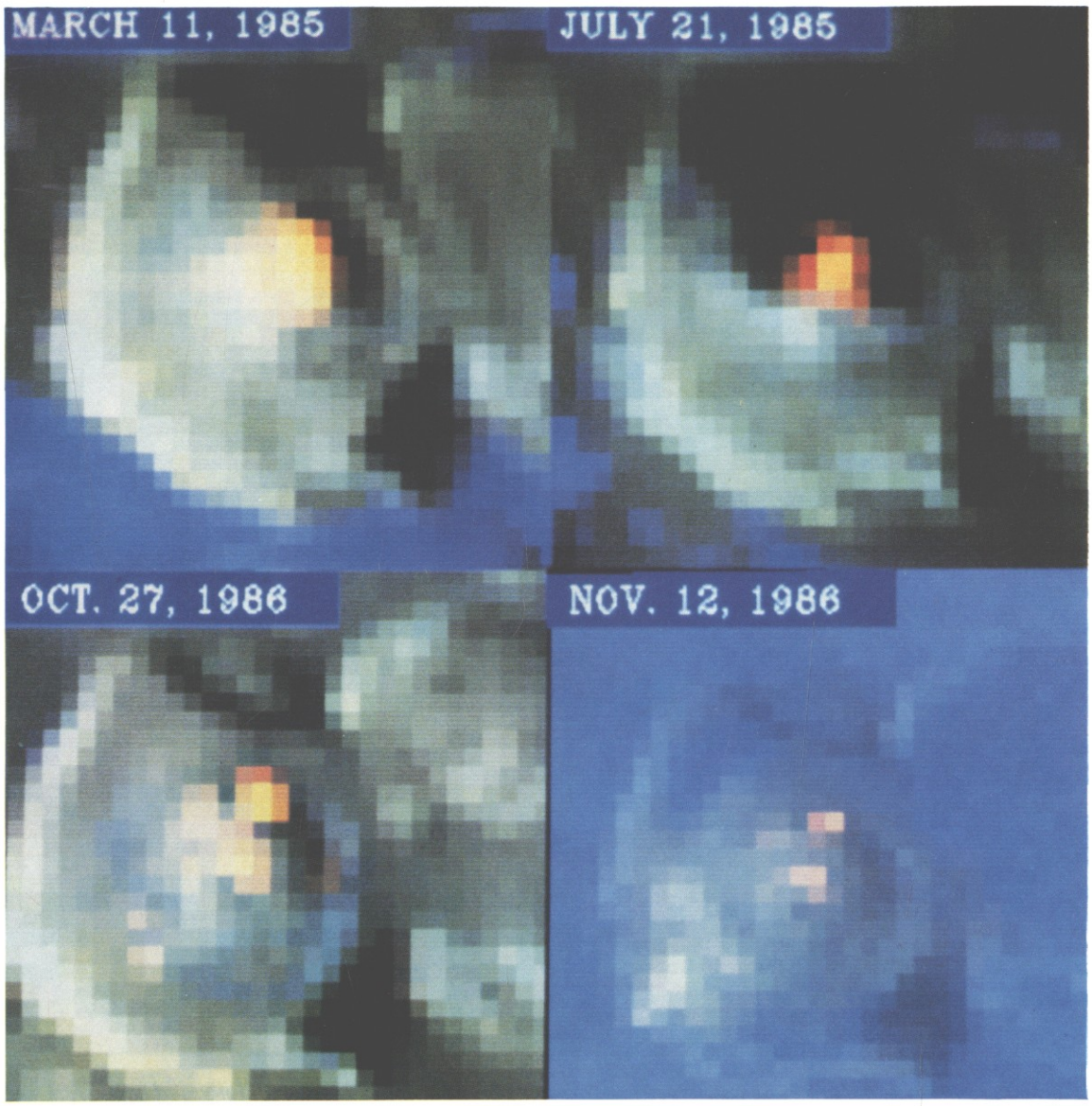

Figure 2.—Subscenes from Landsat 4 TM images showing the temporal evolution of the thermal anomaly within Lascar crater. Width of each subscene is equivalent to 1 km. Dates of acquisition are March 11, 1985; July 21, 1985; October 27, 1986; and November 12, 1986. The major eruption took place 41 days before the October 27 scene was obtained.

nity not from the vicinity of the volcano but from Salta in Argentina, almost 300 km distant, where ash fall was recorded. Two aspects of Lascar's activity have been monitored by the use of satellite sensors that have quite different spectral, spatial, and temporal resolutions. We emphasize, however, that none of these sensors were designed specifically for the analysis of volcanoes; Landsat, for instance, has agriculture and land use as its primary investigations.

Landsat

Near-infrared Landsat TM images having a spatial resolution of 30 m have been used to monitor radiant thermal energy from Lascar volcano on a number of occasions over a period of 7 years. Evidence of previously unsuspected thermal activity at Lascar was discovered serendipitously during examination of a Landsat TM image of the area for another purpose. At this time, an anomaly covering only about 20 pixels in TM bands 5 (1.55–1.75 μm) and 7 (2.08–2.35 μm) was revealed as a bright spot in the center of Lascar's active crater (Francis and Rothery, 1987). In a subsequent study, Rothery and others (1988) determined that the temperature of the anomaly was in the range 800–1,000 °C, which is clearly consistent with magmatic temperatures and possibly was related to hot lava within the summit crater or to high-temperature fumaroles. In order to monitor the thermal flux from the volcano, retrospective and contemporary TM images have been acquired that span the date of the 1986 eruption from 1984 to the present day (fig. 2). Prior to the 1986 eruption, the radiant thermal energy flux showed a marked decrease. Immediately after the eruption, the anomaly, previously a single well-defined entity, appeared weak and fragmented into smaller centers. In subsequent months, radiant thermal energy flux increased

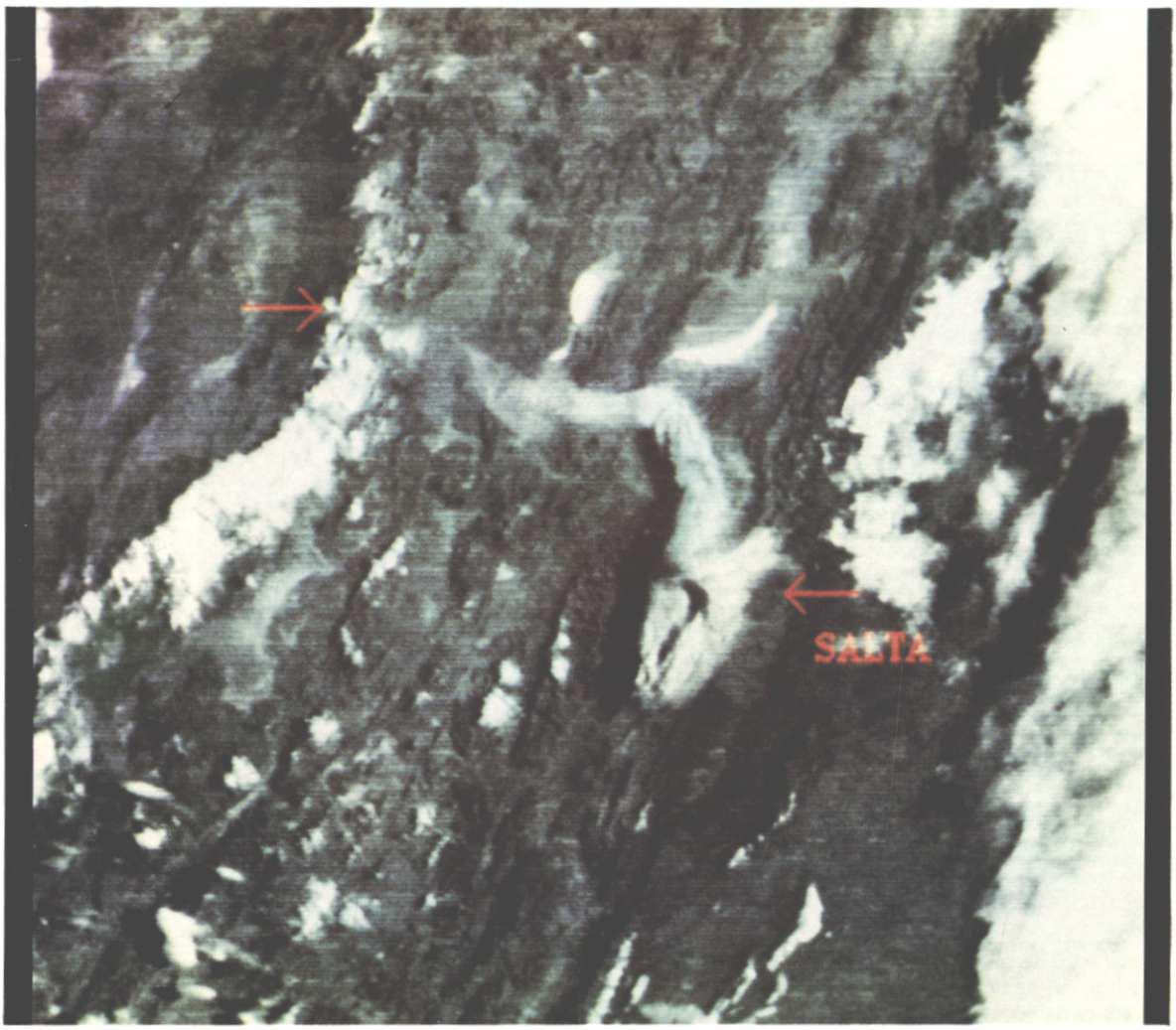

Figure 3.—GOES image collected at 12:12 UT (Chilean time=UT minus 4 hours), September 16, 1986, taken with the visible band, showing the eruption plume near the town of Salta approximately 93 minutes after the eruption. Lascar volcano is marked by the unlabeled arrow. North is to the top. Width of image is ~550 km.

dramatically, and it reached unprecedented high levels in 1988, which indicated that Lascar was in an unusually active state. Field investigations in 1987 and 1988 revealed a growing andesitic lava dome in the summit crater. This was the first record of lava extrusion in the central Andes and the first time that any such event had been detected exclusively by the use of remote sensing techniques. Thermal monitoring of Lascar and other volcanoes continues. An important research objective thus lies in characterizing the thermal signatures of different kinds of volcanic phenomena and in determining how thermal data can be used best in the assessment of likely future volcanic activity.

GOES

1.2 km resolution visible (0.55–0.75 μm) images acquired every 30 minutes from the GOES geostationary satellite were used to monitor the downwind dispersal of the September 16 eruption cloud from Lascar volcano (Glaze, Francis, Self, and Rothery, 1989). The eruption of Lascar, which took place at 10:39 UT (universal time) (+2 minutes) on September 16, 1986, lasted less than 5 minutes and produced a Vulcanian-type eruption column that rose to a height of about 15 km and was borne downwind rapidly. Ground observations and GOES images showed that the eruption plume formed a discrete extended slug about 2 km thick at altitudes between about 10 and 14 km and passed over the city of Salta, Argentina, 285 km distant from Lascar, less than 2 hours after the eruption (fig. 3). The velocity of the leading edge of the cloud was derived from its position on successive GOES images, and its altitude was determined from shadow length measurements to be ~14.5 km (Glaze, Francis, Self, and Rothery, 1989). By 14:12 UT, the plume had diffused, having traveled 400 km in 3.5 hours, and covered an area greater than 100,000 km^2. Thermal infrared GOES images were used to measure the plume temperature at different points along its track. The temperature at the top of the plume 1 hour after the eruption was −40.2 °C, which corresponds with an altitude inferred from radiosonde data to be 10.6 km, significantly lower than that derived by shadow measurement. This unexpected discrepancy has focused research on various aspects of volcanic plume physics. Understanding of the ascent and dispersal of volcanic plumes will be of first importance not only for volcanological studies but also for broader problems of atmospheric circulation. Additionally, the Lascar study drew attention to a more immediate problem: the rapid downwind transport of the ash

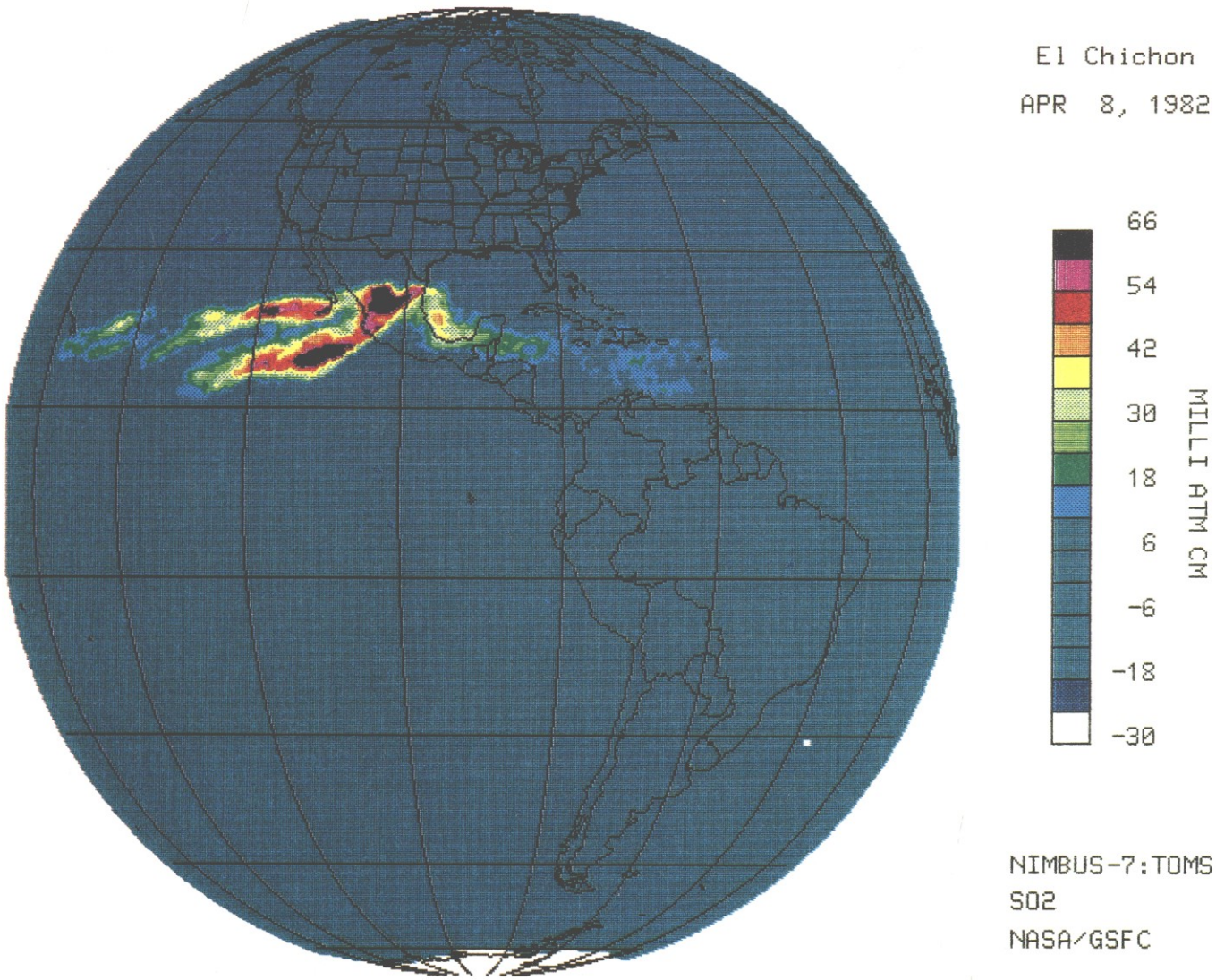

Figure 4.—The dispersal of the sulfur dioxide cloud from the eruption of El Chichón volcano was mapped by the TOMS instrument on Nimbus 7, April 8, 1982. Abbreviation: MILLI ATM CM, milliatmosphere, in centimeters. Image provided by L. Walter, Goddard Space Flight Center, Greenbelt, Maryland, USA.

cloud could abruptly place at risk aircraft flying to and from cities such as Salta, far removed from the volcano. Incidents where large passenger aircraft have lost power in all engines after unexpectedly entering an ash cloud, such as that of Redoubt Volcano, Alaska, in 1990, demonstrate the major hazard that such plumes present and the urgent need to develop means of providing rapid warning of their location (Steenblik, 1990).

GOES (East) and GOES (West) geostationary satellites and the polar-orbiting NOAA 7 satellite also were used earlier to monitor the dispersal of a far larger eruption cloud, one that was injected into the stratosphere. An eruption of El Chichón volcano, southern Mexico, in April 1982 took the lives of many hundreds of people who were living on the flanks of the volcano (Rampino and Self, 1984). Just before the eruption of April 3, the wind in the stratosphere began to blow in its summer pattern from the east. A dense aerosol plume from the eruption, centered at about 20° N., reached Hawaii by April 9, Japan by April 16, and the Red Sea by April 20, and it encircled the Earth completely by April 26. The cloud traveled westward at an average speed of about 20 m per second but expanded rather little to north and south and only covered about 25 degrees of latitude (Kent and McCormick, 1988).

TOMS

On board the Nimbus 7 satellite, the TOMS instrument normally is used to measure the level of ozone absorption in the upper atmosphere at ultraviolet wavelengths. Because sulfur dioxide also absorbs at two wavelengths near 0.3 μm, it too can be detected with the TOMS. TOMS data, for example, were used to map the distribution of sulfur dioxide from the El Chichón eruption (fig. 4). As much as 3.3 million tons of gaseous sulfur dioxide appear to have been injected into the stratosphere during this event (Krueger, 1983). Within 3 months of the El Chichón eruption, all of this sulfur dioxide appears to have been converted to sulfuric acid, which, in the form of

an aerosol, is the medium that mostly is responsible for the attenuation of solar radiation and consequent surface cooling and weather effects observed after large volcanic eruptions. (Ash particles fall out relatively rapidly). El Chichón's aerosol cloud may have caused a reduction in average monthly temperatures of about 0.2 °C in June 1982. Data from TOMS experiments also have been used to track the aerosols that were generated by several other major explosive eruptions, such as the 1985 eruption of Nevado del Ruiz, Colombia (Krueger and others, 1990).

AVHRR

The NOAA AVHRR is operating today on three spacecraft, NOAA–9, 10, and 11. These meteorological satellites are designed primarily for synoptic mapping of clouds and ocean-surface temperatures measuring radiance at visible to near-infrared (0.55–1.10 μm), mid-infrared (3.55–3.93 μm), and thermal infrared (10.3–12.5 μm). The AVHRR sensor has a spatial resolution of ~1 km. Because each satellite can observe an area on the Earth's surface twice each day (once during the day and once at night), it is possible to compile a high temporal-resolution data base of dynamic phenomena. Several scenes of an area may be obtained each 24 hours (the exact number of images depending upon the latitude of the target), which permits the rate of dispersal of a volcanic plume or the advance of lava flows to be monitored (S.K. Rowland and others, unpublished data, 1991). Thermal anomalies due to ongoing volcanic eruptions, such as the Pu'u O'o and Kupaianaha eruptions on the southeast flank of Kilauea volcano in Hawaii (fig. 5), thus can be studied in order to determine the evolution of a lava flow field over a period of weeks to months. The locus of surface activity has been seen to move from the Pu'u O'o and Kupaianaha vents down to the midlevel break in slope, where compound lava flows occasionally break out to the surface, and on to the coast, where the individual lava flows reach the ocean. Although these Hawaii AVHRR measurements do not replace the more detailed local measurements of the movement of flows as determined on the ground, they do demonstrate the advantage of using daily satellite measurements to track the large-scale motion of lava flows should they be detected on volcanoes that are less well monitored than those in Hawaii.

SAR

Optical and infrared sensors such as the Landsat TM and AVHRR have the major disadvantage that they only can observe a volcano during cloud-free conditions. Microwave sensors such as SARs do not suffer from this limitation and offer complementary information to the optical sensors for monitoring volcanoes. In volcanology, SARs have been used only in an exploratory manner until now. Data collected during the space shuttle radar flights in 1981 (fig. 6) and 1984 have been used to map the distribution of lava flows, cinder cones, and fault zones (see, for example, Gaddis and others, 1989). Starting in September 1991 with the operation phase of ERS–1, SAR data for the volcanoes in the Aleutian Islands and on the Alaskan peninsula will be obtained every 35 days (the timing of the spacecraft's repeat orbit). Topographic and deformation maps of these volcanoes will be compiled by using radar interferometry techniques (Gabriel and Goldstein, 1988; Gabriel and others, 1989) in order to search for dome growth, the formation of new lava flows or cones, or changes in summit ice cover that might be related to the onset of volcanic activity.

Earth Observing System (EOS)

Over the next decade, a major effort in remote sensing in volcanology will be 1 of 28 interdisciplinary investigations for EOS, due to be launched by NASA starting in 1998 (Mouginis-Mark and others, 1991). EOS is an ambitious "Mission to Planet Earth" and is intended to deploy NASA's unrivaled expertise in the scientific exploration of remote planets to a broad range of problems that are related to global change on Earth. The volcanological investigation, which includes about 20 volcanologists and remote sensing specialists in the United States and United Kingdom, will include both long-term and short-term monitoring of selected volcanoes, the detection and analysis of precursor activity associated with eruptions, and the monitoring of ongoing eruptions.

The data collected by EOS will allow two aspects of volcanism to be addressed. First, it will further our knowledge about the distribution of volcanic landforms, their temporal evolution, and the nature of the potential hazards posed by individual volcanoes. Second, it will provide a means for documenting, both in the immediate vicinity of the volcano and on a hemispheric scale, the compositions, flux rates, and total atmospheric budgets of the gases, particulates, and aerosols that are injected into the atmosphere by volcanoes. This category of EOS interdisciplinary investigations also will address the links between the magnitude and style of specific eruptions and the other components of the Earth system, such as the distribution of sea-surface temperatures, weather, short-term climate, and different ecosystems.

A variety of instruments on the NASA EOS platforms, together with additional data from NOAA and Japanese platforms, will enable the study of local to regional scale thermal and topographic features of volcanoes, and these will complement ground-based studies. On a larger scale, the same instruments will permit the study of the chemical and structural features of volcanic eruption plumes and aerosols, a critically important area of investigation that can be addressed only by using the synoptic view that is provided by spacecraft. Studies of the composition of plumes are particularly important because, at the present time, little is known about the rates at which gases other than sulfur dioxide are transmitted to the atmosphere by volcanic activity. The determination of the fluxes of H_2O, HCl, CO_2, and H_2S would be especially valuable.

The principal instruments on EOS that will be used for volcanology include the following:

(1) MODIS will obtain daily synoptic visible to near-infrared data at 1-km resolution, will be used for the detection of new eruptions by the identification of thermal and SO_2 anomalies, and will track the dispersal of plumes.

(2) The EOS SAR will not only provide images of ongoing eruptions under day and night and all weather conditions but will also permit (by the use of interferometry) the generation of topographic maps of volcanoes and the study of topographic change. This last attribute will detect the emplacement of a new lava flow or cone, will measure the swelling of a volcanic dome or rift zone, and will enable temporal studies of lava effusion. Imaging radar studies of volcanoes are now in their infancy, but given the facts that many volcanoes in tropical latitudes are frequently covered by clouds and that others at high latitudes are in darkness for long periods, imaging radars ultimately are likely to prove crucial to the successful development of routine volcano-monitoring techniques.

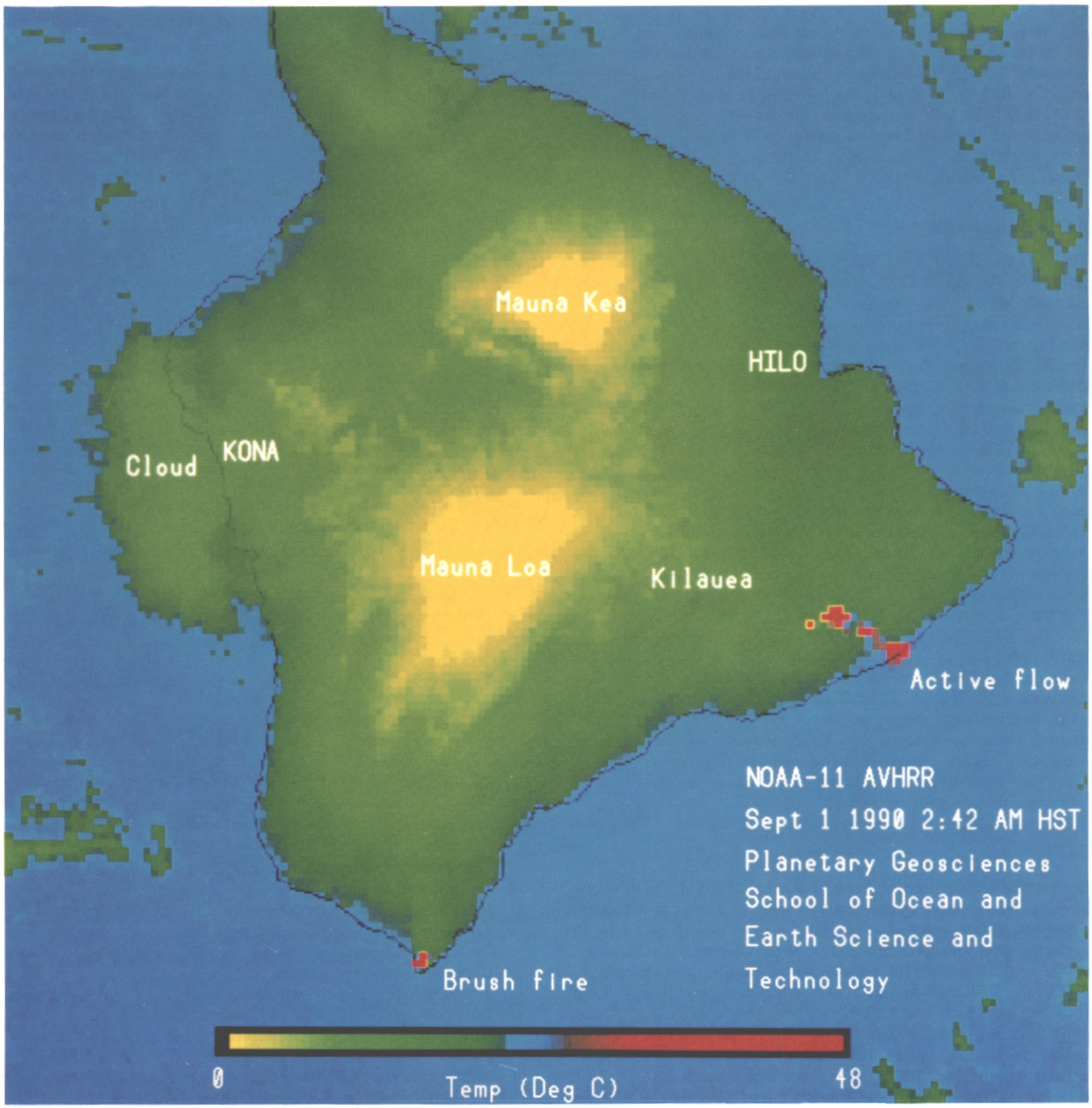

Figure 5.—AVHRR image of Kilauea volcano, Hawaii, obtained by the University of Hawaii on September 1, 1990. This nighttime thermal infrared scene (11.5–12.5 μm), obtained at 2:42 a.m. local time (HST, Hawaiian standard time), has been processed to show surface temperatures between 0 and 48 °C (see temperature bar at bottom). The active lava flow (east side of island) and a brush fire (extreme southern tip of island) were both detected in these data that have 1-km spatial resolution. The Big Island of Hawaii is ~130 km in an east-west direction. Mauna Loa and Mauna Kea volcanoes appear yellow in this rendition because of their height and resultant cold temperatures. A large cloud (green) is indicated off the west coast at Kona. Image provided by P. Flament and H. Garbeil, University of Hawaii, Honolulu, Hawaii, USA.

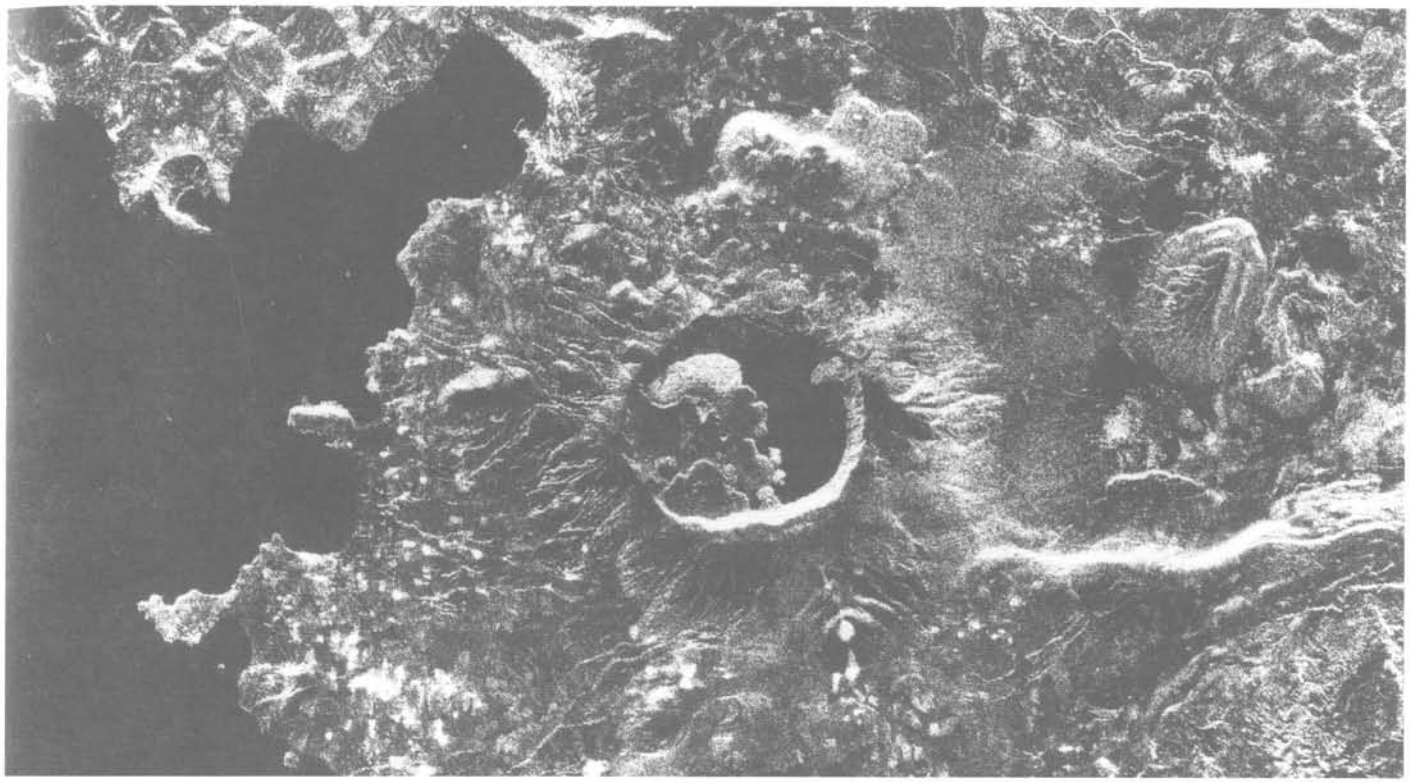

Figure 6.—Nemnut Dagi caldera (center) and Lake Van (black area at left) in southeastern Turkey were imaged by the SIR–A radar experiment, flown on the space shuttle in November 1981. The caldera is 5×9 km in diameter and shows several radar-bright flows within its interior. Several parasitic lava domes and cones are also visible in this image. Radar look direction is from the top. SIR–A data take 35/36.

(3) The ASTER instrument is a set of three sensors that will operate in the visible to near-infrared and thermal infrared, and it will obtain 15 m/pixel stereo images in the visible part of the spectrum. ASTER will be used to study lava flow and eruption plume temperatures and the topography of volcanic cones and plumes, and it will be the principal instrument for monitoring volcanoes for changes in fumarole distribution and temperature (at relatively low temperatures, that is, <100 °C), which may be precursors of new activity.

(4) Several EOS instruments also will be used extensively to study volcanic gases. MISR, SAGE III, and EOSP will be used for distribution studies of volcanic aerosols. Particularly in the case of MISR, high-resolution (~250 m/pixel) stereo images of volcanic plumes will be obtainable, and the distribution of tropospheric aerosols will be determined from their light-scattering properties at multiple viewing angles. TES will be able to measure tropospheric SO_2, CO, COS, H_2S, and HCl and qualitative amounts of H_20 and CO_2. Vertical profiles of SO_2 (between 15 and 30 km in altitude) and HCl (15–60 km) will be obtainable from MLS.

Other satellite missions

Prior to the launch of EOS, existing polar-orbiting remote sensing satellites, such as Landsat 5, SPOT, and meteorological satellites, will continue to provide valuable data. It will also be possible to use experiments flown on the space shuttle and other satellites to collect data on volcanoes. Three radar systems (JERS–1, ERS–1, and Radarsat) will be flown in the 1991–1994 timeframe, and the space shuttle will carry the third Shuttle Imaging Radar (SIR–C) experiment in 1993 and 1994. From the shuttle, volcanoes in Hawaii, the Galapagos Islands, the Indian Ocean, and the Andes will be imaged. From ERS–1, the topography and morphology of volcanoes in the Aleutian Islands also will be investigated.

Atmospheric studies will continue to be an important part of volcanology investigations from satellites even before EOS is launched. Although the primary objective of the TOMS instrument is the measurement of ozone, this instrument has been used successfully since 1978 on the Nimbus-7 spacecraft to study the SO_2 released into the stratosphere by major eruptions. A series of TOMS instruments is planned for launch starting with the Soviet Meteor-3 spacecraft in 1991 and is to be followed by a dedicated Earth Probe satellite in 1993 and the Japanese ADEOS satellite in 1995. SAGE III, which will measure the stratospheric aerosol concentration, either will fly on an Earth Probe-class satellite in the middle 1990s or will be part of an EOS platform.

The SeaWIFS, which is an 8-band visible to near-infrared radiometer, is scheduled for launch in late 1993 and may provide the first opportunity to search for shallow marine eruptions on the basis of the resultant discoloration of the sea surface.

Issues related to satellite monitoring of volcanoes

The advent of satellite investigations of volcanoes and volcanic eruptions anywhere in the world, sometimes in near real-time, raises

several important administrative and political issues. The geological remote sensing community rarely has had to face these issues, but they are encountered commonly by volcanologists in the field (Tilling, 1989). Some of these issues follow.

Involvement of local scientists and government authorities

How do we involve local scientists and government authorities? Access to satellite data does not make an investigator in a laboratory an immediate expert on a remote volcano. Given the volume and breadth of remote sensing data that EOS will provide, it should be possible to monitor remote volcanoes, to detect changes in volcanic activity, and when experience has been accumulated over many years, to detect precursors of some kinds of eruption. But understanding or even predicting the eruptive behavior of a volcano is a separate issue from assessing the hazard that an eruption might present because a volcanic hazard involves many more complex issues, such as timing and topography. Remote sensing techniques may be able to show, for example, that temperatures on a previously dormant volcano have increased significantly and that an eruption may take place within days or weeks. But predicting eruptions is only part of the problem. Several of the worst volcanic disasters in history have taken place on volcanoes that already were very obviously active, such as Mt. Pelée in Martinique in 1902. In such instances, the volcanic hazard arises from very sudden, short-lived events, such as the eruption of nuées ardentes.

Thus, the unique perspective given by spacecraft observations cannot necessarily provide the remote sensing volcanologist with the range of measurements and local knowledge that are required to interpret the behavior of an individual volcano and then provide useful advice to local authorities on potential volcanic hazards. Indeed, local geologists will continue to provide essential information from firsthand observations and the details of the eruptive history of a volcano. Previous volcanic crises have demonstrated that casual interactions with local authorities, the usual modus operandi of scientists, can lead to serious misunderstandings. Investigators working with remote sensing data will find it essential, therefore, to focus on specific areas of investigation that will be carried out in collaboration with local scientific institutions and officials and will be formalized through appropriate protocols. Within the framework of EOS investigations, the lack of real-time data will constrain most investigations to basic research and data gathering, rather than hazard assessment and prediction.

Coordination with similar programs

The EOS volcanology project is not synonymous with NASA's efforts in volcanology, nor is it the only program that will study volcanoes in remote parts of the world. Coordination with the Smithsonian Institution's GVN (Washington, D.C., USA) and the U.S. Geological Survey's volcano observatories (HVO, AVO, CVO) will be essential if the broader U.S. community is to take full advantage of the modern sensors. Similarly, cooperation between the U.S. programs and international groups that are interested in volcanic hazards would benefit from a formal definition of roles, data exchanges, and collaborative research.

Cooperation with international programs

Several international programs could interface with the U.S. satellite volcanology experiments. For example, the potential use of the existing French ARGOS system in order to monitor volcanoes and provide "early warning" of anomalous behavior of selected volcanoes on a global basis could provide the early information that is necessary for retargeting the spacecraft sensors.

Linkage with other disciplines

The EOS volcanology investigation fits well within the overall goal of the EOS project, which is to study the regional and global interrelationships among components of the Earth system, because it specifically investigates the links among volcanism, atmospheric chemistry, and short-term (1–3 year) climate change. Linkage between these EOS studies and other international programs is also a possibility, but the precise mechanism for coordination remains unclear. For example, many volcanoes around the world could be monitored in detail by using the EOS satellite sensors. An obvious group of volcanoes to be studied could be those selected specially as "Decade Volcanoes" by the IAVCEI for the IDNDR. The IGBP and RIDGE could interface with the NASA studies of volcanism and volcano-climate interactions. However, interagency planning and, probably, joint funding of research programs most likely would be required in order to develop these interdisciplinary ties substantially.

Conclusions

Remote sensing offers the potential for significantly increasing our knowledge of volcanoes around the world, as well as for collecting data of uniform quality over sufficiently large areas that will allow us to interpret volcanic processes such as eruption plume dynamics and the growth of lava flow fields. Certain measurements, such as the ones that give us the ability to use SAR to map the distribution of topographic change over areas of several hundred square kilometers on cloud-covered volcanoes, also offer the promise (as yet unproven by actual measurements on volcanoes) of significant new types of measurements. A crucial issue presented by this unprecedented volume of data is the ability of earth scientists to access and interpret the information in a timely manner. We hope that the whole scientific community will have free access to the EOS data set, but in many instances, the ability to locate the appropriate information within the data archive, obtain the calibrated data sets, and make timely use of the data will be a challenge for the foreseeable future. In addition, particularly in the case of volcanic hazard monitoring, the strong links between the remote sensing expert on one hand and the volcanologists and local civil defense experts on the other have to be developed with care and respect for the roles and abilities of the respective groups. Remote sensing of volcanoes will make the greatest contribution to the earth sciences if the resulting information is used in conjunction with the detailed knowledge of the region that is derived by volcanologists in the field.

Acknowledgments

Research described in this article was supported under grants from NASA's Geology Program (NAGW–1162 and NAGW–1929) and the Earth Science and Applications Division (NAS5–33012). This is Planetary Geosciences Paper No. 664 and the School of Ocean and Earth Science and Technology Contribution No. 2664 of the University of Hawaii, Honolulu, Hawaii, USA.

References

de Silva, S.L., and Francis, P.W., 1990, Potentially active volcanoes of Peru—Observations using Landsat Thematic Mapper and Space Shuttle imagery: Bulletin of Volcanology, v. 52, p. 286–301.

Francis, P.W., and de Silva, S.L., 1989, Application of the Landsat Thematic Mapper to the identification of potentially active volcanoes in the Central Andes: Remote Sensing of Environment, v. 28, p. 245–255.
Francis, P.W., and Rothery, D.A., 1987, Using the Landsat Thematic Mapper to detect and monitor active volcanoes: An example from the Lascar volcano, northern Chile: Geology, v. 15, p. 614–617.
Francis, P.W., and Wells, G.L., 1988, Landsat Thematic Mapper observations of large volcanic debris avalanche deposits in the Central Andes: Bulletin of Volcanology, v. 50, p. 258–278.
Gabriel, A.K., and Goldstein, R.M., 1988, Crossed orbit interferometry: Theory and experimental results from SIR–B: International Journal of Remote Sensing, v. 9, p. 857–872.
Gabriel, A.K., Goldstein, R.M., and Zebker, H.A., 1989, Mapping small elevation changes over large areas: Differential radar interferometry: Journal of Geophysical Research, v. 94B, p. 9183–9191.
Gaddis, L.R., Mouginis-Mark, P.J., and Hayashi, J.N., 1990, Identification of lava flow surface textures: SIR–B radar image texture, field observations, and terrain measurements: Photogrammetric Engineering and Remote Sensing, v. 56, p. 211–224.
Gaddis, L.R., Mouginis-Mark, P.J., Singer, R.B., and Kaupp, V., 1989, Geologic analyses of Shuttle Imaging Radar (SIR–B) data of Kilauea Volcano, Hawaii: Geological Society of America Bulletin, v. 101, p. 317–332.
Glaze, L.S., Francis, P.W., and Rothery, D.A., 1989, Measuring thermal budgets of active volcanoes by satellite remote sensing: Nature (London), v. 338, p. 144–146.
Glaze, L.S., Francis, P.W., Self, S., and Rothery, D.A., 1989, The Lascar September 16, 1986, eruption: Satellite investigations: Bulletin of Volcanology, v. 51, p. 149–160.
Kent, G.S., and McCormick, M.P., 1988, Remote sensing of stratospheric aerosol following the eruption of El Chichón: Optics News, May, p. 11–19.
Krueger, A.J., 1983, Sighting of El Chichón sulfur dioxide clouds with the Nimbus 7 Total Ozone Mapping Spectrometer: Science, v. 220, p. 1377–1379.
Krueger, A.J., Walter, L.S., Schnetzler, C.C., and Doiron, S.D., 1990, TOMS measurement of the sulfur dioxide emitted during the 1985 Nevado del Ruiz eruptions: Journal of Volcanology and Geothermal Research, v. 41, p. 7–15.
Matson, M., 1984, The El Chichón volcano eruptions—A satellite perspective: Journal of Volcanology and Geothermal Research, v. 23, p. 1–10.
Mouginis-Mark, P.J., Rowland, S., Francis, P., and others, 1991, Analysis of active volcanoes from the Earth Observing System: Remote Sensing of Environment, v. 36, p. 1–12.
Mouginis-Mark, P.J., Pieri, D.C., Francis, P.W., Wilson, L., Self, S., Rose, W.I., and Wood, C.A., 1989, Remote sensing of volcanos and volcanic terrains: EOS (American Geophysical Union Transactions), v. 70, no. 52, p. 1567, 1571, 1575.
Pieri, D.C., Glaze, L.S., and Abrams, M.J., 1990, Thermal radiance observations of an active lava flow during the June 1984 eruption of Mount Etna: Geology, v. 18, p. 1018–1022.
Rampino, M.R., and Self, S., 1984, The atmospheric effects of El Chichón: Scientific American, v. 250, p. 48–57.
Rothery, D.A., Francis, P.W., and Wood, C.A., 1988, Volcano monitoring using short wavelength infrared data from satellites: Journal of Geophysical Research, v. 93B, p. 7993–8008.
Steenblik, J.W., 1990, Volcanic ash: A rain of terra: Journal of Airline Pilots Association, v. 59, no. 6, p. 9–15.
Tilling, R.I., 1989, Volcanic hazards and their mitigation: Progress and problems: Reviews of Geophysics, v. 27, p. 237–269.□

Peter Mouginis-Mark *is a Professor of Geology and Geophysics at the University of Hawaii at Manoa, Hawaii, USA, and is the Director of the Hawaii Space Grant College program. His interests lie in the geomorphic analysis of landscapes on Mars, Earth, and Venus, especially the features produced by volcanism. He also is deeply involved in educating future generations of space explorers through school programs and public outreach. Pete is Team Leader for the NASA Earth Observing System's interdisciplinary Volcanology Team and is a member of the Space Shuttle Imaging Radar (SIR–C), ERS–1 radar, and JERS–1 verification teams. His field experience has included volcanological research in Hawaii, Iceland, the western Galapagos Islands, northeastern Chile, Réunion Island, Sicily, and the Canary Islands.*

Peter Francis *is a Reader at the Open University in Milton Keynes, England, and a Visiting Scientist at the University of Hawaii. His research interests include over 20 years of field mapping and satellite investigations of Quaternary volcanoes in the central Andes, analyses of planetary volcanism, and the application of remote sensing to geologic problems. Peter is a member of the NASA Earth Observing System's Volcanology Team.*

by Robert E. Crippen

Measurement of subresolution terrain displacements using SPOT panchromatic imagery

Satellite-derived imagery can be used to measure subresolution horizontal terrain displacements that are associated with present-day earthquakes, sand dune migration, coastal processes, glacial motion, and, perhaps, preeruptive volcanic processes. This use of these data will increasingly facilitate the understanding of natural hazards and the determination of the rates of many environmental processes worldwide.

Introduction

Satellite image data provide maps of the surface of the Earth that are detailed, uniform, and spatially comprehensive over wide areas. These attributes allow researchers to use these data in order to solve significant problems in the earth sciences that are not practical to solve by any other means. Research is now underway to extend the use of satellite imagery to the detection and measurement of surface processes occurring at scales below the limits of resolution.

The premise of the method is that areally extensive, subresolution spatial differences in ground patterns between images acquired at differing times can be measured accurately to high precision and also can be distinguished from systematic image differences, such as those due to sensing-system attitude variations. The idea for this approach was conceived while considering the tectonic effects of the October 17, 1989, Loma Prieta ("San Francisco") earthquake and their possible effects upon image data (Crippen, 1990). Thus far, testing of a preliminary algorithm shows that the approach is reasonable.

The data currently used are from the French SPOT satellite, which has a "pushbroom" sensor array that provides 10-m panchromatic imagery. In some cases, the terrain displacements one may seek to measure may be a small fraction of the pixel size. In other cases, the displacements may exceed the pixel size, but one may seek subpixel precision. The general approach is to match spatially the "after" image to the "before" image at each point on a grid by iteratively interpolating one and testing its correlation with the other. The statistical sample of each image at each grid point is typically thousands of pixels. Spatial variations in the results correspond both to changes on the ground ("geometric signal") and to image distortions ("geometric noise"). However, most image distortions are attributable to sensor-attitude variations that can be identified and removed through recognition and measurement of their distinct spatial characteristics. This allows us the possibility of isolating and revealing patterns of environmental change.

Note that the objective is not to resolve subresolution objects, nor is it necessary to resolve subresolution objects. Instead, the goal is to detect and measure surface processes by matching statistically the radiometric patterns in the data that differ spatially in a consistent direction over many pixels.

Advantages of imageodesy

The name coined for this method is "imageodesy," which is both a concatenation of "image geodesy" and a partial acronym for "Image Multitemporal Analysis Geodesy." Clearly, there are limitations to the application of imageodesy, but it also has several potential advantages over currently available alternatives.

In the study of seismotectonic deformation along a fault, for example, comparable methods require the establishment of benchmarks at selected locations followed by labor-intensive surveys. In order to map the strain field associated with an earthquake, scientists must wait years, decades, or centuries for an earthquake to occur on that segment of that fault. In contrast, by using satellite image data, an earth scientist need not anticipate the time and location of an earthquake nor concentrate his effort in any one region in the hope of an opportunity to collect data (that is, an earthquake) during his lifetime. The before images are available and continue to accumulate in image libraries (collected by other people for other purposes at no cost to the imageodesist until needed), and the after images can be ordered as needed for any location in the world. Problems of accessibility due to terrain or political factors do not exist, and the data are spatially comprehensive.

Similar advantages of labor savings, spatial uniformity and detail, and global coverage and access are applicable to studies of sand dunes, coastal processes, glaciers, and volcanic processes. Significantly, imageodesy enhances the value of imagery collections as historical records of environmental change.

General approach

Fundamental concept

Basically, the imageodesy method relies upon the fundamental statistical concept of a normal distribution. The essence of this concept is that accurate and precise measurements can be obtained statistically from a set of measurements that are individually unreliable and even relatively crude. If measurements have errors that are random, then their probability distribution is symmetrical and bell-shaped and has a peak at the true value. If enough measurements are made, then the shape of the "bell" can be defined sufficiently well to determine the peak accurately. Thus, the probability of accuracy of the statistical determination (at any given level of precision) improves as the number of measurements increases.

Each pixel value is a measure of radiance weighted at subresolution scales by the point-spread function that is imposed by the atmosphere and sensor optics. Each pixel value is, therefore, variable in relation to its geographic position at subresolution scales and thereby indirectly measures geographic position. Imageodesy typically compares thousands of pixels in the before image to thousands of pixels in the after image in determining each displacement vector,

d it can, as a result, be capable of high accuracy at high levels of atial precision.

Clearly, the problem faced is not this simple. The measurement rors that must be overcome (radiometric and geometric noise in the iage) are not fully random, and other data inadequacies are possi-e. These difficulties are discussed in the "Sources of error" section.

asic algorithm

he idea for the procedure is an outgrowth of image-matching work iat was developed and used to register misaligned bands in a multi-pectral data set (Crippen, 1987). A vector is calculated at each node n a grid by the use of (for example) 1 square kilometer of data 10,000 pixels) from each image. Several improvements can be xpected as this research continues, but the basic correlation "hill limbing" routine for each vector, as used in initial tests, is as ollows. (1) The before and after scenes are best-fit matched to the earest pixel, as determined by visual inspection. (2) The before mage is used still as the mapping base and is held "constant." (3) For ach vector determination, 100×100 pixels of the before image are ompared statistically for maximum correlation to a moving template f 100×100 pixels in the after image, as follows.

For full-pixel steps:

(A) Correlation is determined at the starting (full-scene visual) match position and at the 24 neighboring full-pixel steps, which results in a 5×5 array of correlation coefficients.

(B) If the maximum correlation in the array is not at the starting match position, a vector is "drawn" (in effect) to the point of maximum correlation, and a new 5×5 array of correlation coefficients is calculated (without redundancy) at that point.

(C) Maximum correlation is determined again, and the vector is "redrawn," if necessary. (Further iterations are allowed but were not necessary in the initial tests. As verified visually, the best-fit starting position provided image registration to within a few pixels at all locations within the scene.)

For subpixel steps:

(A) Repeated bilinear interpolation of the after image is applied in order to create a set of images that are translationally shifted by half-pixel steps for comparison to the before image. These include the peak-correlation full-pixel shift location and its eight neighbors (a 3×3 array of correlation coefficients). The highest correlation in this array is determined, and the vector is "redrawn" to it, if necessary.

(B) Quarter-pixel image shifts that include the peak-correlation half-pixel shift location and its eight neighbors (again, a 3×3 array) are calculated, their peak correlation value is determined, and the vector is again "redrawn," if necessary.

(C) This routine is repeated in seven steps down to shift steps of 1/128 pixel (about 8 cm on the ground). Not surprisingly, 1/128 pixel appears to be well beyond the random noise level of precision, as shown by separate tests (see "Indication of precision limit" section).

After the full array of vectors across the image is generated, trends that are clearly attributable to differences in data collection between the before and after images are characterized and removed. If these trends are related to detector array distortions, then they are distinctly constant along the satellite path (and appear as differences among entire columns of pixels). If they are related to attitude variations through time, then they are distinctly constant across the satellite path (and appear as differences among entire rows of pixels). If they are related to static differences between scenes, such as a difference in scale, then they form distinctive two-dimensional patterns across the entire image. Thus, these trends are spatially distinct and generally can be removed in order to isolate and reveal image differences that are due solely to ground deformations.

Results of initial tests

A test site at the Superstition Hills, an arid area in southernmost California, USA, was chosen in order to attempt the detection of fault offsets related to the magnitude 6.6 earthquake on November 24, 1987. The maximum combined coseismic and postseismic offsets along the Superstition Hills fault for this quake are on the order of 1 m (McGill and others, 1989; Burgmann and others, 1989), which posed a challenge for the imageodetic method at its current level of implementation. The available before image was acquired by the SPOT–1 satellite on November 11, 1987, and the after image selected was acquired on February 21, 1989. Both scenes were acquired from nearly the same orbital position and so provided matching look angles. Although the dates were not optimal for matching the sun positions and other seasonal effects, the image dates were approximately symmetrical around the winter solstice such that the sun positions were similar. Also, the arid and rugged, yet fairly low relief, character of this terrain provided strong feature patterns that allowed us to match features statistically, and yet they minimized the impact of potential differences between the scenes.

Unfortunately, the fault offsets were not clearly distinguishable in the imageodetic results. This is likely due to the fairly simplistic implementation used thus far and to the small size of the offsets, which are only slightly larger than the best precision expected from the technique under optimal conditions. Several refinements to the technique, now under investigation, may prove critical to this particular tectonic application.

Fortunately, however, the imageodetic method was demonstrated successfully in this same image pair by the subresolution measurement of barchan and longitudinal sand dune migration in an area immediately west of the Superstition Hills. The dune movement was detected because the dunes and their shadows (in contrast with the underlying terrain) form the dominant radiometric patterns in this local area. Figure 1 shows the SPOT panchromatic imagery for the dune site (top) and displays the corresponding temporal difference vector pattern (bottom). Note that the large, anomalous vectors correspond distinctly to the geographic positions of the dunes, point downwind for the barchan dunes (as verified by dune morphology), and measure up to 7 m. This amount of movement is very reasonable for the timespan between the images (15 months) for dunes of this size (about 50–70 m across). Movements of one nearby dune (in an area likely to have stronger winds) have averaged 15 m per year over past decades (Shelton, 1966).

Error types and limitations

Sources of error

The primary challenge in this work is to overcome measurement errors of a wide variety such that adequate levels of precision and accuracy can be attained in the image comparisons. Sources of error are of two primary types: radiometric and geometric problems.

Errors due to radiometric problems result primarily from differences across the detector array, difficulty in detecting patterns in the image (signal-to-noise inadequacies), and radiometric changes in scene content between the dates of image acquisition. SPOT image data have very high radiometric quality; however, radiometric quality requirements for imageodesy are unusually high.

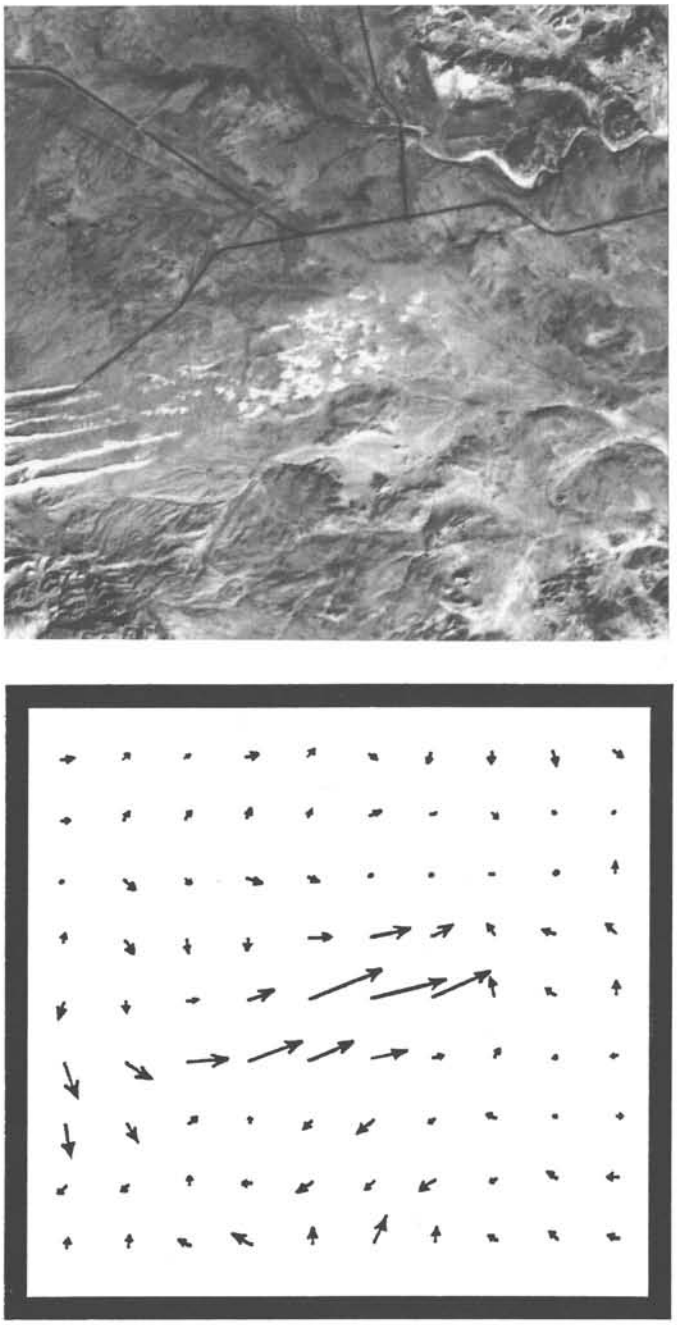

Figure 1.—Top: SPOT panchromatic image of Superstition Hills sand dune site in southernmost California, USA (average of before and after scenes). © CNES. Bottom: Vector ray of imageodesy results of dune site. Array spacing is 500 m, and vector exaggeration factor is 100. Note that anomalous vectors closely correspond to the dunes and indicate up to about 7 m of displacement. Background noise is mostly less than 1 m.

Minor differences across the detector array (which may be significant in some cases) are evident as vertical striping, especially in data that have been filtered to enhance high spatial frequencies. A time-variable error that results in horizontal striping is also evident. It may be possible to adjust for both of these error types by characterizing and correcting them on a column-by-column and row-by-row basis. In order to allow this and to avoid unnecessary image degradation due to resampling, imageodesy uses unrectified "level 1A" SPOT data.

An inherent limitation of the method is that patterns in the image data are required in order to conduct image comparisons. In some cases, the terrain will be flat and featureless and very difficult to match between images (signal variance will be inadequate). A map of correlation coefficients can be used to identify such problem areas, but it is unlikely that this problem can be fully solved. Fortunately, such areas are seldom of interest anyway.

Radiometric differences between the scenes can be a problem also. Natural vegetation can grow or die, drainage channels across alluvial terrains can migrate, and roads can be modified. In some cases, entirely new features will not be problems because they will not spatially match anything in the older scene and will not, therefore, spatially bias the correlation patterns (the peak correlation will decrease in magnitude but will not shift spatially). In general, however, major radiometric features should be identified by image differencing and then removed from the correlation procedures by image masking. In areas where radiometric change is pervasive (as, for example, agricultural fields), the subresolution matching of edges in the image (such as field boundaries) may be possible as an alternative procedure.

The problems of "geometric noise" also are critical but not insurmountable. Sun-angle and view-angle differences between scenes should be avoided. Shadows will not match between scenes having differing sun positions. Likewise, radial distortion of topographic features in images will differ between images of differing view angles. In many cases, one must, therefore, compare scenes taken from the same orbit path (SPOT is a pointable sensor) on approximately the same day of the year. SPOT is in a sun-synchronous orbit, so matches of time of day are not a problem.

The other major source of geometric noise results from sensor-attitude (and altitude) differences during the two periods of image acquisition. Variations between scenes in yaw, pitch, and roll (and scale) are all possible. Ancillary data on these variations are provided on SPOT digital data tapes and are described in the "SPOT User's Handbook" (CNES, 1988). However, the best way of dealing with these problems is to identify, measure, and remove their fairly distinct spatial patterns in the initial imageodetic results, as discussed in the "Basic algorithm" section. In initial tests, the primary differences were found to be constant (static) differences in yaw and scale and constantly changing (dynamic) differences in pitch and roll.

Indications of precision limit

The precision of image matching varies as a function of the image signal-to-noise ratio, the number of pixels involved, the image pattern textures, and the interpolation method (Forstner, 1982; Sutton and others, 1988). However, a general statement on precision may be possible.

Tests were used to map out broad arrays of correlation coefficients at each level of precision for a few sites. The resulting maps showed correlation increasing smoothly to a peak at the coarser levels of precision, but it increased irregularly at the finer levels of precision, and a transition took place at about 1/16 to 1/32 of a pixel. This may indicate the limit of precision for an accurate single-vector result, exclusive of the problems of broader image distortions and exclusive of image preprocessing steps or image-matching algorithm changes that possibly could improve these results.

Also encouraging is the work of other researchers who have used image matching and analyses in different contexts. Although they have used a variety of data types and processing routines,

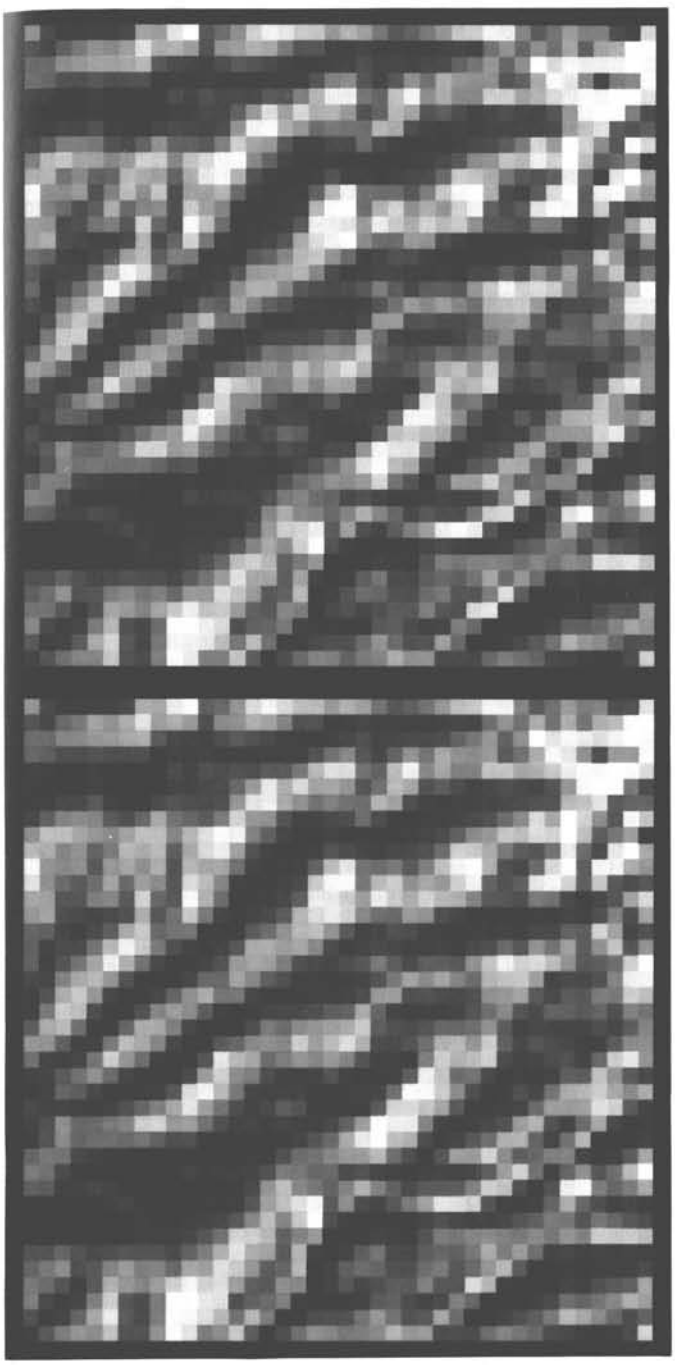

Figure 2.—Simulations of left-lateral (top) and right-lateral (bottom) subresolution fault offsets showing before images in cyan and after images in red. In each case, the fault is located at a color fringe boundary, and the sense of offset is indicated by the locations of color fringes relative to shadows (see text).

several have found a limit of precision at about 1/20 of a pixel (Qi and Huhns, 1986; Berenstein and others, 1987; Mort and Srinath, 1988; Morgan and others, 1989; Havelock, 1989; Lyvers and others, 1989; Li, 1990). A precision of 1/20 of a pixel corresponds to 50 cm on the ground. This precision would be extremely useful for many purposes.

Related image-analysis methods

In addition to vector calculations, at least two alternative methods are possible for determining relative displacements in multitemporal image pairs. Both involve coregistering the images as closely as possible (by subresolution resampling) in order to provide an overall best fit. One method is to flicker (temporally alternate) the two images (both in gray tones) on an image-display monitor at substantial enlargement so that individual pixels can be seen. The directions and magnitudes of subresolution shifts can be seen easily (barring major radiometric noise), although their significance may be difficult to ascertain in the context of image distortions resulting from attitude variations. The other method is simply to display the two images in complementary colors simultaneously and to judge the patterns of subresolution misregistrations as indicated by color fringes.

Two examples of the color fringe method are simulated in figure 2. A single SPOT image was used (thus avoiding radiometric and geometric noise) and was resampled in order to simulate a fault offset in the after image. The fault runs vertically as a north-south trace (north to the top) directly through the middle of the image, and displacements are uniform within the west block and within the east block. The before image is displayed in cyan (blue and green), and the after image is displayed in red.

In the upper simulation, movement along the fault is left lateral at one-half pixel (5 m), and the east block has been given perfect registration. Note that the color fringes in the west block demonstrate the general direction of offset (for example, bright red has moved relatively southward and impinged upon dark cyan, which has produced a red color fringe on the north side of each shadow). Also note that the location of the fault is evident as the eastern boundary of the color fringes. Thus, both the location of the fault and its sense of motion can be determined from the image pair, despite the subresolution amount of fault displacement.

In the lower simulation, movement along the fault is right lateral at three-fourths pixel (7.5 m), the west block again having a misregistration of one-half pixel (5 m) and the east block now having a misregistration of one-fourth pixel (2.5 m) in the opposite direction. Note that (1) the color fringes on the west block have reversed in color compared to the upper version (red fringes are now south of shadows), (2) on the same sides of shadows, the color fringes are opposites between the east and west blocks (cyan on the north side of shadows on the west block and red on the north side of shadows on the east block), and (3) the saturation of the color fringes is greater on the west block because of its greater offset (misregistration) amount. In this case, the fault can be located by the abrupt changes in the hue of given fringes as the fault is crossed, and the sense of motion can again be determined by the relative positions and hues of the fringes.

These techniques provide useful tools that augment the imageodesy vector method. The vectors provide statistically significant results that can be modeled to remove geometric noise and thereby obtain precise displacement magnitudes and directions over wide areas. Fault breaks in remote locations might be located by the vectors although only to within the 1-km breadth of the image-sampling area. Image-display methods can be used then to locate a fault to within one pixel (10 m for SPOT images).

Related studies and possibilities

Image analyses similar to imageodesy have been used previously in the study of cloud motions (Leese and others, 1971), sea-ice movements (Ninnis and others, 1986), sea-surface velocities (Emery and

others, 1986; Garcia and Robinson, 1989), and glacial ice streams (Bindschadler and Scambos, 1991). The purpose of the current work has been to develop this approach to a level that is useful for solving geologic problems, especially tectonic problems.

The particular challenge of tectonic problems is the small scale of deformation associated with even the largest tectonic events over short time intervals. Maximum fault offsets are typically no more than 8 m for even the greatest earthquakes. Thus, if we use 10-m resolution imagery, subresolution measurements are essential, which is not the case in the study of clouds, sea surfaces, or glaciers. Further, the lessons learned from the challenges faced in tectonic applications should prove to be valuable across the full spectrum of applications. The importance of the work lies in the understanding of natural hazards, such as earthquakes, and in the determination of the rates of environmental processes in general, particularly as concern grows about global change.

The range of possible applications of imageodesy varies according to sensor characteristics, particularly spectral sensitivities, spatial resolutions, and repeat coverage cycles. One interesting possibility is the acquisition of image pairs that are separated by only a few seconds and are used for the study of rapidly moving features. The SPOT satellite currently provides this capability. It has two image sensors per satellite, which can be used simultaneously. In acquiring panchromatic (10-m) data, the sensors point slightly forward along the satellite path, and in acquiring multispectral (20-m) data, they point slightly backward (CNES, 1988). This results in simultaneous data acquisitions that are separated by about 15 km (one-quarter scene length) on the ground. At a scene acquisition period of 9.024 seconds, the time difference for the two modes to view the exact same terrain is about 2.3 seconds. One study already has demonstrated that velocities of boats, trains, aircraft, roadway vehicles, and clouds can be determined by using such image pairs (Stern, 1987). Comparable applications having appropriate sensors might allow, for example, nearly instantaneous, precise determinations of sediment or thermal pattern flow in rapidly moving coastal currents.

Another useful application (over a period of days or weeks) could be the detection of topographic changes associated with magmatic migration prior to volcanic eruptions, such as those that occurred at Mount St. Helens in the USA in 1980. Even more applications may become evident as refinements increase the robustness of the technique.

Future work

Future work on the imageodesy technique will include refinements aimed at assuring high precision and optimum accounting for systematic spatial noise. The former may require filtering of the data, selective masking of temporal differences in land cover, and (or) use of alternative interpolation and image-matching schemes. The latter will require refined models of the possible results of attitude variations and other factors. Much experimentation will be needed.

A particularly alluring goal of this research is to produce a spatially comprehensive map of horizontal terrain displacements associated with at least one large earthquake. So far, only one prime-candidate earthquake has occurred since the launch of the first SPOT satellite in 1986, namely, the Luzon, Philippines, earthquake (magnitude 7.9) of July 16, 1990 (Newhall and others, 1990). One useful before image exists, but a cloud-free after image of comparable season and look angle has not become available for this tropical location. Meanwhile, refinements are being developed on the Superstition Hills imagery, the worldwide collection of before images continues to grow, and the next great earthquake gets closer, day by day.

Acknowledgments

This work was carried out at the Jet Propulsion Laboratory (JPL), California Institute of Technology, Pasadena, California, USA, under a contract with the National Aeronautics and Space Administration. Support for this project was provided by a grant from the JPL Director's Discretionary Fund. Assistance was provided by the JPL Supercomputer User Support Staff. Thanks to Ronald Blom and several other colleagues for their critiques, encouragement, and support of this research.

References

Berenstein, C.A., Kanal, L.N., Lavine, D., and Olson, E.C., 1987, A geometric approach to subpixel registration accuracy: Computer Vision, Graphics, and Image Processing, v. 40, no. 3, p. 334–360.

Bindschadler, R.A., and Scambos, T.A., 1991, Satellite-image-derived velocity field of an antarctic ice stream: Science, v. 252, no. 5003, p. 242–252.

Burgmann, R., Behr, G., and Bilham, R., 1989, Creep events and interevent slip on the Superstition Hills fault, California: EOS (American Geophysical Union Transactions), v. 70, no. 43, p. 1348.

CNES (Centre National d'Etudes Spatiales), 1988, SPOT user's handbook: Reston, Virginia, USA, SPOT Image Corporation, v. 1 and 2.

Crippen, R.E., 1987, The regression intersection method of adjusting image data for band rationing: International Journal of Remote Sensing, v. 8, no. 2, p. 137–155.

———1990, Concept for the measurement of horizontal terrain displacements associated with the Loma Prieta earthquake of 17 October 1989 using SPOT panchromatic imagery: Geological Society of America Abstracts with Programs, v. 22, no. 3, p. 16.

Emery, W.J., Thomas, A.C., Collins, M.J., Crawford, W.R., and Mackas, D.L., 1986, An objective method for computing advective surface velocities from sequential infrared satellite images: Journal of Geophysical Research, v. 91, no. C11, p. 12865–12878.

Forstner, W., 1982, On the geometric precision of digital correlation, *in* Hakkarainen, J., Kilpelä, E., and Savolainen, A., eds., Mathematical models, accuracy aspects and quality control, proceedings of the symposium: International Archives of Photogrammetry, v. 24–III, p. 176–189.

Garcia, C.A.E., and Robinson, I.S., 1989, Sea surface velocities in shallow seas extracted from sequential Coastal Zone Color Scanner data: Journal of Geophysical Research, v. 94, no. C9, p. 12681–12691.

Havelock, D.I., 1989, Geometric precision in noise-free digital images: IEEE [Institute of Electrical and Electronics Engineers] Transactions on Pattern Analysis and Machine Intelligence, v. 11, no. 10, p. 1065–1075.

Leese, J.A., Novak, C.S., and Clarke, B.B., 1971, An automated technique for obtaining cloud motion for geosynchronous satellite data using cross correlation: Journal of Applied Meteorology, v. 10, no. 1, p. 118–132.

Li, M., 1990, High-precision relative orientation using feature-based matching techniques: ISPRS [International Society for Photogrammetry and Remote Sensing] Journal of Photogrammetry and Remote Sensing, v. 44, no. 6, p. 311–324.

Lyvers, E.P., Mitchell, O.R., Akey, M.L., and Reeves, A.P., 1989, Subpixel measurements using a moment-based edge operator: IEEE Transactions on Pattern Analysis and Machine Intelligence, v. 11, no. 12, p. 1293–1309.

McGill, S.F., Allen, C.R., Hudnut, K.W., Johnson, D.C., Miller, W.F., and Sieh, K.E., 1989, Slip on the Superstition Hills fault and on nearby faults associated with the 24 November 1987 Elmore Ranch and Superstition Hills earthquakes, southern California: Bulletin of the Seismological Society of America, v. 79, no. 2, p. 362–375.

Morgan, J.S., Slater, D.C., Timothy, J.G., and Jenkins, E.B., 1989, Centroid position measurements and subpixel sensitivity variations with the MAMA detector: Applied Optics, v. 28, no. 6, p. 1178–1192.

Mort, M.S., and Srinath, M.D., 1988, Maximum likelihood image registration with subpixel accuracy, *in* Tescher, A.G., ed., Applications of digital image processing XI: SPIE [Society of Photo-Optical Instrumentation Engineers] Proceedings, v. 974, p. 38–45.

Newhall, C.G., Sharp, R.V., Wieczorek, G.F., Wennerberg, L., and Bicknell, J.D., 1990, The July 16, 1990, Luzon earthquake: U.S. Geological Survey and Philippine Institute of Volcanology and Seismology, unpublished final report, 59 p.

Ninnis, R.M., Emery, W.J., and Collins, M.J., 1986, Automated extraction of pack ice motion from Advanced Very High Resolution Radiometer imagery: Journal of Geophysical Research, v. 91, no. C9, p. 10725–10734.

Qi Tian and Huhns, M.N., 1986, Algorithms for subpixel registration: Computer Vision, Graphics, and Image Processing, v. 35, no. 2, p. 220–233.

Shelton, J.S., 1966, Geology illustrated: San Francisco, W.H. Freeman and Company, 434 p.

Stern, M., 1987, A new tool: SPOT imagery for studying rapid movements, *in* Symposium on Remote Sensing of Environment, 21st, Ann Arbor, Michigan, USA, 1987, Proceedings: Ann Arbor, Michigan, USA, Environmental Research Institute of Michigan, v. 2, p. 917–924.

Sutton, M.A., McNeill, S.R., Jang, J., and Babai, M., 1988, Effects of subpixel image restoration on digital correlation error estimates: Optical Engineering, v. 27, no. 10, p. 870–877.□

Dr. Robert E. Crippen *is a Research Geologist at the National Aeronautics and Space Administration's Jet Propulsion Laboratory, California Institute of Technology, Pasadena, California 91109, USA. He has developed new approaches to the extraction of geologic information from remotely sensed imagery and other spatial data sets. His primary research centers on neotectonic activity, particularly for sites in the arid lands of the southwestern United States.*

by Yasushi Yamaguchi, Hirokazu Hase, and Katsuro Ogawa

Remote sensing for geothermal applications

Remote sensing can contribute to geothermal studies and exploration by detecting surface thermal anomalies by the use of thermal infrared imagery, mapping lineaments that are conduits for geothermal fluids, depicting the regional volcanic framework, and delineating hydrothermally altered areas by the use of spectral patterns in the short-wave-infrared regions. In particular, the Optical Sensor on the Japanese Earth Resources Satellite, launched February 11, 1992, will be useful for discriminating hydrothermal alteration zones. Another future remote sensor that will be applicable to geothermal surveys is the Advanced Spaceborne Thermal Emission and Reflection radiometer, a research facility instrument that will be launched in 1998 on the United States National Aeronautics and Space Administration's Polar-Orbiting Platform.

Introduction

Geothermal energy is one of the alternative energy sources that is being used in various ways, including for electric power generation and local heating systems. Countries like the United States, Philippines, Mexico, Italy, New Zealand, Japan, Indonesia, El Salvador, Kenya, Iceland, Nicaragua, Turkey, China, and Russia are operating geothermal power plants. The world's total electric output from geothermal energy reached approximately 6,000 megawatts in 1989. The majority of the current geothermal power plants are using high-temperature fluids that are composed of hot water and steam.

In Japan, most hydrothermal convection systems are developed in areas related to Quaternary volcanism, and these systems are associated with surface activity such as hot springs, fumaroles, hydrothermal alteration, and anomalously high surface temperatures, which can be the targets for remote sensing. For instance, remote sensing techniques have contributed to national and regional geothermal surveys by detecting topographic features related to geothermal activities and by detecting surface thermal anomalies by the use of thermal infrared imagery. These techniques also are used to map and discriminate hydrothermally altered areas that produce spectral patterns in the visible to short-wave-infrared regions. This paper provides some examples of the remote sensing methods that have been applied to geothermal studies and exploration, and we discuss the future trends in this area.

Mapping surface thermal anomalies

The first application of thermal infrared imagery to detect thermal anomalies in volcanic areas was done by Fischer and others (1964). In Japan, an experimental study employing a laboratory-use, prototype thermal infrared imaging instrument was started in 1965 on some Japanese geothermal fields by members of the Geological Survey of Japan and the NEC Corporation. These tests were successful in obtaining useful data. In the following year, an airborne single-band thermal infrared scanner was constructed (Matsuno and others, 1969), and the scanner continued to be improved by the NEC Corporation until 1968. However, more advanced imaging scanners were developed by the United States and Sweden, and these were used in the early stage of regional geothermal studies (Hase, 1971, 1974).

For instance, the thermal infrared image (fig. 1) obtained in the Sengan area, one of the most promising geothermal fields in northern Japan, was used for historical thermal evaluation of the geothermal activity by measuring the area of "dead" and "live" geothermal phenomena (Hase and Miyazaki, 1988). Geothermal activity at Fukenoyu hot spring in the center of the area is known to wander about because of the sealing effect of hydrothermally altered soil and (or) rocks. This wandering seems to be rather common and is observed in many geothermal areas. The extent of the geothermally anomalous area was measured on the thermal infrared imagery and then was compared to the surrounding hydrothermally altered background area. The empirical field study, which found the limits of detectable thermal anomalies at the natural geothermal surface in terms of heat flow, showed a range of 200 to 800 $\mu cal/cm^2$ s, and the surveys effectively mapped the geothermally anomalous surface beyond this heat intensity (Hase, 1974).

Another example of mapping surface thermal anomalies was presented by Kawamura and Yamaguchi (1982), who studied the Onikobe geothermal area in northern Japan by using an airborne thermal infrared scanner. As most of this area is covered by thick vegetation, an interpolation method that makes use of the double Fourier progression was employed to infer the ground-surface temperature distribution from the data of open bare ground.

In addition, multiband sensors in the thermal infrared region have been developed. These make it possible to know the spectral emittance patterns of surface material, as well as provide more accurate surface temperatures. The Thermal Infrared Multispectral Scanner (TIMS) developed by the National Aeronautics and Space Administration's (NASA) Jet Propulsion Laboratory (JPL) (Kahle and Goetz, 1983) and the Geoscan Airborne Multispectral Scanner (AMSS) (Honey and Daniels, 1985) are examples of the multiband thermal infrared imager. Japan is developing a multiband thermal infrared sensor known as the Advanced Spaceborne Thermal Emission and Reflection radiometer (ASTER), which is detailed later in this article.

Lineaments as conduits of geothermal fluids

Lineaments interpreted from remotely sensed imagery provide important information on subsurface fractures that may control the convective movement of geothermal fluids. In the summer of 1980, the Japanese New Energy Development Organization (NEDO) car-

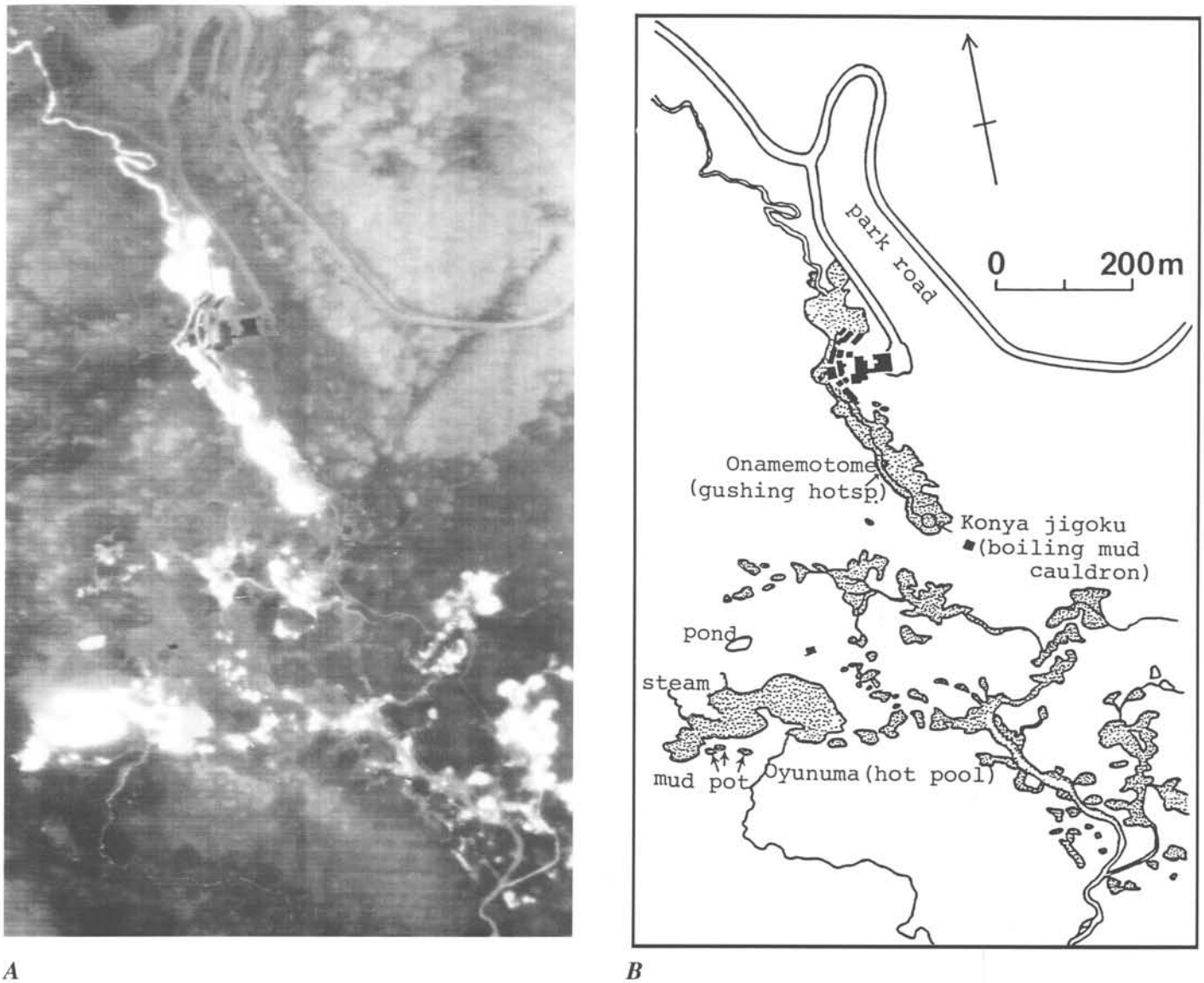

Figure 1.—Goshogake in the Sengan geothermal area, northern Japan. A, Thermal infrared image of the area. B, Interpretation of the thermal infrared image. Dotted areas are thermal anomalies. Abbreviation: hotsp, hot springs.

ried out an airborne Synthetic Aperture Radar (SAR) mapping survey over all the Japanese islands. Yamaguchi and others (1985) interpreted the lineaments from the SAR images obtained in this project, and they made a detailed field survey of a set of specific lineaments for the Hohi geothermal area in southwestern Japan. The test area for this geothermal assessment is covered mostly by vegetation and young volcanic ash deposits. A soil-gas method was employed at several survey lines across the lineament trace, and it showed concentrations of radon and CO_2. Although the soil gas was not of deep origin, as determined from analysis of the gas constituents measured by gas chromatography, the anomalously high radon and CO_2 indicated the existence of a concentration mechanism of radioactive materials and biochemical activation. This concentration mechanism suggests the existence of subsurface fractures.

Regional volcanic framework

Many hydrothermal convection systems are situated at or near Quaternary volcanoes in Japan, and photogeologic interpretation is quite helpful in volcano-stratigraphic studies of these areas. Molten or solidified magma beneath such areas generally is accepted as the heat source for the volcano-related geothermal systems.

Large-scale circular features are observed in volcanic terranes from synoptic Landsat imagery. These features are known sometimes to be Quaternary calderas. Other features are concealed partly by sediments or are obscured by dissected geomorphology. The Okiura area in the northernmost part of the main island of Japan was studied in order to (1) clarify the geologic meaning of its large circular

feature and (2) assess the geothermal potential of the area. The researchers concluded that the area was the center of early Pleistocene, large-scale volcanism and that the circular feature is a caldera, which was formed by the eruption of voluminous acidic tuff and was given the name of Okiura caldera (Muraoka and Hase, 1981). The Okiura area was selected as a geothermal exploration target. A combination of several new types of data obtained in drilling and in the assessment of geothermal resources assisted in interpreting the caldera structure.

Landslide topography also is observed on remotely sensed imagery in volcano-related geothermal areas. In the Sengan area, the geothermally active spots are located in landslide areas (Hase and others, 1983). Lineaments mapped on initial volcanic surfaces are the straight segments of streams as opposed to consequent streams. Valley heads of landslide topography have, in many cases, straight escarpments and correspond to lineament directions. The SAR image demonstrates the situation where the collapse of volcanic bodies is accelerated by the development of fractures and circulation of geothermal fluids along fracture systems below the young volcanic ejecta.

Detection of hydrothermal alteration: JERS–1 OPS

A hydrothermally altered area is a typical surface manifestation of geothermal activities and is, therefore, an important target for remote sensing techniques applied to geothermal areas. Multiband sensors in the short-wave-infrared region should be useful for mapping hydrothermal alteration halos because phyllosilicate minerals exhibit diagnostic absorption features in the short-wave-infrared region.

The Optical Sensor (OPS) of the Japanese Earth Resources Satellite (JERS–1), which was launched on February 11, 1992, has four bands in the short-wave-infrared region and four bands in the visible to near-infrared region including one forward-viewing band for stereoscopic imaging along the nadir track of the satellite (table 1). The visible to near-infrared bands have band passes similar to those of the Landsat Thematic Mapper (TM), whereas OPS bands 6, 7, and 8 in the short-wave-infrared region are three subdivisions spectrally of TM band 7. As shown in figure 2, the OPS short-wave-infrared bands are clearly targeting the absorption features of phyllosilicate and carbonate minerals for the purpose of lithologic mapping. According to a preliminary investigation that used simulated OPS response patterns (Yamaguchi, 1987), we can expect that the OPS data will allow us to distinguish three different alteration types: the alunite-pyrophyllite group, the kaolinite-montmorillonite-sericite group, and the epidote-chlorite-carbonate group. Figures 3 and 4 show the simulated OPS images of the Yerington and Silver Bell areas, western United States, from the airborne multispectral scanner data (Akiyama and others, 1989), where the different lithologies and alteration types are displayed in different colors. This proves the usefulness of the OPS for discriminating hydrothermally altered areas.

Table 1.—Major characteristics of JERS–1 sensors

System	Subsystem	Band no.	Spectral range (μm)
OPS	Visible to near-infrared	1	0.52–0.60
		2	0.63–0.69
		3	0.76–0.86
		4	0.76–0.86
		(forward viewing)	
	Short-wave-infrared	5	1.60–1.71
		6	2.01–2.12
		7	2.13–2.25
		8	2.27–2.40
	Item	**Performance**	
	Ground resolution	18.3×24.2 m	
	Stereo B/H ratio	0.3	
	Swath width	75 km	
	Digitization	6 bits	
	Data rate	60 Mbps	
SAR	Frequency	1275 MHz (L-band)	
	Ground resolution	18×18 m (3 looks)	
	Off-nadir angle	35 degrees	
	Swath width	75 km	
	NEΔρ	−20.5 dB maximum	
	Transmitting power	Approximately 1.3 kW	
	Digitization	3 bits	
	Data rate	60 Mbps	

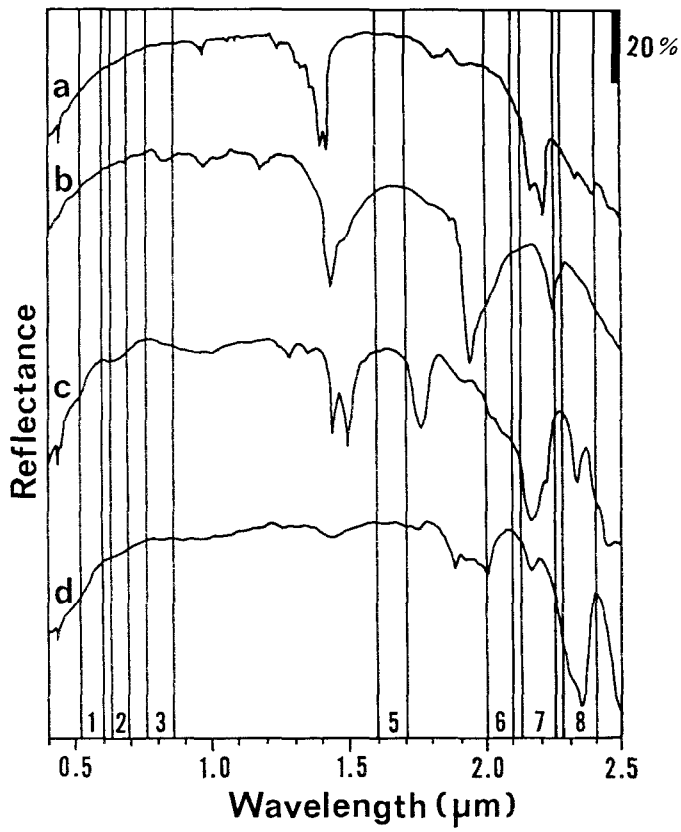

Figure 2.—Reflectance spectra of selected minerals and the band passes (1–8) of JERS–1 OPS. Explanation: a, kaolinite; b, montmorillonite; c, alunite; d, calcite. Spectra are displaced vertically, and 20 percent indicates percent reflectance.

A future remote sensor: ASTER

One of the future remote sensing systems that will be useful to geothermal applications is ASTER, formerly known as Intermediate and Thermal Infrared Radiometer (ITIR). ASTER is a research facil-

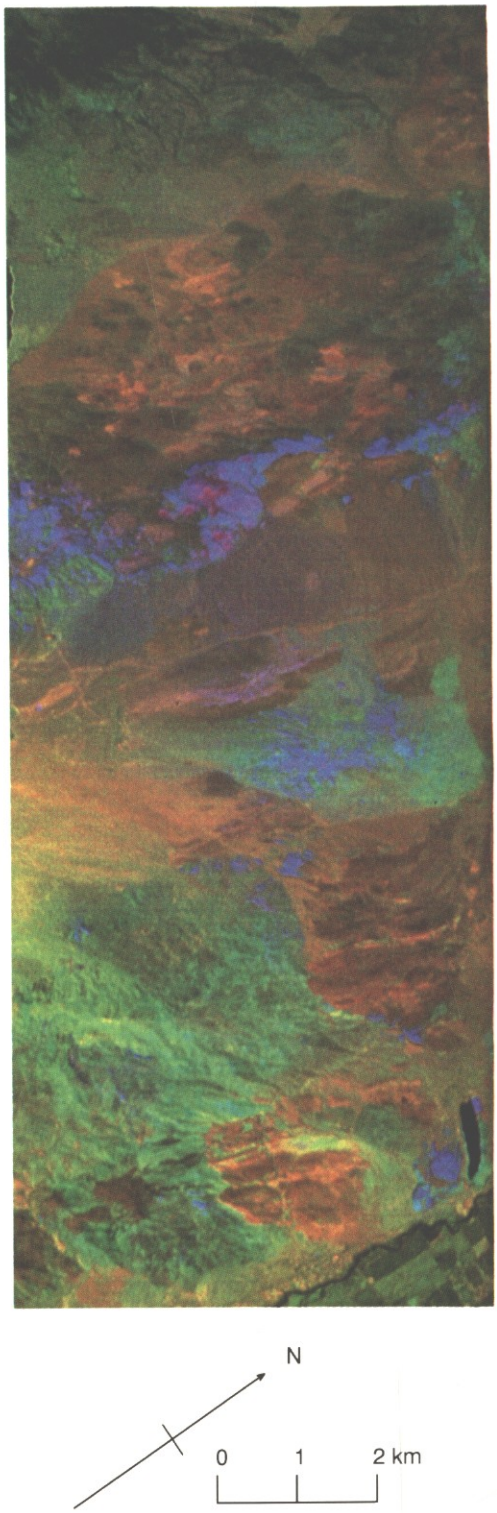

Figure 3.—A JERS–1 OPS simulation image of the Yerington area, Nevada, USA. Band 6 shown as blue, band 7 shown as green, and band 8 shown as red. Decorrelation stretching has been applied (Akiyama and others, 1989).

ity instrument proposed by the Japanese Ministry of International Trade and Industry (MITI) to be launched on NASA's Earth Observing System AM1 (EOS–AM1) platform in 1998 (Yamaguchi and others, 1991). The ASTER inherits the technologies that were developed for the JERS–1, and it is being designed in order to meet the requirements given by the ASTER science team. Table 2 shows its major performance requirements. The ASTER instrument is a multispectral imaging radiometer that has 14 spectral bands and consists of 3 subsystems: the visible to near-infrared, short-wave-infrared, and thermal infrared subsystems. All three subsystems will cover the same 60-km imaging swath and have a pointing capability in the crosstrack direction within a range of 232 km. ASTER has three bands in the visible to near-infrared region, six bands in the short-wave-infrared region, and five bands in the thermal infrared region, and these have 15-, 30-, and 90-m ground resolutions, respectively. In addition, ASTER has one backward-viewing visible to near-infrared band for stereoscopic observation in the along-track direction.

ASTER will provide surface-temperature and emissivity data at the highest spatial resolution among all the EOS–AM1 instruments. High spatial resolution data in the visible to near-infrared and short-wave-infrared regions will be obtained within the same 60-km imaging swath as in the thermal infrared bands. Because these data have a wide spectral coverage and relatively high spatial resolution, we will be able to discriminate a variety of surface materials and reduce the problems resulting from mixed pixels.

For geothermal applications, the thermal infrared data will provide surface-temperature information. In very high temperature areas like a lava lake in the crater of an active volcano, the short-wave-infrared bands can measure surface temperature. Therefore, geological mapping will be carried out efficiently by combining the high-resolution stereo data obtained by the visible to near-infrared bands, information on alteration mineralogy recorded by the short-wave-infrared bands, and temperature and emissivity data provided by the thermal infrared bands.

Table 2.—ASTER baseline performance requirements

Subsystem	Band no.	Spectral range (μm)	Radiometric resolution	Spatial resolution
Visible to near-infrared	1	0.52–0.60	≤0.5%	15 m
	2	0.63–0.69		
	3	0.76–0.86		
Short-wave-infrared	4	1.60–1.70	≤0.5%	30 m
	5	2.145–2.185	≤0.8%	
	6	2.185–2.225	≤0.8%	
	7	2.235–2.285	≤1.0%	
	8	2.295–2.365	≤1.0%	
	9	2.36–2.43	≤1.3%	
Thermal infrared	10	8.125–8.475	≤0.3 k	90 m
	11	8.475–8.825		
	12	8.925–9.275		
	13	10.25–10.95		
	14	10.95–11.65		

Item	Performance
Stereo B/H ratio	0.6
Swath width	60 km
Total coverage in crosstrack direction by pointing capability	232 km

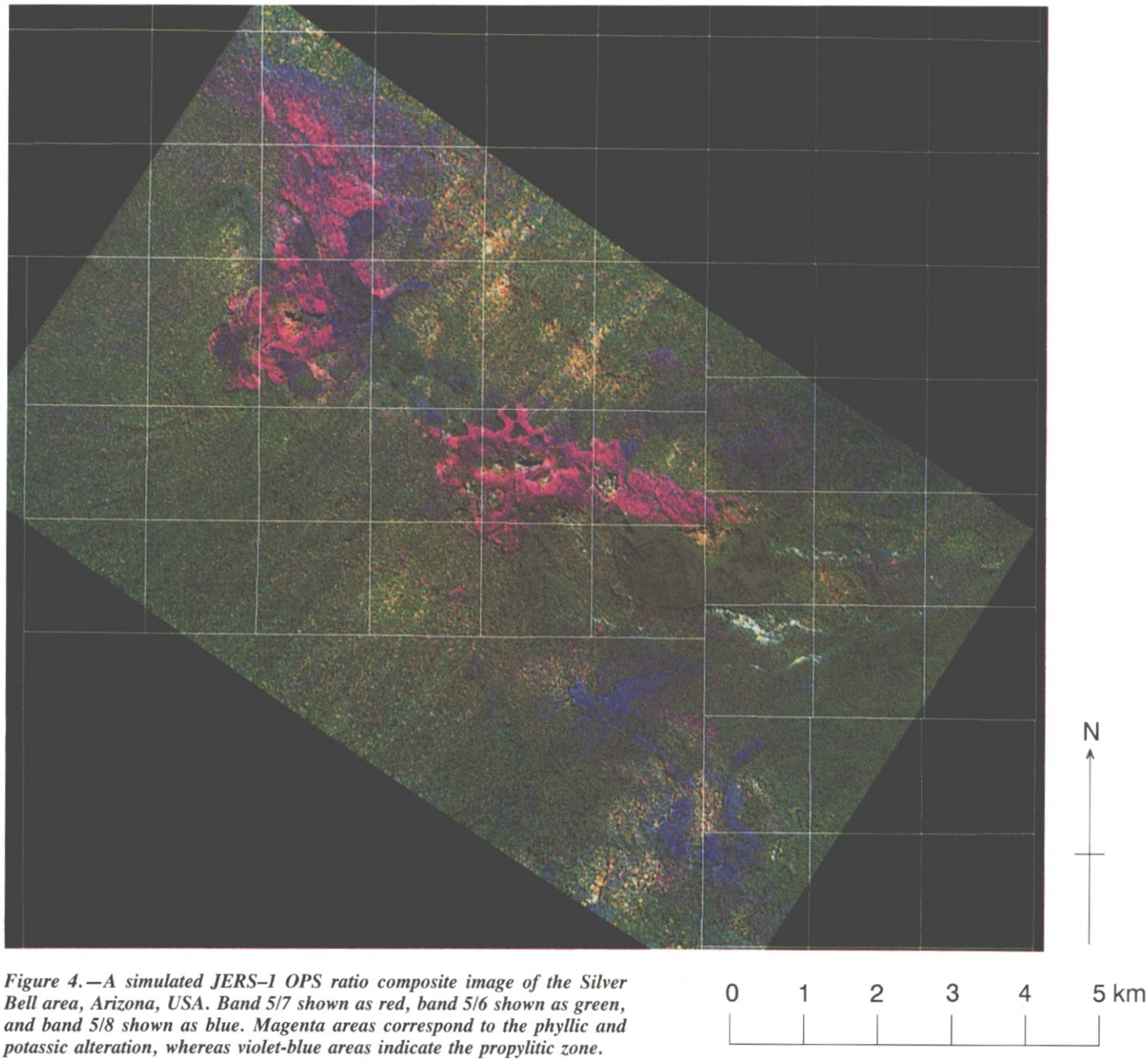

Figure 4.—A simulated JERS–1 OPS ratio composite image of the Silver Bell area, Arizona, USA. Band 5/7 shown as red, band 5/6 shown as green, and band 5/8 shown as blue. Magenta areas correspond to the phyllic and potassic alteration, whereas violet-blue areas indicate the propylitic zone.

Conclusions

Geothermal energy has been attracting public attention lately because it discharges a smaller amount of CO_2 into the atmosphere than hydrocarbons discharge. Therefore, as geothermal studies become more necessary, remote sensing techniques will contribute more to these geothermal studies, as shown here. In the near future, when more advanced sensors like ASTER become available, our understanding of geothermal systems will increase.

References

Akiyama, Y., Komai, J., Yokoyama, T., and Okada, K., 1989, Preliminary assessment of JERS–1 optical sensor based on the simulated airborne data, *in* Thematic Conference on Remote Sensing for Exploration Geology, 7th, Calgary, Alberta, Canada, 1989, Proceedings: Ann Arbor, Michigan, USA, Environmental Research Institute of Michigan, p. 519–529.

Fischer, W.A., Moxham, R.M., Polcyn, F., and Landis, G.H., 1964, Infrared surveys of Hawaiian volcanoes: Science, v. 146, p. 733–742.

Hase, H., 1971, Surface heat flow studies for remote sensing of geothermal resources: Journal of the Japan Society of Photogrammetry, v. 10, no. 3, p. 9–17.

———1974, Geologic remote sensing of the Kusatsu-Manza geothermal area, central Japan: Geological Survey of Japan, Report 252, p. 1–56.

Hase, H., and Miyazaki, Y., 1988, Geothermal resources map aided by remote sensing data: International Archives of Photogrammetry and Remote Sensing, v. 27, no. B7, p. 212–221.

Hase, H., Muraoka, H., Yamaguchi, Y., and Kamata, H., 1983, Fracture and geothermal fluid induced collapse of volcanic body defined by radar remote sensing: Mining and Metallurgical Institute of Japan and Australasian Institute of Mining and Metallurgy Joint Symposium, Sendai, Japan, 1983, Session JA (Geology and Mineral Exploration), Proceedings, p. 1–14.

Honey, F.R., and Daniels, J.L., 1985, Application of Carr Boyd Minerals Limited airborne multispectral scanner to spectral discrimination of hydrothermally altered areas, *in* International Symposium on Remote Sensing of Environment—Remote Sensing for Exploration Geology, 4th, San Francisco, California, USA, 1985, Proceedings: Ann Arbor, Michigan, USA, Environmental Research Institute of Michigan, p. 227–231.

Kahle, A.B., and Goetz, A.F.H., 1983, Mineralogic information from a new thermal infrared multispectral scanner: Science, v. 222, p. 24–27.

Kawamura, M., and Yamaguchi, Y., 1982, Infrared airborne survey on Onikobe geothermal field, Miyagi Prefecture: Butsuri-Tanko (Society of Exploration Geophysicists of Japan), v. 35, no. 6, p. 13–29. [In Japanese, English abstract.]

Matsuno, K., Hase, H., and Nishimura, K., 1969, On IR imagery and its application to the mapping of geothermal distributions: Photogrammetria, v. 25, p. 61–74.

Muraoka, H., and Hase, H., 1981, Okiura caldera, discovery of a Valles-type caldera in the northern Honshu, Japan: International Association of Volcanology and Chemistry of the Earth's Interior Symposium, Tokyo, 1981, Abstracts, p. 242–243.

Yamaguchi, Y., 1987, Possible techniques for lithologic discrimination using the short-wavelength-infrared bands of the Japanese ERS–1: Remote Sensing of Environment, v. 23, p. 117–129.

Yamaguchi, Y., Hase, H., Yano, Y., and Kinugawasa, Y., 1985, Lineament analysis of radar images and associated soil gas surveys in the Hohi geothermal area: Energy Developments in Japan, v. 7, p. 369–391.

Yamaguchi, Y., Tsu, H., and Sato, I., 1991, Japanese mission overview of JERS–1 and ASTER: SPIE [Society of Photo-Optical Instrumentation Engineers] Proceedings, v. 1490, p. 324–334.□

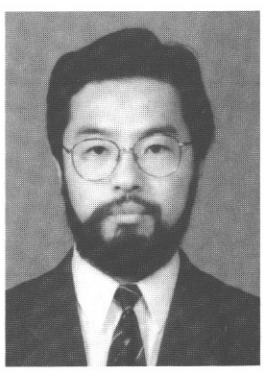

Yasushi Yamaguchi, *a Research Geologist with the Geological Survey of Japan (GSJ) (1–1–3 Higashi, Tsukuba 305, Japan) since 1980, graduated from the Institute of Geology and Paleontology, Tohoku University, Japan, in 1978 and obtained his doctorate from the same university in 1989 by doing geological remote sensing work. From 1980 to 1982, he was transferred to the New Energy Development Organization from the GSJ to be in charge of the radar mapping project. He was a Visiting Scientist at Stanford University, USA, from 1984 to 1986. Recently, he has been engaged in the JERS–1 and ASTER programs.*

Hirokazu Hase *has been working for the Geological Survey of Japan (1–1–3 Higashi, Tsukuba 305, Japan) since 1964. He was one of the earliest scientists involved in remote sensing research work in Japan and has applied the technique to Japanese geothermal surveys. He was at Stanford University, USA, from 1969 to 1970 under Professor R.J.P. Lyon, where he did a geological remote sensing study. He worked at one time for the New Energy Development Organization, where he did a nationwide geothermal survey involving remote sensing. He is now the Director of the Geothermal Research Department of GSJ.*

Katsuro Ogawa *has been working for the Geological Survey of Japan (1–1–3 Higashi, Tsukuba 305, Japan) since 1964, and he has completed a study of the method for interpreting aeromagnetic data. He also has conducted studies on the assessment of geothermal and petroleum resources based on various geophysical data. He is the Director General of the GSJ and serves as one of the Executive Directors of the Remote Sensing Society of Japan.*

by Valentina S. Shibakova, Aleksey V. Sadov, and Aleksander L. Strom

Engineering geology and remote sensing in the USSR

Remote sensing techniques are an integral part of engineering geology studies in the USSR. The use of these techniques improves the reliability and quality of engineering geology studies, as well as decreases both the time required to perform the studies and their costs.

Many types of remote sensing are employed at a variety of scales, and these include airborne photography, space imagery, satellite scanner imagery, thermal infrared surveys, and radar remote sensing. The widespread applications of remote sensing data encompass seismic risk and dam safety assessment, permafrost zone mapping, mountain hazard mapping, and the assessment of man's impact on the geological environment, among others. (Ed.)

Introduction

Remote sensing techniques that incorporate photographic, video, thermal infrared, radar, and multispectral surveys are used widely in engineering geology investigations in the USSR. In fact, these techniques are considered to be an integral part of the general complex of methods that are employed in geological investigations for engineering purposes. They are applied to (1) mapping and zonation, (2) ranking of geological and engineering geology processes, (3) revision and renewal of engineering geology maps, and (4) the study of today's geological environment and the prediction and definition of changes as a result of the impacts of technology.

Reliable engineering geology interpretations of remote sensing data are provided by contrast-analog, landscape-indicative, and morphostructural image analyses. When interpreting images, we use various techniques including successive approximation; analysis and synthesis of decoded information; individual, consulting, and comparative interpretation; and typification and extrapolation. Also, we apply methods of image transformation and automation. The results of our engineering geology interpretations are presented in various graphic, numerical, and descriptive models, as well as in airborne and space images and photographic maps. The use of remote sensing improves the reliability and quality of engineering geology studies. The length of time that is required to perform the necessary studies is shortened, and the cost of these studies is minimized (Komarov and Sadov, 1984).

Types of imagery

Aerosurveys in the optical (visible) ranges have been used in engineering geology since 1940, and the techniques are well developed. Surveys are carried out at different scales from 1:5,000 to 1:50,000 in black and white or in colored multizonal and spectrozonal versions. The methods for analysis of engineering geology also are well developed. Useful information is provided about potential intensive technological impacts in the vicinity of a site, as well as for the wider region, although the possibility of using landscape-indicative methods is decreased strongly in areas where natural landscapes already have been disturbed by man. Under these conditions, geomorphological and geobotanical aspects of analysis are of great importance. Special photogrammetric techniques are used for the characterization of the relief (Sadov and Revson, 1979). Generally, studies of airborne photography help us define counters and squares for the areas of development of different geomorphological processes, observe morphometric characteristics, determine the dynamics of observed processes, and define some factors that control the development of the processes.

Space imagery studies have been used in engineering geology since 1970. Remote sensing materials have been prepared that have different levels of generalization and are applied to engineering geology investigations. The combined interpretations of aerial and space imagery are used as well. We have methods for processing an image in order to extract a significant local structure or a geologic process from data for a larger area. Our engineering geology maps show many small or local geological processes, such as karst, erosion, subsidence, landslides, or rockfalls. Therefore, the ground resolution of space imagery is of great importance. Analyses of space images in the visible ranges are carried out in two versions, both in black and white and in colored multizonal versions. Black and white photographs often provide less information than colored photographs do, but this information has higher resolution. Therefore, black and white photographs are used when detailed images are necessary. Colored multizonal photographs that have resolutions between 10 to 50 m and 5 to 8 m are used for the compilation of specialized medium-scale and small-scale maps.

Satellite scanner imagery is used for the identification, observation, monitoring, and assessment of hazardous processes.

Thermal infrared (airborne) surveys are carried out in 2 to 5 m/km and 8 to 14 m/km ranges in both profile and areal versions. These techniques are used to observe regions for special purposes such as changing water-table levels, surficial soil-moisture analysis, surface-water contamination, and spontaneous combustion of coal and peat material.

Radar remote sensing (in microwave ranges from 1 mm to 30 cm and in the radio wave range up to 50 m) is conducted in both active and passive versions. It can be used to measure the thickness of superficial deposits, soil moisture, and depth to ground-water level (Komarov and others, 1988).

Selected research topics

Seismic risk and dam safety assessment

In the mountainous regions of central Asia, one of the most tectonically and seismically active areas of the USSR, a series of major

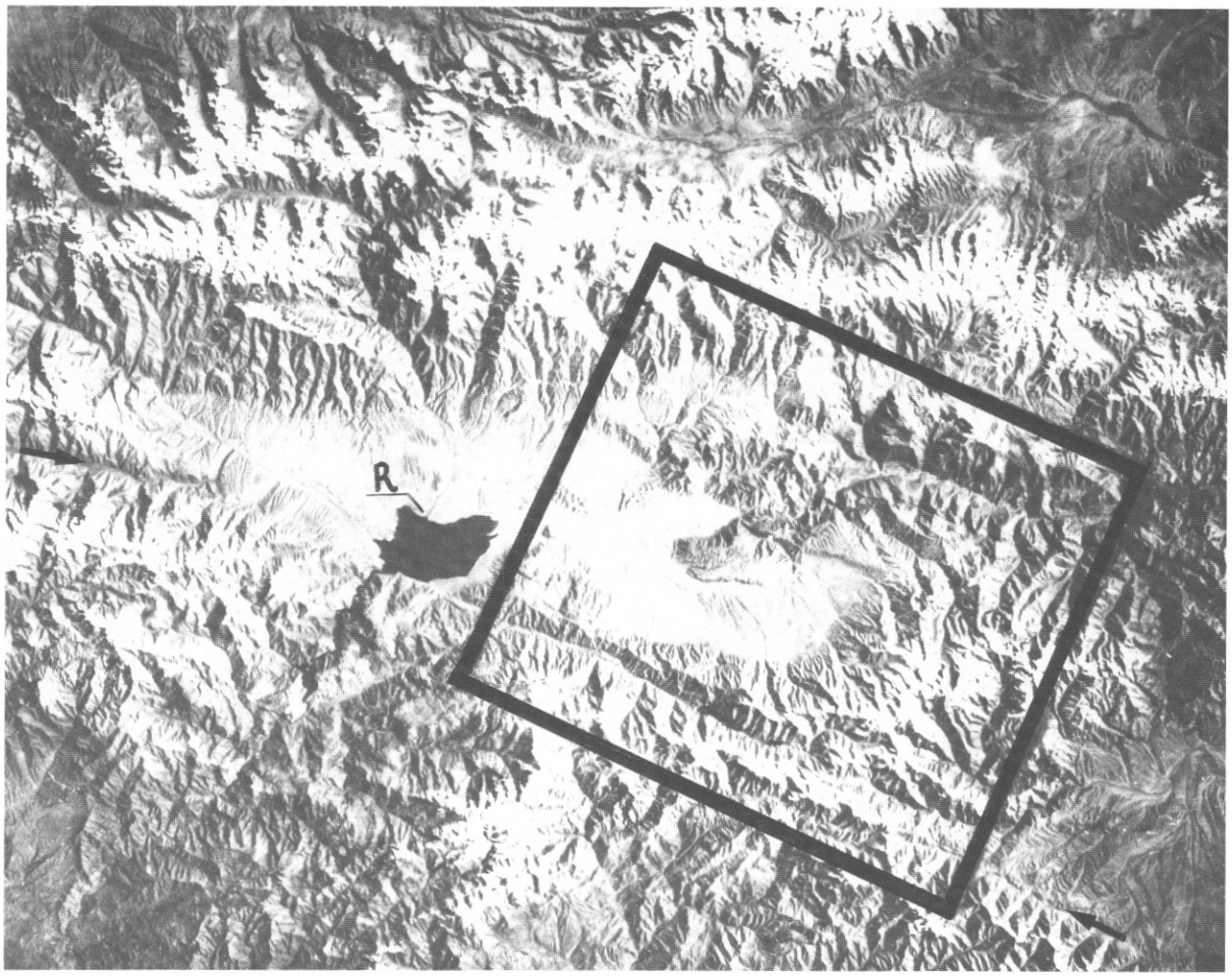

Figure 1.—Space photograph showing part of the Naryn River basin in the Kirgiz Republic. Arrows show the Talas-Fergana wrench fault, and R is the Toktogul reservoir. The outlined area is figure 2.

hydroelectric projects have been developed in order to provide irrigation water and electricity for the central Asian republics. These projects are at Toktogul, a 215-m-high concrete gravity dam; at Nurek, a 300-m-high earthfill dam; and at Rogun, a 335-m-high earthfill dam. The Hydroproject Association has performed analyses of potential seismic hazards for dam sites such as these by applying remote sensing methods.

Space images and airborne photographs are used for the geological investigations of dam sites and tunnel alignments. Images at different scales and resolutions, which range from satellite shots having scales of about 1:1,000,000 to detailed large-scale aerial photographs, are analyzed in order to identify, locate, and investigate faulting and slope processes. Methods have been developed that reveal special imagery features, such as landslides, rockfalls and rock avalanches, and broken watersheds and disrupted drainage patterns, for locating active faults. Data obtained from these space and aerial images are compared with geological maps and seismological data. These types of surficial dislocations can be interpreted (after specialized investigation) as residual deformations resulting from prehistoric, strong earthquakes.

The Kambarata project is in the Naryn River basin, which occupies the internal part of the eastern Tien Shan (mountain chain), in the Kirgiz Republic. The project, located to the east of the active Talas-Fergana wrench fault (fig. 1), is illustrated as an example. A design has been worked out for a 255-m-high rockfall dam that will be built by an oriented rock blast.

One of the difficult problems is the definition of seismic hazard at individual project sites. No strong earthquake has been recorded in this study region during the whole period of observation, and no historical data report such events. On the seismic zoning map of the USSR, the study region was included in seismic zones that have an intensity from seven to eight points on the MSK scale (similar to the Modified Mercalli scale).

Special analysis of stereoscopic satellite photographs, which have better than 10-m resolution (fig. 2), shows a number of recent faults, landslides, and other dislocations in the eastern part of the Naryn basin (fig. 3). Areas were identified that needed more detailed ground investigations. The features were analyzed next on large-scale aerial photographs (fig. 4) and then were verified in the field. On the basis of this data, we delineated seismogenetic zones having high seismic potential (Mmax=7.0) and long recurrent intervals for the strongest events. The resulting seismic hazard of the project's dam sites within the study region was determined and received a nine on the Modified Mercalli scale.

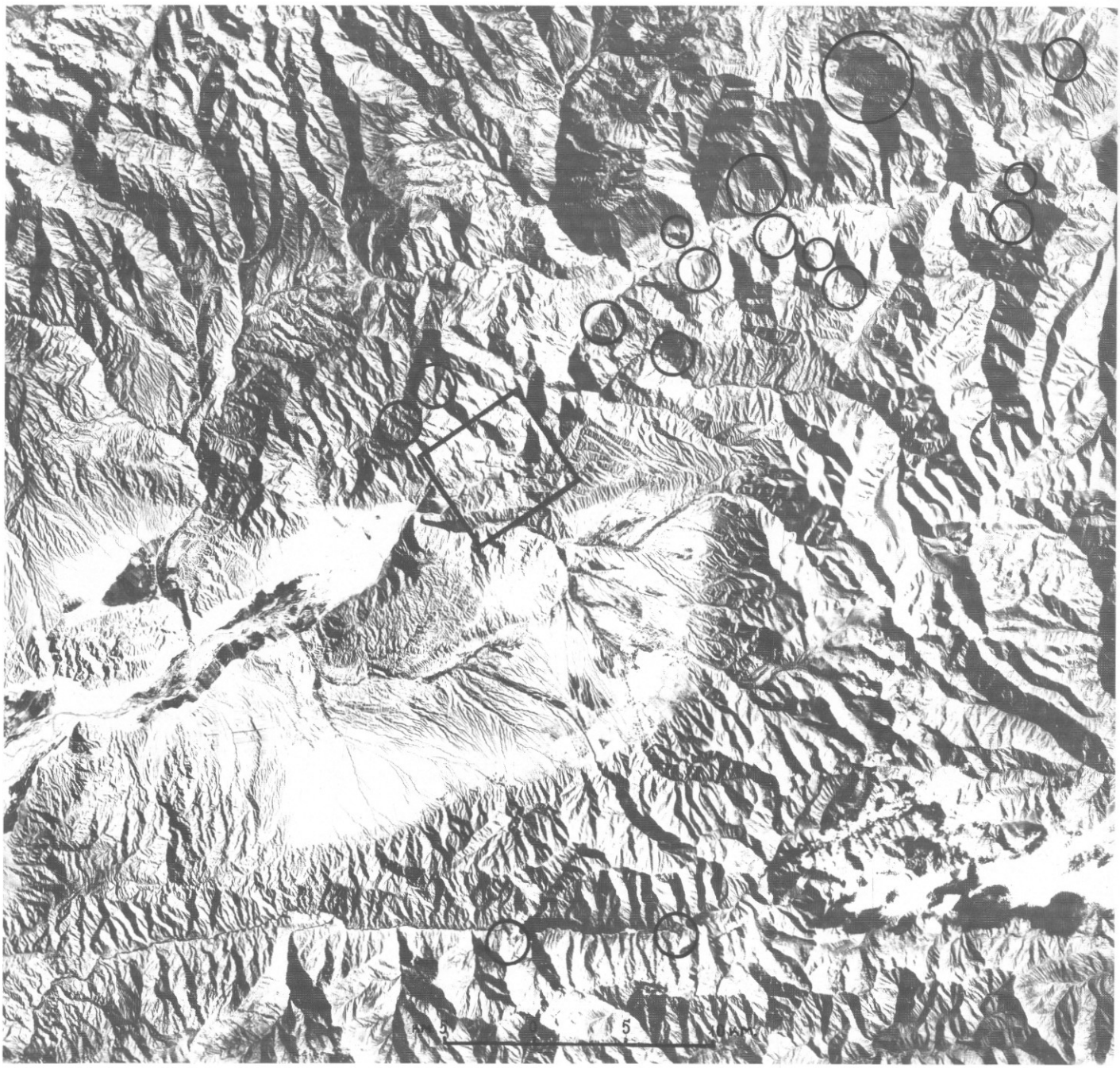

Figure 2.—Detailed space photograph of the central part of the area shown in figure 1. Circles mark some recent dislocations. The outlined area is figure 4.

Permafrost zone mapping

The permafrost zone extends over vast areas of the USSR. This zone is characterized by unique geological conditions and engineering requirements. Trofimov (1989) defined the most important aspects of the permafrost as follows:

(1) Permafrost represents a specific class of deposit, in which the properties of the ground depend largely upon the amount of embedded ice. These properties are dependent upon temperature and undergo abrupt alterations relative to changes in temperatures.

(2) A wide variety of freezing processes are active in these areas. Cryogenic processes lead to the progressive development and formation of new permafrost and types of cryogenic relief, whereas the postcryogenic processes lead to the degradation of permafrost and the formation of typical landforms. Such landforms include thermokarst of varying size and morphology and hummocky ground.

(3) The presence of perennially frozen ground evokes a radical change in the hydrogeological structure of the region. As a consequence, the role of permafrost is a factor that controls the

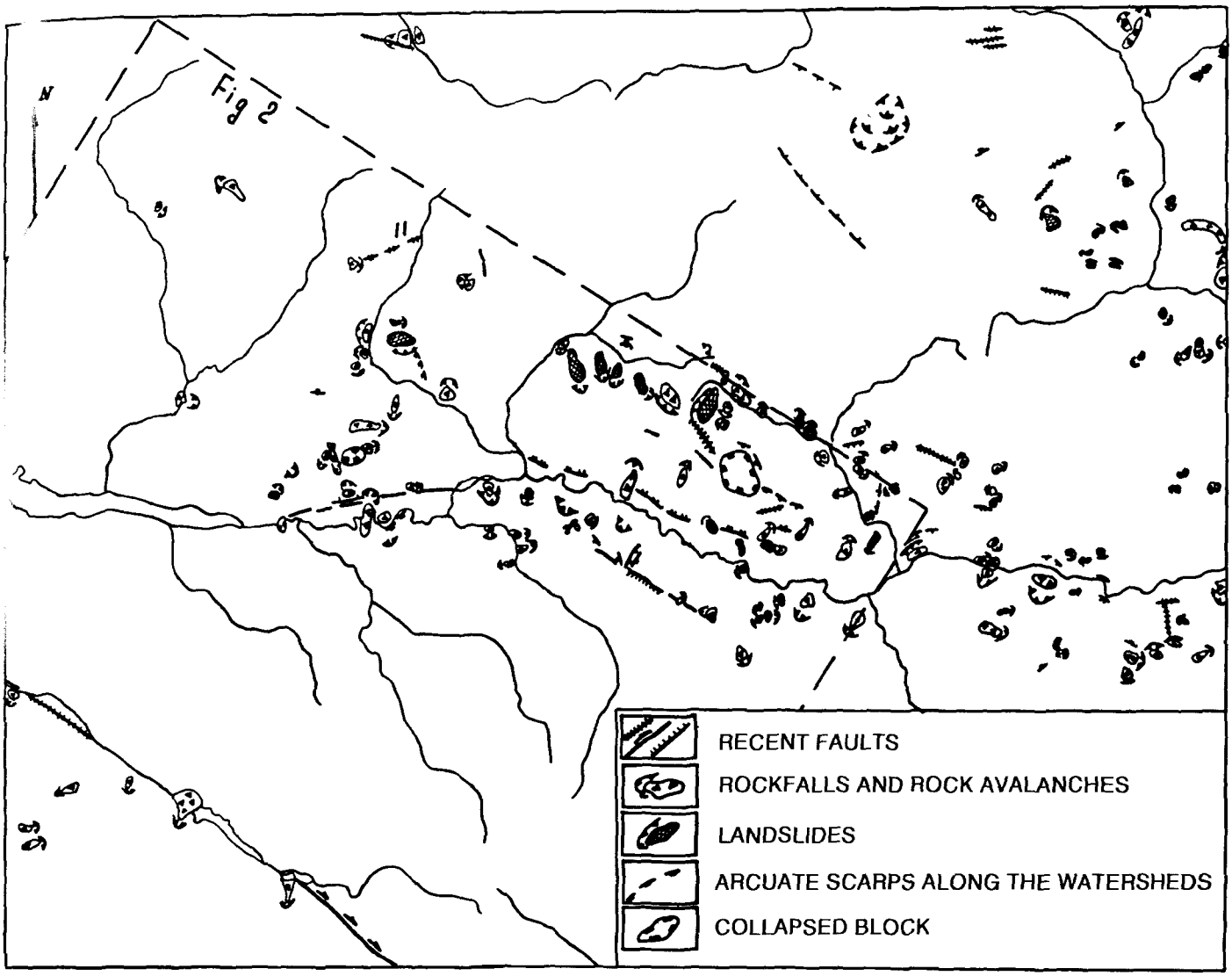

Figure 3.—Recent dislocations of the Naryn River basin interpreted from space and aerial photographs.

formation of geological conditions and that must be addressed during engineering studies.

(4) Many characteristics of the frozen-ground environment are highly sensitive to the effects of humankind.

Because of all these factors, the permafrost zone requires the application of specialized techniques for the investigation, estimation, and prediction of changes in geological conditions. As industrial development has increased in permafrost regions, we have seen a series of engineering and geological problems unfold, as well as various problems involving the ecological balance and environmental protection.

A geocryological map of the USSR has been prepared at a scale of 1:2,500,000 at Moscow State University. This map is the primary summary of research in regional geocryology. It was compiled on the basis of geological, geophysical, and remote sensing data. These data included satellite imagery and aerial photography of continental, regional, and local scope (Ershov and others, 1984). The main content of the map is defined by the display of the most important geocryological characteristics:

(1) Geological formations that have identified cryogenic structures. These formations allow the establishment of the dependence of composition and cryogenic structure upon sedimentation, history of tectonic and geocryological evolution, and climatic and altitudinal zoning.

(2) Spreading of the cryolithozone and its types according to the thermoexchange capacity of the rock. The thermoexchange capacity is characterized by average annual temperatures of rocks that fluctuate from 1 to 2 °C within this zone.

(3) Thickness of the cryolithozone.

(4) Permafrost phenomena and thaws.

The map compilers used the landscape pe-key method and regions at small, medium, and large scales as key areas. These key areas were correlated next with one another by extrapolating these data over the range of the map.

Mountain hazard mapping

Remote sensing is used widely in the study of hazard processes in mountainous regions. In particular, these observations are valuable

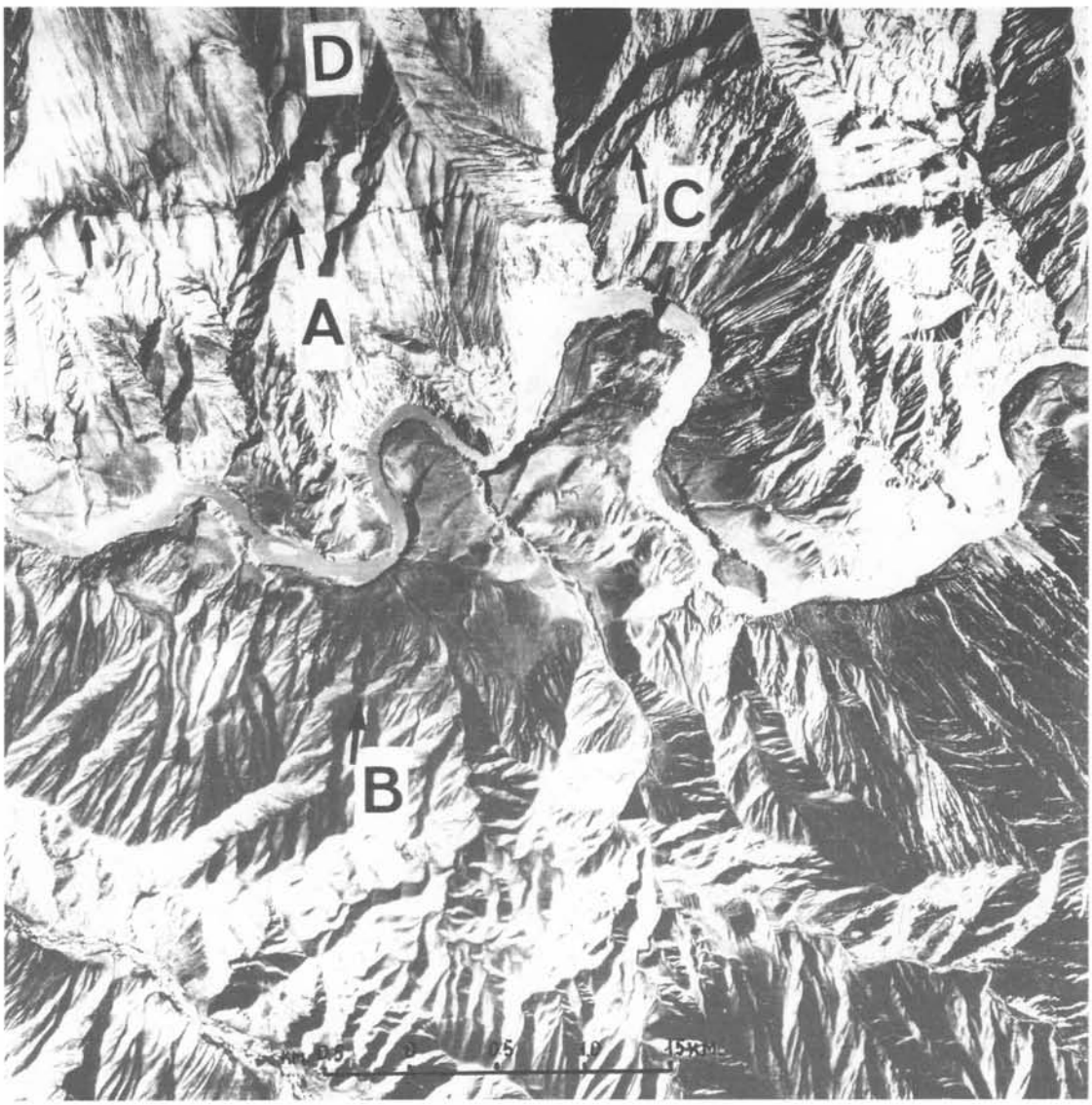

Figure 4.—Aerial photograph of the area marked in figure 2. Arrows show recent dislocations. A and B are faults, and C and D are rockfalls.

for the risk assessment of landslides, mudflows, rockfalls, erosion, and karst topography. Aerospace photographs help to assess the roles of climatic zones and structural and tectonic factors in the dynamics of these processes.

In order to map these hazard processes, techniques of comparative analysis of photographs taken at different times, chronomorphostructural analysis, principles of identifying images, and systems of electronic-optical transformation are used. The Kuramin-Chatkal mountain area of central Asia, mapped at a scale of 1:200,000 (fig. 5), shows different lithological deposits, tectonic structures, and the development and evolution of landslides, mudflows, and mud avalanches.

Environmental aspects

The geological environment is undergoing continuous changes that are caused either by natural geological processes or by anthropogenic and technological processes. Different remote sensing methods are employed in order to study man's impact on the geological environment. For example, the engineering-geodynamics map of the Aral Sea, compiled at a scale of 1:1,000,000, shows changes in the area and provides a forecast for changes continuing to the year 2000 (fig. 6).

Conclusions

This paper has discussed briefly some examples of the use of remote sensing in engineering geology in the USSR. Remote sensing methods and techniques are used for many purposes such as hydrogeology, irrigation projects, mining, the development of urban and coastal areas, and linear construction. Furthermore, a remote sensing system is now under development for monitoring areas of intensive human impact.

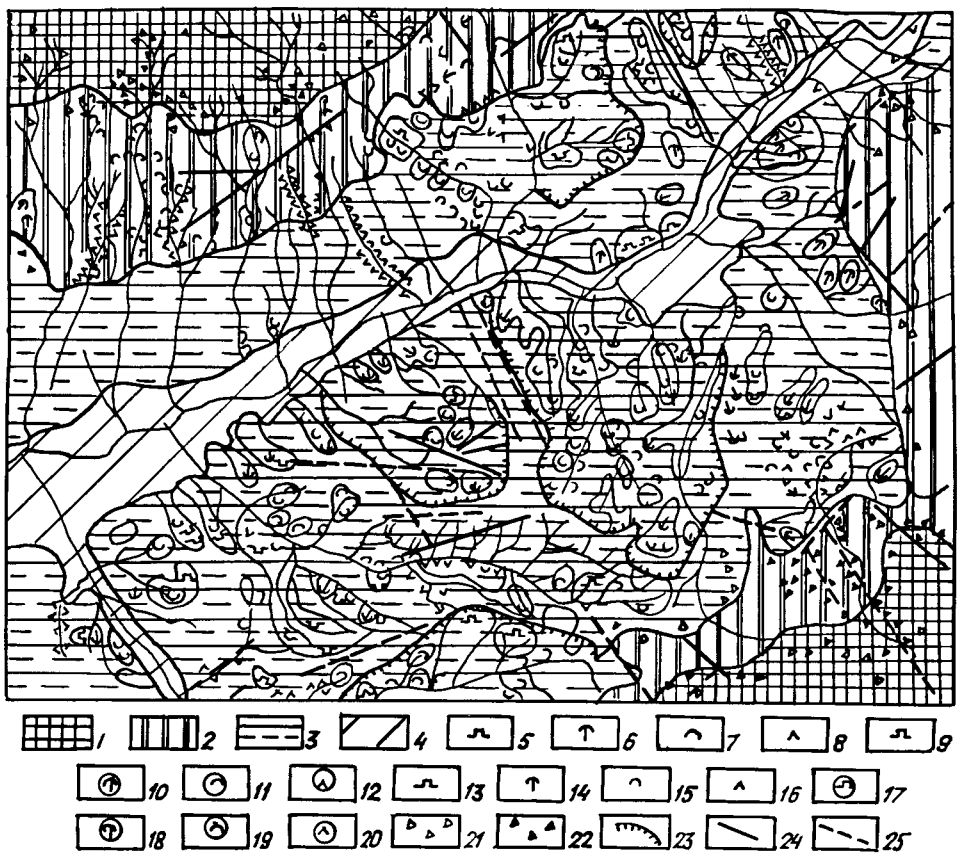

igure 5.—Kuramin-Chatkal mountainous territory of central Asia ***iowing engineering geology classification areas mapped at a scale*** *f* ***1:200,000.*** *Explanation: 1, highlands showing erosional-enudational relief in hard rocks of the Paleozoic Era; 2, middle-eight lands and lowlands showing erosional-denudational relief on ard and semihard rocks mainly of the Paleozoic Era but with a thin over of loose sediments; 3, piedmonts showing erosional relief on emihard and binder rocks of the Mesozoic and Cenozoic Eras and a iick cover of loessal soils; 4, piedmonts showing erosional-ccumulative relief on semihard and binder rocks of the Cenozoic ra and a thin cover of loessal sediments. Fresh landslides: 5, locks; 6, flows; 7, mud streams; 8, mud avalanches. Areas of fresh andslides: 9, blocks; 10, flows; 11, mud streams; 12, mud avalanches. Old landslides: 13, blocks; 14, flows; 15, mud streams; 16, nud avalanches. Areas of old landslides: 17, blocks; 18, flows; 19, nud streams; 20, mud avalanches; 21, fresh debris; 22, old debris; 23, ancient sliding cirques. Tectonic dislocations having a break in ontinuity: 24, proven; 25, inferred.*

References

Ershov, E.D., Kondratieva, K.A., Zomolotchikova, C.A., Trush, N.I., and Gavrilov, A.B., 1984, Geocryological map of the USSR, scale 1:2,500,000: International Geological Congress, 27th, Moscow, 1984, Abstracts, v. 8, p. 39–40.

Komarov, I.S., Akinfiev, C.A., Lyalko, V.I., Ogilivi, A.A., and Sheko, A.I., 1988, Methods of the study of geological processes in the regions of intensive technological impact: Problems of the geoenvironment: Moscow, Nauka Publishers, p. 61–84. [In Russian.]

Komarov, I.S., and Sadov, A.V., 1984, Aero-space methods in hydrogeological and engineering geological studies in the USSR: International Geological Congress, 27th, Moscow, 1984, Abstracts, v. 8, p. 71–72.

Radchenko, E.K., 1984, Methods of remote sensing of hydrogeological and engineering geological changes in the areas of drainage and irrigation: International Geological Congress, 27th, Moscow, 1984, Abstracts, v. 8, p. 131–133.

Sadov, A.V., and Revson, A.L., 1979, Aerospace methods in engineering geodynamics: Moscow, Nedra Publishers, 206 p. [In Russian.]

Trofimov, V.T., 1989, Engineering geology of the permafrost zone, *in* Dearman, W.R., Sergeev, E.M., and Shibakova, V.S., eds., Engineering geology of the Earth: Moscow, Nauka Publishers, p. 40–63.□

Dr. Valentina S. Shibakova *is a Senior Scientist in the Geological Institute of the USSR Academy of Sciences, Pizevsky 7, 109917 Moscow, USSR. She is the Scientific Secretary of the Council on Engineering Geology and Hydrogeology of the USSR Academy of Sciences. Dr. Shibakova specializes in the study of soil and rock properties and in the development of the method of soil stabilization by the use of microwaves. She is a member of the International Association of Engineering Geology (IAEG) and recently served as coeditor of the IAEG publication entitled "Engineering Geology of the Earth."*

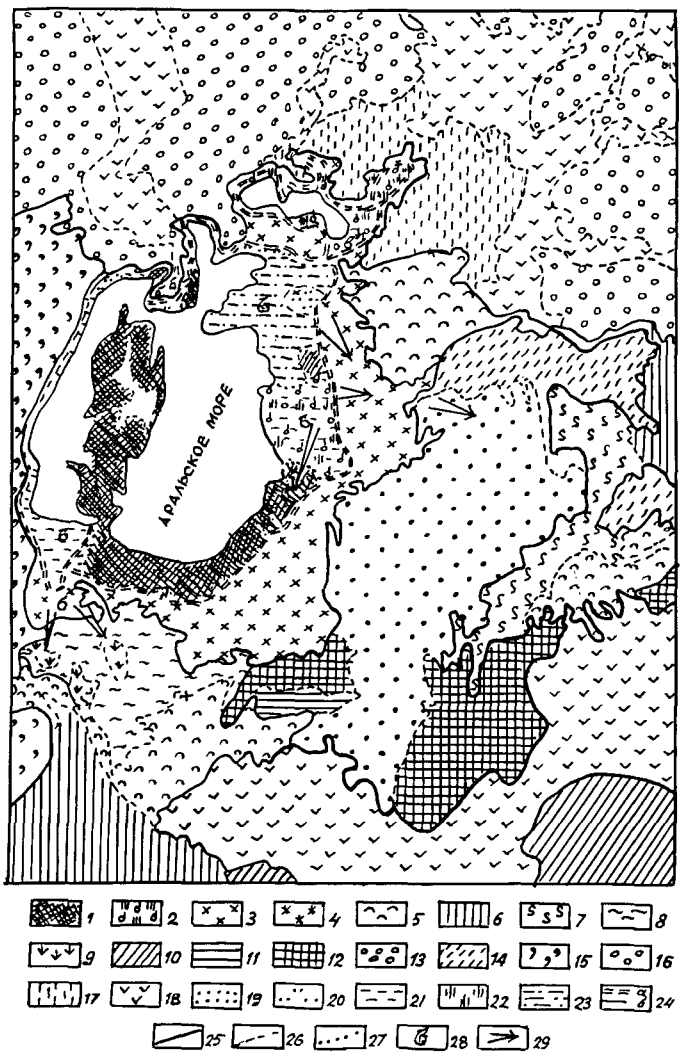

Figure 6.—Aral Sea region showing the classifications of the engineering geodynamicsm of a changing geological environment that is predicted will result from the impact of humankind.

Area I of the Aral Sea and adjacent zones changing as a result of the lowering of sea level. Explanation: 1, sandy beaches undergoing deflation and subsequent redeposition of sand (I_1); 2, wet and swelling Solonchak soils on exposed marine clays and loams and subsequent deflation of swelling Solonchaks (I_2); 3, drying of wet Solonchaks, destruction of gypseous crusts, desalinization of rocks, and deflation of sands of the earlier exposed sea floor (I_3); 4, damping of sliding processes due to sea retreat (I_4).

Area II of changing environment that has been influenced by land-reclamation measures. 5, Induced rise in phreatic water level from 5 to 10 m up to 1 to 5 m below the land surface and the resulting changes in chemical composition and mineral content, incidental salting of deposits and waste lands, and formation of tugai vegetation along irrigation canals (II_1); 6, stable hydro-reclamation regime of oasis lands (II_2); 7, improvement of pastures and growth of phreatophytes as a result of the rise in phreatic water level caused by discharge of irrigation water into old riverbeds and restoration of black-saxaul forests (II_3); 8, lowering of the phreatic water level from 0.5 m to 10 m, partial desalinization of soils, death of tugai vegetation, and deflation of intradelta sands (II_4); 9, formation of swelling Solonchaks on the areas of dried lakes and subsequent deflation of salts (II_5).

Area III containing changes due to man-induced impacts that are not related to land-improvement measures. 10, Disturbances in soil and vegetation covers and formation of land dumps and ravine system as a result of mining works (III_1); 11, moderate deflation due to pasturing and salt pulverization (III_2); 12, extension of near-well lakes and Solonchaks, as well as tugai formation and secondary redistribution of sand resulting from intensive pasturing (III_3); 13, extension of near-well and natural Solonchaks due to salt pulverization from the dried sea bottom and formation of secondary salt-deflation sites (III_4); 14, secondary deflation of small sandy masses resulting from increased pasturing (III_5); 15, surface destruction of high gypsum-content soils in Ustyurt plateau and subsequent deflation due to intensive traffic (III_6).

Area IV showing moderate changes as a result of slight impacts induced by man. 16, Moderate evolution of ravine erosion, salting, and takyr formation (IV_1); 17, Solonchak degradation of takyrs, salting of sands, and increase in salt pulverization from the dried sea bottom (IV_2); 18, moderate deflation of sands (IV_3). Lithological differences of exposed marine soils resulting in the prevalence of 19, sand; 20, sands and sandy loam; 21, sandy loam, loam, and silt; 22, salted soils; 23, loam and sandy loam. Also shown are 24a, Aral Sea level in 1986; 24b, predicted Aral Sea level for the year 2000; 25, areas of changes in the geological environment due to different man-induced activities; 26, areas showing prevalence for particular changes in the geological environment; 27, lithological differences in soils of the exposed sea bottom; 28, sites of the most active salt deflation; and 29, basic directions of salt movement.

Dr. Aleksey V. Sadov *is Professor and Chief of the Aerocosmic Research Methods Laboratory at the All-Union Research Institute for Hydrogeology and Engineering Geology (VSEGINGEO), 142452 Zeleniy-village, Noginsk district, Moscow region. He is an Expert-Supervisor for Remote Sensing at the USSR Ministry of Geology.*

Dr. Aleksander L. Strom, *a graduate of Moscow State University, is the Group Supervisor of the Geophysical Department of the Hydroproject Association, Volokolamskoje Shosse, 2, A–80, 125812 Moscow, USSR. He works in the fields of seismogeology and the applications of remote sensing methods for seismogeological investigations.*

by Jay R. Eliason

Mapping fractures remotely for earthquake hazard assessment by the use of topographic and seismic hypocenter data

Research tools are being developed in order to study the structure of fracture zones remotely by the use of topographic and seismic hypocenter data. These techniques have been employed in analyses of a complex segment of the San Andreas fault that includes its intersection with the Sargent fault in California, USA. These analyses also include the area where dominant surface rupturing resulted from the Loma Prieta earthquake of October 17, 1989. Results of this study indicate that a zone of complex fracturing marks the Pacific-North American plate boundary in this area. Brittle structures appear to be developing in response to uplift, northeast-southwest transpression, and right-lateral shear. Research also suggests that primary surface faulting on the San Andreas fault in this area has developed 2 kilometers northeast of the zone that now is mapped as the surface trace of the fault. Topographic fracture analyses identify the dominant regional fracture zones northeast of the mapped fault zone. These fracture zones correlate with the near-surface fracture zones that have been determined from seismic hypocenters and the surface projection of the modeled fault plane that has been determined from geodetic data. Right-lateral strike-slip motion, which was not observed in surface ruptures produced by the Loma Prieta earthquake, may be developing in this area.

Introduction

Digital fracture analysis techniques have been investigated since 1983 for the purpose of identifying potential fracture zones on the basis of their subtle topographic imprints and the distribution of their seismic hypocenters (Eliason, 1984; Eliason and Eliason, 1985a, b). We have used topographic data obtained from aerial and satellite platforms to develop and demonstrate the topographic analysis technique, and as part of this study, we have analyzed the seismic hypocenters that have been determined for a segment of the San Andreas fault south of San Francisco, California, USA. In addition, this work has included analysis of the available data on the surface topography for the study area located northwest of the Loma Prieta earthquake, which took place on October 17, 1989, at a depth of 17.6 km on the San Andreas fault.

Our analysis area (fig. 1) is centered over the Summit Road-Skyland Ridge area northeast of Santa Cruz, California. This area developed the most dominant surface ruptures that were related to the Loma Prieta earthquake (U.S. Geological Survey Staff, 1989). The objective of this research project was to correlate the potentially dominant surface fracture zones, as determined from topography, and the potentially active subsurface fracture zones, as determined from the aftershock sequence from the Loma Prieta event. The potential fracture zones that were identified in this complex segment of the fault show a strong spatial correlation between the fracture zones at the surface and the active subsurface fracture zones. We have devel

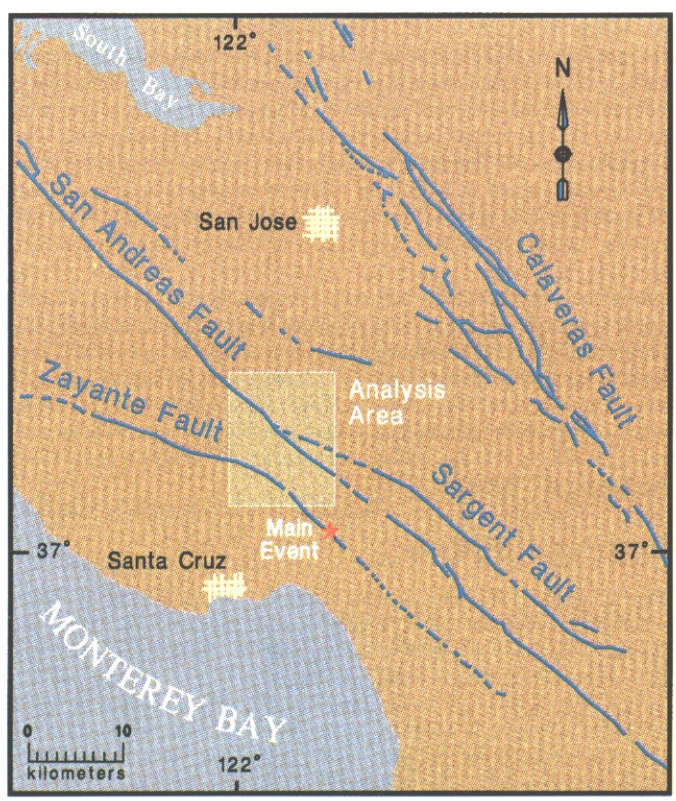

Figure 1.—Analysis area and dominant fault systems in the vicinity northeast of Santa Cruz, California, USA. Also shown is the location of the main event of the Loma Prieta earthquake of October 17, 1989. Dashed faults are inferred.

oped a generalized structural model based on the potential fracture zones that we identified in the analysis area.

Digital fracture analysis techniques, which use topographic and seismic hypocenter data, provide geologists another structural analysis tool that will complement classic field mapping of geologic units and structural forms. Dominant near-surface fracture zones typically cut various geologic units and structural forms and can, in most areas, be mapped only locally by the field geologist. On the other hand, the spatial correlation of dominant fracture zones is not obvious in the field in most areas because of limited exposure. Therefore, the digital fracture analysis techniques that are being developed as part of this research program provide unique tools for mapping the regional correlations of these natural fracture systems. This mapping is done in three dimensions and uses the topographic imprint and seismic signature of the fracture systems.

Analysis techniques

Spatial fracture analysis techniques for the identification of dominant near-surface and subsurface fracture zones are based on the identification of locally planar segments of these zones. Near-surface planar segments of fracture zones locally control the orientation of aligned topographic lows by influencing erosional processes. In the subsurface, these zones of crustal weakness accommodate local strain and produce clusters of seismic hypocenters. Topographic fracture analysis is limited primarily by the accuracy of the available topographic data that are required to define accurately the aligned topographic lows in three-dimensional space. These analyses also are limited currently to the identification of fracture zones having dips that range from 50° to 90°. This limitation removes many of the structural identification problems that are associated with slope, bedding, and other shallowly dipping structural features. Research is focused on developing advanced algorithms that will be capable of handling the identification and classification of these shallowly dipping structures. Topographic data that are capable of defining 10-m contours accurately at a scale of 1:24,000 or larger in areas having local relief of 500 m or greater have provided us the ability to define fracture zones in areas that are as small as 8 km by 8 km. In contrast, the study of seismic hypocenters is not limited by the degree of dip and can be used to identify structures that dip from 0° to 90°. Indeed, the analysis of the seismic hypocenters is limited primarily by the accuracy of the location of seismic events. The work presented here is based on seismic events recorded by the U.S. Geological Survey's seismic array on the San Andreas fault, which has relative location errors of significantly less than 300 m for the epicenter location and less than 600 m for the vertical location in the analysis area (Dietz and Ellsworth, 1990).

Topographic analysis

The topographic fracture analysis technique assumes that dominant underlying fracture systems locally control segments of valley and sidewall canyons and are expressed as aligned topographic lows. The three-dimensional location and orientation of such a topographic low can be thought of as a vector included in a fracture zone in three-dimensional space. If a dominant fracture zone has developed in an area, the imprint of this zone will likely control several locally aligned topographic lows. All these topographic low vectors will lie in the plane of the dominant fracture zone (fig. 2). Coplanar analysis of these vectors defines the orientation and location of the fracture zone. Topographic low vectors that are not related to the dominant fracture zone will fail the coplanar analysis test and thus will be eliminated from the analysis. The coplanar test calculates poles to all possible planes that can be defined by three of the four vector end points. In order to pass the coplanar test, all these poles must be within specified limits of trend and plunge. An average plane strike, dip, and spatial location are calculated for each vector pair that passes the coplanar test. These coplanar detections are then sorted in order to identify dominant clusters of planes that fall within specified limits of orientation (strike and dip) and spatial location. Next, these potential fracture zones are ranked from the most dominant to the least dominant. The average fracture orientation and location in three-dimensional space for each cluster can be used in conducting classic structural analysis methods, as field measurements would be, or they can be used for projecting potential fracture zones to local altitude datums, as detailed later.

Seismic hypocenter analysis

Seismically active fracture zones develop along local zones of crustal weakness that are compatible with the local stress field. Seismic activity associated with these tectonic structures occurs dominantly within these fracture zones, but many events also occur on minor secondary structures during local deformation and dilation. In seismic fracture analysis, we assume that a significant number of these events will be located on the primary plane of a dominant fracture zone. This analysis technique uses the same coplanar algorithm that is involved in topographic fracture analysis. The algorithm uses four seismic hypocenters (in place of the four vector end points in the topographic analysis) for defining coplanar sets of seismic events.

Figure 2.—Aligned valley vector segments of the topographic fracture studies of the analysis area are plotted on the Universal Transverse Mercator (UTM) projection, zone 10S, 1,000-m grid.

All possible combinations of four events are analyzed in order to determine every possible seismically active set of planes. The coplanar test calculates poles to all the planes that can be defined by three of the four events. In order to pass the coplanar test, all these poles must fall within specified trend and plunge limits. As in the topographic fracture analysis, the coplanar seismic planes are sorted next for the purpose of identifying clusters of planes and for ranking the dominant fracture zones.

Other seismic hypocenter analysis techniques

Other research has been conducted on techniques for the identification of major crustal fractures that are seismically active in three-dimensional space. This research includes the principal parameter method (Michelini and Bolt, 1986), the planes defined by three earthquakes (Fehler and others, 1987), and the counting box method (Rieken, 1985). In the principal parameter method (Michelini and Bolt, 1986), the strongest cluster of seismic events are fitted to a matrix of three perpendicular eigenvectors. Data from specific aftershock sequences are selected on the basis of time after a major event. A single average fault plane orientation and a location are determined for each sequence. In the method using planes defined by three earthquakes (Fehler and others, 1987), these planes are calculated for all possible combinations of three events in order to define every possible plane. Dominant fracture plane orientations then are selected from the planes identified. In the counting box method (Rieken, 1985), a series of thin counting boxes that have a specified strike and dip are superimposed over the seismic data in three-dimensional space. The strike and dip of the boxes are incremented by 5-degree steps through all the possible orientations, and the number of events in each box is recorded. Box orientations and locations containing high numbers of events define the potentially active fracture zones. The distribution of these events can be used then for defining a planar fracture, or a surface can be fitted to the events identified.

The four-point coplanar analysis algorithm, developed for the analysis of both topographic and seismic hypocenter data, has capabilities that avoid many of the limitations encountered by these other methods. If we use four vector end points, or four seismic hypocenters, for the initial identification of coplanar structures, this significantly reduces the number of potential structures that are identified initially. As a result, this eliminates most of the random planar structures and simplifies the cluster sorting. It also reduces the effect of the plane distribution that results from the shape of the input data set, which is a major limitation of three-point methods. Analyzing overlapping subregions within a study area allows us to resolve complex intersecting fault structures by the use of four-point coplanar analysis algorithms. In addition, analyses at various scales provide us information about both the dominant through-going fracture zones and the local fracture zones.

Results and discussion

Topographic fracture studies and seismic fracture studies have been conducted in the analysis area shown in figure 1. This area includes the lower half of the Los Gatos 7.5-minute quadrangle and the upper half of the Laurel 7.5-minute quadrangle. The area is 15 km from north to south and 12 km from east to west and includes the mapped intersection of the Sargent and San Andreas faults. It also includes most of the northwest half of the rupture zone that is associated with the Loma Prieta earthquake of October 17, 1989 (main event, fig. 1). Seismic aftershocks recorded from October through December 1989 within the analysis area number 997 events, located at depths ranging from 1 km to 20 km, and were used for the seismic fracture analyses.

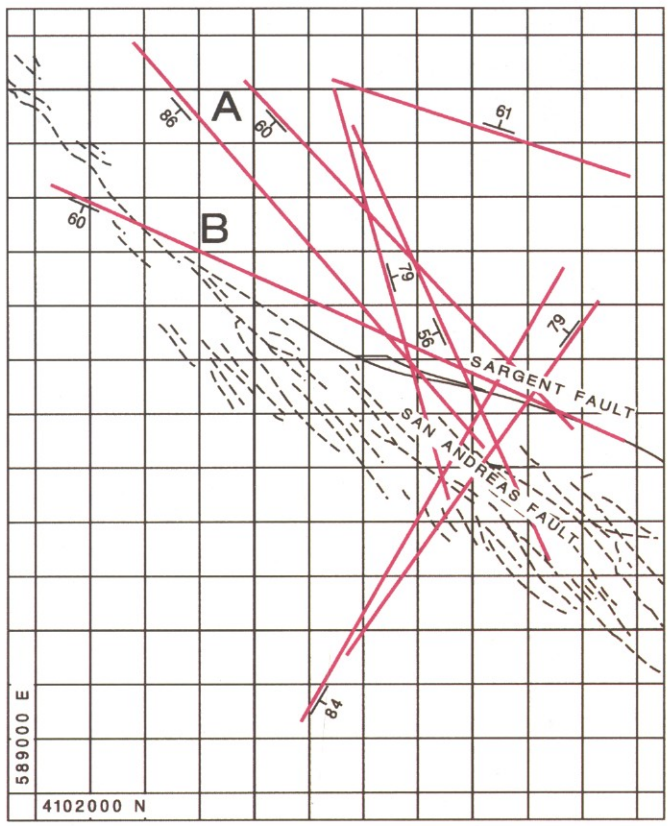

Figure 3.—Mapped surface faults that are related to the San Andreas (dashed black lines) and Sargent (solid black lines) fault zones (Brabb and Hanna, 1981) and potential fracture zones (red) and their dips. The potential fracture zones are related to both the San Andreas (A) and Sargent (B) fault zones and were identified by the regional topographic analysis projected to the 427-m- (1,400-ft-) altitude datum, which is referenced to the UTM, zone 10S, 1,000-m grid.

The vectors for topographic lows (over 5,000) used in this research project were digitized from the topographic data that are available on the 1:24,000-scale 7.5-minute maps, which have a 12.2-m contour interval. These vectors, plotted in figure 2, are referenced at each end of an aligned topographic low by Universal Transverse Mercator (UTM) north and east coordinates and altitudes.

Regional topographic analysis

We conducted a regional study of the topographic low vectors in order to identify dominant through-going fracture zones. From this work, we selected potential fracture zones containing clusters of eight or more planes. These dominant through-going structures were defined by a total of 60 valley vectors from the more than 5,000 input vectors, and more than 98 percent of the input valley vectors were rejected in this regional analysis. The intercepts of these potential fracture zones with a near-surface datum (427 m) are plotted in figure 3. These regional potential fracture zones, which have typical lengths of 10 km, are anticipated to be the most likely structures that may correlate with segments of major through-going fault systems.

The San Andreas and Sargent fault zones, as mapped by Brabb and Hanna (1981), are included in figure 3. The San Andreas fault zone correlates closely with the dominant surface rupture zone that

developed in response to the Loma Prieta event and was mapped by the U.S. Geological Survey Staff (1989).

Regional potential fracture zones identified from the topography that are most likely related to the San Andreas fault (A in fig. 3) are offset to the northeast of the mapped fault zone by approximately 2 km. This 2-km offset corresponds with the surface projection of the fault plane as modeled by Lisowski and others (1990) from the geodetic data for this northwest segment of the rupture zone. The model developed from the geodetic data indicates that the rupture zone strikes N. 44° W., dips 70° SW., and rakes 144°. This orientation agrees with the main shock mechanism (strike N. 50±15° SW., rake 140°) determined from fault-plane solutions by Oppenheimer (1990). The geodetic modeling indicates that the coseismic deformation for this event can be explained by oblique slip (1.66±0.05 m right-lateral strike slip and 1.19±0.06 m reverse slip) on a 37-km-long buried rupture extending from −5 km to −17.5 km below the land surface. This event may not have produced measurable surface rupture, but the correlation between the modeled rupture zone projection to the surface and the dominant structures determined from the regional topographic analysis suggests that this is a zone of weakness that has influenced the surface topography. One of the dominant regional structures (B in fig. 3) correlates closely with the mapped traces of the Sargent fault.

Subregional seismic hypocenter analysis

We conducted seismic hypocenter studies on overlapping subregions for the purpose of defining locally active, potential fracture zones. These studies used seismic hypocenters from three depth ranges: −1 to −6 km, −8 to −12 km, and −14 to −18 km. From these analyses, we selected potential fracture zones that contained clusters of six or more planes. These seismically active zones have been projected to subsurface datums of −3.5 km, −10 km, and −16 km, respectively, and are shown in figure 4.

The seismically active, potential fracture zones identified at -3.5 km and the mapped surface structures related to the San Andreas and Sargent faults are plotted in figure 4. The locations of all these seismically active, potential fracture zones correlate closely with the potential regional fracture zones that were determined from the topography and are shown in figure 3. The seismically active structures also suggest that the surface projection of the San Andreas rupture zone is approximately 2 km northeast of the mapped surface structures. Several structures related to the Sargent fault also appear to have been involved in the Loma Prieta aftershock sequence.

At the −10-km depth (fig. 4), seismically active structures show complex orientations that may be related to the San Andreas and Sargent fault intersection. A more organized fracture set developed along a northwest trend, which is consistent with the San Andreas fault orientation, and it extends to the northwest.

At the −16-km depth (fig. 4), the seismically active structures show a dominant trend that is consistent with the orientation of the slip plane derived for the main event of the Loma Prieta earthquake, N. 130±10° E. (Oppenheimer, 1990). Fault structures at the −16-km datum dip from approximately 60° to 90° to the southwest, and several of the dominant sets range from 75° to 80° southwest. These dips correlate closely with the 70±15° reported by Oppenheimer (1990).

Figure 5 shows the three-dimensional spatial relationships of the topographic and seismic hypocenter analyses. Included are the surface traces of mapped fault structures, the potential regional fracture zones determined from the topographic analysis, and the seismically active structures projected to the −3.5-km, −10-km, and −16-km datums. This model shows the spatial correlation of the surface and subsurface structural traces, as well as the southwest dip of the San Andreas fault zone, which appears to dip more steeply from the surface to −10 km than it does from −10 km to −16 km.

Subregional topographic analysis

We analyzed the topographic low vector data by using overlapping subregions in order to define the near-surface, local, potential fracture zones. From the results, we selected potential fracture zones having clusters of six or more planes. A composite plot of these dominant local structures projected to the 427-m- (1,400-ft-) altitude datum is shown in figure 6. The local surface structures plotted as dark blue and green in the figure are on or are southwest of the San Andreas and Sargent faults, as defined by the previous regional analyses of the topography and seismic hypocenters. These structures are postulated to be on the Pacific plate side of the San Andreas fault, which was uplifted approximately 0.4 m by the Loma Prieta event as determined by geodetic modeling (Lisowski and others, 1990). The potential fracture zones appear to be developing in two different structural domains. The structures in the southwest, plotted in dark blue, trend dominantly west-northwest-east-southeast and east-west and have dips ranging from 50° to 60°. These structures appear to be normal-faulting structures that are developing in order to accommodate extension related to the uplift. The fracture sets that are plotted in green trend dominantly northeast-southwest and dip steeply (70° to 90°). These structures appear to dominate the boundary of the Pacific plate and include the area now mapped as the San Andreas fault zone. A complex boundary zone along this section of the San Andreas fault, which includes the Sargent fault intersection, is defined by these structures. Northeast-southwest transpression and right-lateral shear could account for the development of these structures. Northeast of the San Andreas and Sargent fault zones on the North American plate is a local topographic high containing Mount Umanhum. This area appears to be a relatively competent crustal block that is bounded by several dominant structures plotted in light blue. The spatial relationship of these structural domains is shown in a generalized block diagram (fig. 7). Of necessity, our structural interpretations are limited by the extent of the analysis area, which includes only the part of the Loma Prieta earthquake rupture zone that is northwest of the main event.

Conclusions

This study of the brittle structures that are forming on a segment of the San Andreas fault, including its intersection with the Sargent fault, has provided a rigorous test of the research tools being used for structural analysis of fracture systems. These tools are being developed in order to provide quantitative methods for the remote determination of complex crustal fracture patterns from data sets that can be collected from aerial platforms, satellites, and microseismic arrays. Although the topographic analysis will not be applicable to areas of low relief and recent sedimentary deposits, these tools should contribute to the study of brittle structures in areas of moderate topographic relief. Fortunately, most seismically active continental areas have significant topographic relief.

The Loma Prieta topographic analyses have identified dominant, regional, potential fracture zones northeast of the mapped San Andreas fault zone. These potential fracture zones correlate closely both with the near-surface potential fracture zones that have been determined from seismic hypocenters and with the surface projection of the modeled fault plane that has been determined from geodetic data (Lisowski and others, 1990). It is unlikely that the seismic activity and crustal displacement related to the Loma Prieta event are occurring on new or unique crustal fractures. These events most likely are

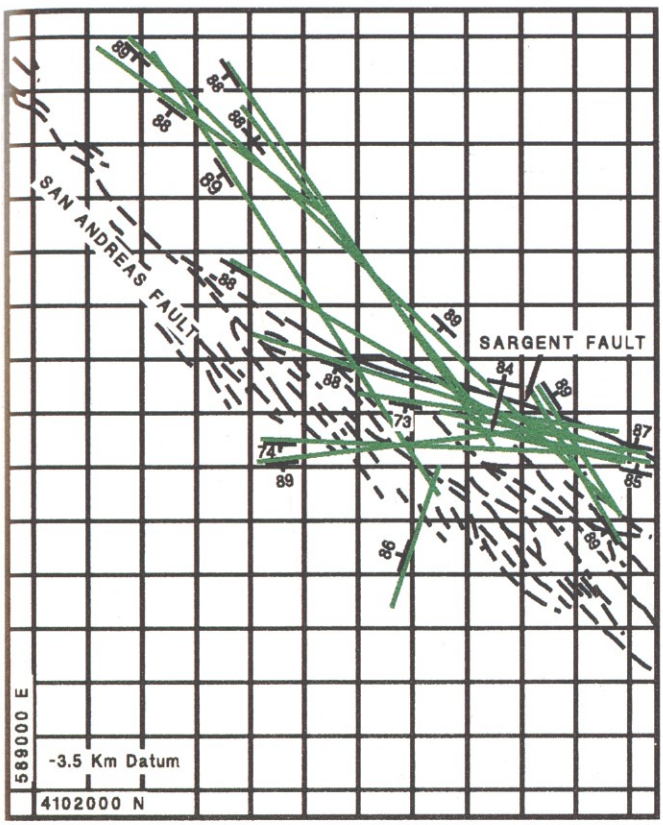

Figure 4.—Locally active, potential fracture zones and their dips projected to the −3.5-km datum (green), −10-km datum (dark blue), and −16-km datum (light blue). The mapped surface faults related to the San Andreas (dashed black lines) and Sargent (solid black lines) fault zones are shown on the −3.5-km datum. The plots are referenced to the UTM, zone 10S, 1,000-m grid.

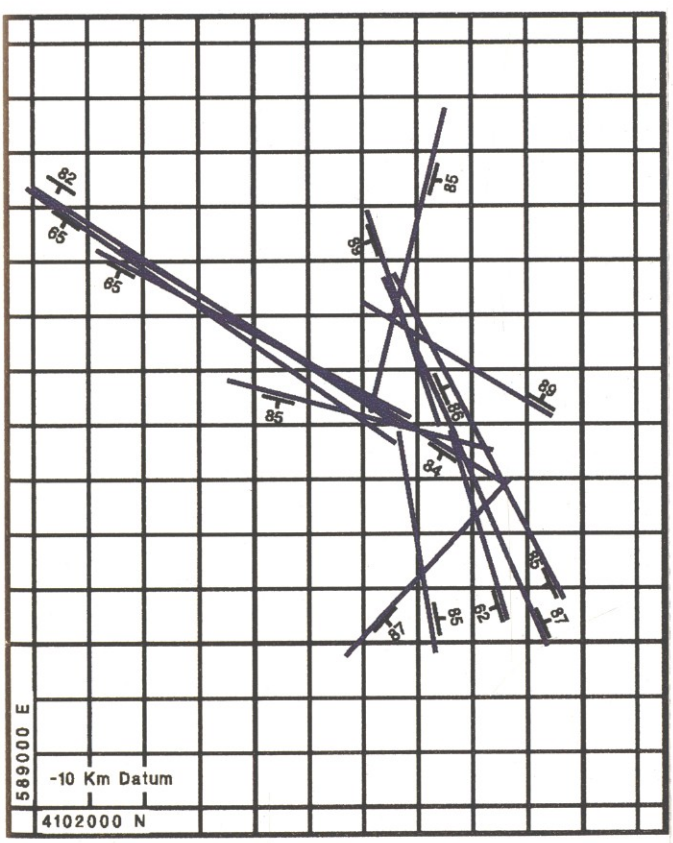

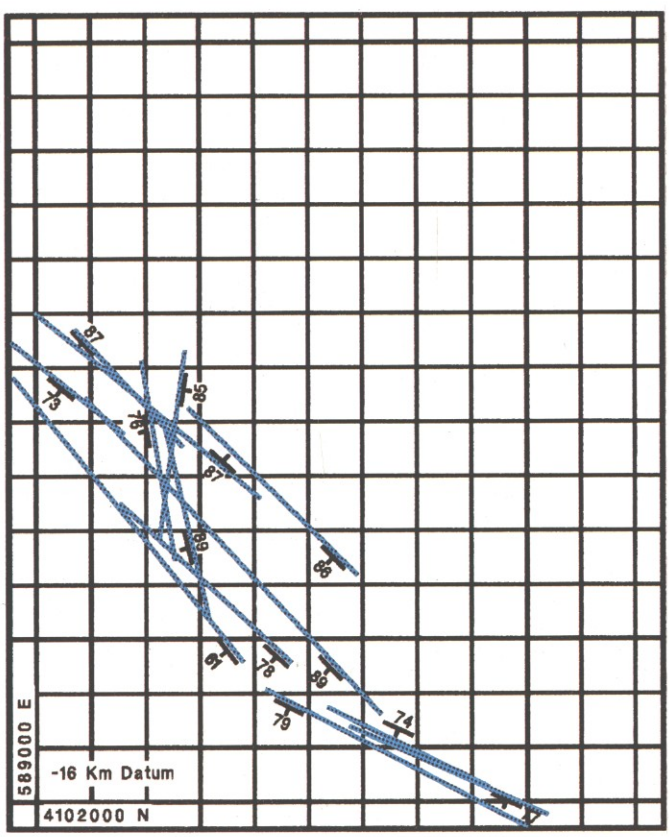

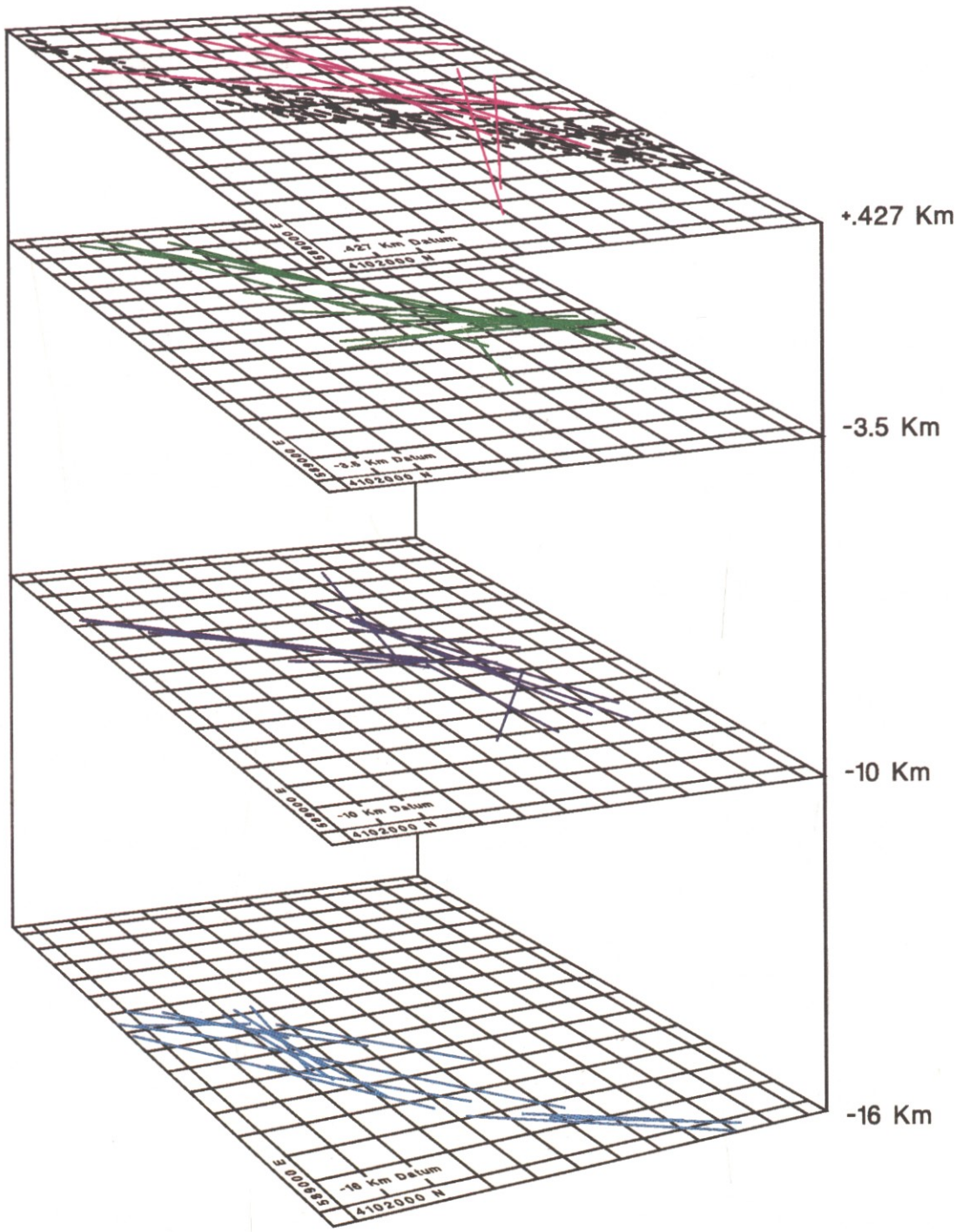

Figure 5.—Spatial relationships of the mapped surface faults related to the San Andreas and Sargent fault zones (black) and the potential regional topographic and seismically active fracture zones (colors) projected to near-surface and subsurface datums, which are referenced to the UTM, zone 10S, 1,000-m grid.

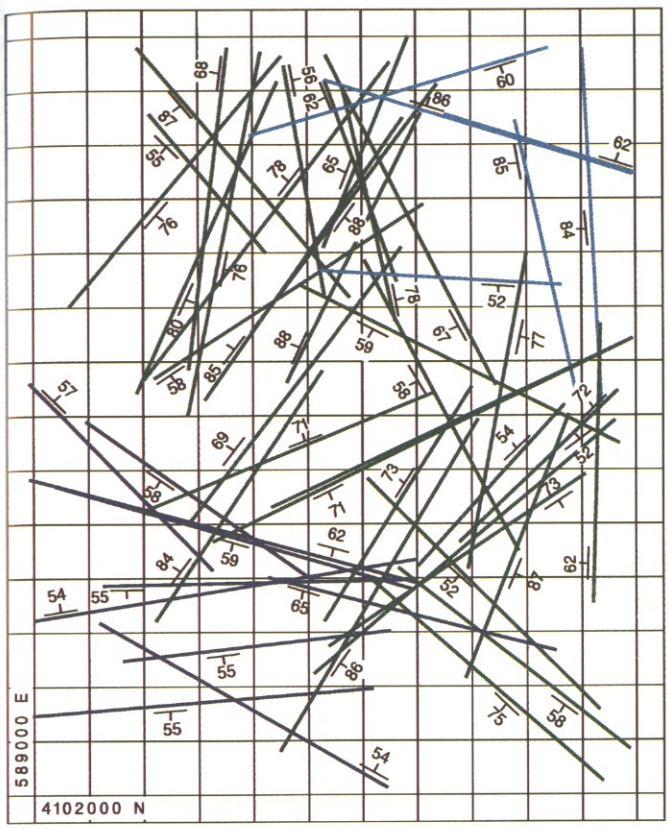

reactivating the dominant crustal weaknesses that represent the local San Andreas and Sargent fault zones. The dominant surface fracture zones that have been determined from the topographic data probably are the surface manifestation of fault zones developing in response to the right-lateral displacement on this segment of the San Andreas fault. Field studies should focus on this area for the purpose of determining whether direct evidence of right-lateral offset exists. Horizontal displacement measured on surface fractures that formed as a result of the Loma Prieta event shows no significant evidence of right-lateral displacement (Hart and others, 1990). These fractures are considered to be developing in response to effects such as lateral spreading of the ridges caused by shaking and secondary faulting. The analyses of topographic data indicate that a complex fracture domain has formed along the fault boundary in this area in order to accommodate deformation and movement of the fault blocks. Secondary motion on these and related minor fault structures that underlie the mapped San Andreas fault zone may account for the fact that the observed surface rupturing is unrelated to the primary right-lateral fault motion in this area.

Mapping of near-surface brittle structures from the subtle, but recoverable, imprint of the underlying fracture systems is a remote sensing research tool that can be applied now to most areas having moderate topographic relief. Stereo imagery collected from aerial and

◀ ***Figure 6.—Potential fracture zones and their dips determined from the subregion analyses of topography projected to the 427-m- (1,400-ft-) altitude datum referenced to the UTM, zone 10S, 1,000-m grid. The color coding is related to structural domains: Pacific plate (dark blue), boundary zone (green), and North American plate (light blue).***

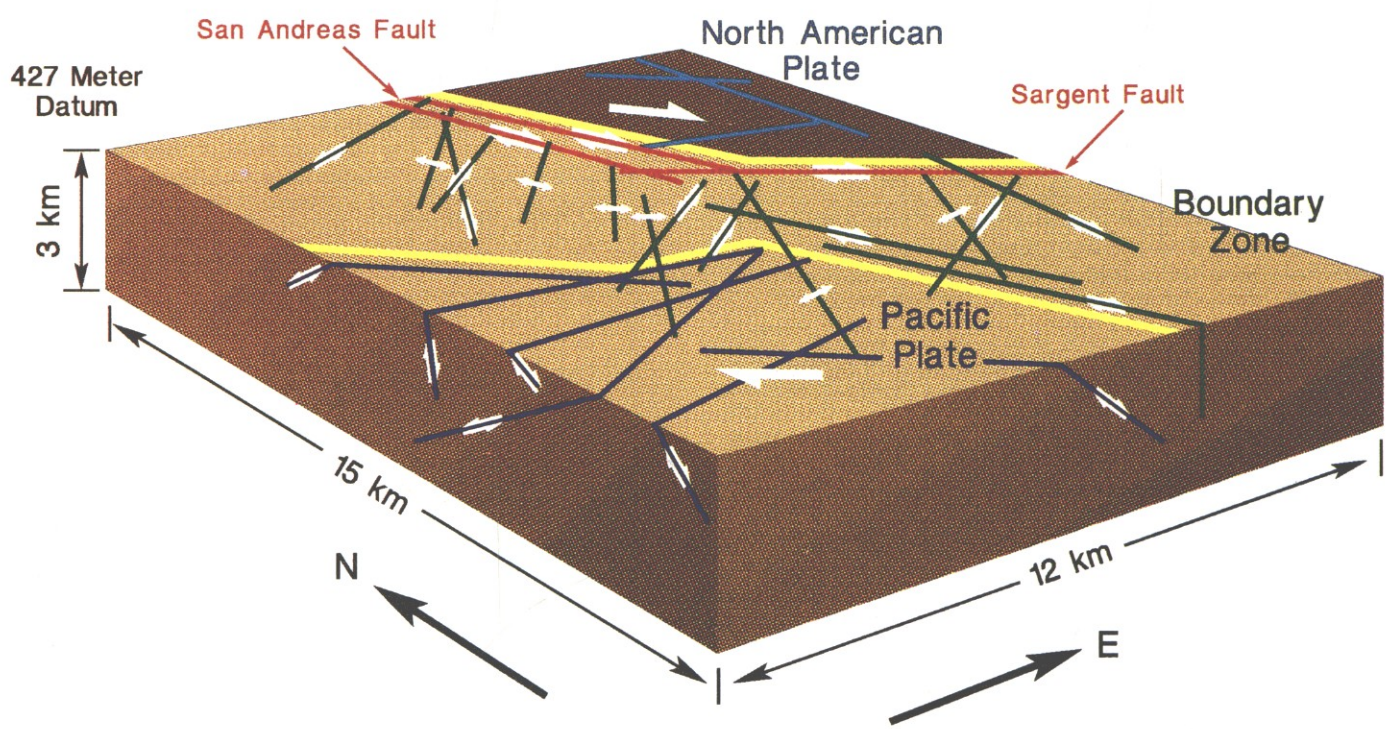

Figure 7.—Generalized structural model of the potential fracture zones determined from the topographic fracture analyses. Arrows show direction of movement.

(or) high-resolution satellite platforms can be used to obtain the topographic data required for the analyses. In the United States, topographic data are available for most areas at a scale of 1:24,000. These data are adequate for conducting topographic fracture analyses. Larger scale topographic data may be required for analyses in areas of low relief and for defining fracture detail in local areas. Current satellite systems are capable of obtaining topographic data that has a 10-m accuracy, and this should be useful for conducting fracture analyses of many areas. In addition, accurately located seismic hypocenters apparently contain a recoverable imprint of the local fracture systems. Both of these methods of analysis are based on the assumption that crustal fracture zones that develop under local stress fields tend to be planar over several kilometers. These fractures subtly influence erosion patterns at the surface and control the location of seismic activity at depth. By studying the spatial relationships of erosional patterns and seismic events, we have been able to recover the three-dimensional locations and orientations of these fractures. This ability will provide another valuable research tool for the investigation of complex fault systems. Data from these investigations will complement the lithologic and structural data that are being collected in the field by classic techniques.

The work presented here provides only a small window into the structural detail that should be recoverable from areas having complex fault systems. Future research hopefully will provide the key data that are needed in order to determine the neotectonic framework of seismically active areas and to provide us with better assessment of local seismic risk.

Acknowledgments

My research partner and wife, Valerie L.C. Eliason, has been responsible for much of the data preparation and analyses required for conducting this research and for completing these demonstration projects.

I would like to thank D.J. Ponti and R.E. Wells of the U.S. Geological Survey in Menlo Park, California, for identifying the areas of maximum surface rupture and for reviewing our initial analyses of the area, as well as D.H. Oppenheimer of the U.S. Geological Survey in Menlo Park, California, for providing the Loma Prieta seismic data set and for reviewing these analyses.

References

Brabb, E.E., and Hanna, W.F., 1981, Maps showing aeromagnetic anomalies, faults, earthquake epicenters, and igneous rocks in the southern San Francisco Bay region, California: U.S. Geological Survey Geophysical Investigations Map GP–932, scale 1:125,000.

Dietz, L.D., and Ellsworth, W.L., 1990, The October 17, 1989, Loma Prieta, California, earthquake and its aftershocks: Geometry of the sequence from high-resolution locations: Geophysical Research Letters, v. 17, no. 9, p. 1417–1420.

Eliason, J.R., 1984, A technique for structural geologic analysis of topography: Pullman, Washington, USA, Washington State University, doctoral dissertation, 196 p.

Eliason, J.R., and Eliason, V.L., 1985a, A comparative study of fracture planes computed from topography and lineaments from imagery with structures and mineralization in the magnesite belt of Washington State, *in* International Symposium on Remote Sensing of Environment—Remote Sensing for Exploration Geology, 4th, San Francisco, California, USA, 1985, Proceedings: Ann Arbor, Michigan, USA, Environmental Research Institute of Michigan, p. 655–664.

———1985b, U.S. Patent 4,698,759, issued October 6, 1987, Process for structural geologic analysis of topography and point data.

Fehler, Michael, House, Leigh, and Kaieda, Hideshi, 1987, Determining planes along which earthquakes occur: Method and application to earthquakes accompanying hydraulic fracturing: Journal of Geophysical Research, v. 92, no. B9, p. 9407–9414.

Hart, E.W., Bryant, W.A., Wills, C.J., and Treiman, J.A., 1990, The search for fault rupture and significance of ridgetop fissures, Santa Cruz Mountains, California, *in* McNutt, S.R., and Sydnor, R.H., eds., The Loma Prieta (Santa Cruz Mountains), California, earthquake of 17 October 1989: California Division of Mines and Geology, Special Publication 104, p. 83–94.

Lisowski, M., Prescott, W.H., Savage, J.C., and Johnston, M.J., 1990, Geodetic estimate of coseismic slip during the 1989 Loma Prieta, California, earthquake: Geophysical Research Letters, v. 17, no. 9, p. 1437–1440.

Michelini, A., and Bolt, B.A., 1986, Application of the principal parameters method to the 1983 Coalinga, California, aftershock sequence: Bulletin of the Seismological Society of America, v. 76, no. 2, p. 402–420.

Oppenheimer, D.H., 1990, Aftershock slip behavior of the 1989 Loma Prieta, California, earthquake: Geophysical Research Letters, v. 17, no. 8, p. 1199–1202.

Rieken, E.R., 1985, Computer generated fault surface determinations for earthquake foci: Pullman, Washington, USA, Washington State University, master's thesis, 126 p.

U.S. Geological Survey Staff, 1989, Preliminary map of fractures formed in the Summit Road-Skyland Ridge area during the Loma Prieta, California, earthquake of October 17, 1989: U.S. Geological Survey Open-File Report 89–686, scale 1:12,000.□

Dr. Eliason *has over 30 years of experience in geological research and development. His work has included the development of quantitative digital analysis techniques for remote sensing and the assessment of geologic structures, hydrogeology, and environmental geology. Currently, his studies focus on the continued development and application of fracture analysis techniques. Dr. Eliason is co-owner of Geologic Analysis and Consulting Services in Deary, Idaho, USA. Previously, he worked for 25 years at the U.S. Department of Energy's Hanford Research Laboratory in Richland, Washington, USA, as a Senior Research Scientist and Manager of geoscience investigations.*